Università
Ca'Foscari
Venezia

CORSO DI LAUREA MAGISTRALE
(ordinamento ex D.M. 270/2004)
IN SCIENZE AMBIENTALI

Curriculum INTERNAZIONALE IN SVILUPPO SOSTENIBILE
(classe LM-75 Scienze e Tecnologie per l'Ambiente e il Territorio)

PROVA FINALE DI LAUREA

Ca' Foscari
Dorsoduro 3246
30123 Venezia

GEOCHEMICAL CHARACTERIZATION OF A SHALLOW FIRN CORE RETRIEVED FROM COLLE GNIFETTI (MONTE ROSA, ITALY)

Relatore: prof. ***Carlo Barbante***

Co-relatore: prof. ***Takao Yamashita*** *(Hiroshima University)*

Laureando: ***Nicolò Ardenghi***

Matricola: ***831166***

ANNO ACCADEMICO
2011/2012

SUMMARY

Colle Gnifetti (4450 m a.s.l. – Punta Gnifetti 4554 m a.s.l.) is a mountain saddle of the Monte Rosa massif, in the Pennine Alps, on the border between Italy and Switzerland. The site is hence located above the local critical limit of 4200 m a.s.l., where the glaciers are not yet significantly affected by melting processes.
Glaciers of this area (that can be seen as the heart of Europe) are excellent paleoenvironmental and paleoclimatic records for the entire continent, as they are affected by pollutant inputs from all the main European industrialised countries, especially Germany, Italy and France.

This thesis aims to gain information about the trace elements and heavy metals inputs for the mentioned area over the last 15-20 years through the analysis of a 11 m shallow firn core recovered from the Colle Gnifetti ice saddle, in August 2011.
The data has then been connected with information from the previously obtained cores from the same glacier, which encompassed a wider time span for trace elements: from a few thousand years ago to 1993.
The dating process was performed by comparing the CG11 high resolution crustal profiles (analysed specifically for the dating process) and other dated crustal elements profiles of previous studies regarding colle Gnifetti ice cores such as the CG03 of Gabrieli (*Gabrieli* 2008) and the CG08, an unpublished Swiss work.
Firstly, some main distinctive summer peaks were identified in the compared profiles of the few elements the studies had in common (such as Ca, Mg, K and Na).
Then the concentration tables of these elements were compared to each other to highlight the peaks and the valleys marking maximum and minimum values and

define, with a certain degree of uncertainty, the season and the year of each section.

The final step was to compare data on dust layers (almost none in CG11) and the distribution of ice lenses to confirm and/or refine the dating. Finally, a seasonal profile was defined and adopted for further calculation, among which the snow accumulation rates.

The study of climatic proxies and pollutants contained in the ice of Colle Gnifetti helped to improve the picture of the climatic and environmental evolution of the surrounding area and of the continent itself in the last decades, by adding data to global databases**.**

The analysis of the trace elements and heavy metals Concentration profiles and Enrichment Factors (EF) trends were analysed for the most significant elements (Pb, Ag, U, Ni, Cu, Cd, Sn, Co, V, Cr, Bi, Tl, Rb, Sr, Cs, Ga, Mn); different groups of elements showed various behaviours revealing a substantial continuity between the concentration trends of previous studies on ice cores with similar origin.

However, for some elements, there is a great difficulty in detecting any trend at all; these apparently random readings are probably the consequence of the high yearly variability and the short time span covered by the ice core.

Also, a small innovation in the ice/firn processing method was successfully tested with the use of ceramic blades instead of steel chisels.

CONTENTS

1. INTRODUCTION

1.1 IMPORTANCE OF ICE CORES FOR CLIMATE AND ENVIRONMENTAL RESEARCH

Ice core proxy records from polar regions and mid-low latitude mountain glaciers are an important source of information for climate reconstruction (both hemispheric and global) and environmental research (*Mann*, *Zhang* et al. 2008).
The environmental tracers are sealed within the snow/ice as it gradually accumulates and is compressed under the weight of the more recent layers. Among the various proxies contained in ice cores, the use of isotopic composition of water, coupled with the analysis of natural and/or anthropogenic tracers, is the most common approach for paleoclimatic reconstructions (*Siegenthaler* and *Oeschger* 1980) (*Araguás-Araguás*, *Froehlich* et al. 2000).
Ice cores are investigated for many environmental proxies.
Sulphur dioxide is one of the first pollutant of interest to be investigated (ex.: acid rains); it is strongly emitted by anthropogenic sources (factories) but it also has natural sources, of which the main is volcanic emissions. SO_2 emissions can be directly related to the concentration of sulphate anion (SO_4^{2-}) in ice cores; to distinguish between natural and anthropogenic sources of SO_4^{2-} (and therefore SO_2) a correction of the total SO_4^{2-} for the contribution of sea-salt (mainly Na^+ and Cl^-) and mineral dust is needed (*Schwikowski*, *Döscher* et al. 1999). Volcanic eruptions input huge amounts of SO_2 into the atmosphere, these episodes are the cause of strong pulses of SO_4^{2-} concentration in ice cores and can easily be used for the dating process (*Palmer*, *van Ommen* et al. 2001).
Two other major ionic aerosol components analysed in Alpine ice cores closely reflect the pollution history of Central Europe: NO3-and NH4+which are, respectively, the products of precursor gases NOx and NH3. NOx are produced during high temperature combustion processes while NH3 emissions are related to animal manure and production of fertilizers (*Schwikowski* 2004).
Other ions such as Cl^-, F^-, methanesulfonic acid (MSA), formiate ($HCOO^-$), acetate (CH_3COO^-) are often determined (*Legrand*, *De Angelis* et al. 1992).
High concentrations of trace elements, especially heavy metals, in Alpine ice cores can be the sign of anthropogenic pollution when they exceed the estimated natural concentration. One of the best studied is Pb, that undergoes various

concentration shift during history, from Roman time to Medieval ages, the industrial revolution and the last decades of the XX century (*Barbante*, *Schwikowski* et al. 2004; *Gabrieli* 2008). Other environmentally important heavy metal proxies are Ag, Au, Cd, Co, Cr, Cu, Mo, Pd, Rh, Sb, Sn, etc. (Barbante, C. et al. 1997; *Barbante*, *Boutron* et al. 2002; *Barbante*, *Schwikowski* et al. 2004; *Hong*, *Barbante* et al. 2004).

Alpine and Tibetan ice cores have been investigated for various kinds of organic compounds like Polycyclic Aromatic Hydrocarbons (PAHs), polychlorinated biphenyls (PCB), polybrominate diphenyl ethers (PBDEs), perfluorinated compounds (PFCs) and other kind of Persistent Organic Pollutant (POPs) as well as for levoglucosan (a biomass burning tracer) (*Villa*, *Vighi* et al. 2003; *Villa*, *Negrelli* et al. 2006; *Gabrieli* 2008; *Gambaro*, *Zangrando* et al. 2008; *Kirchgeorg*, *Weinberg* et al. 2010).

Nuclear testing and nuclear reactor accidents have been the emission sources of strong pulses of many radioactive isotopes like ^{3}H, ^{36}Cl, ^{129}I, ^{137}Cs, $^{235}U/^{238}U$ and $^{239}Pu/^{240}Pu$. These episodes are historically known and the correspondent concentration pulses of the most prominent among them (such as the Chernobyl accident) in the ice core have often been used for the dating process of the core itself (*Warneke*, *Croudace* et al. 2002; *Olivier*, *Bajo* et al. 2004; *Gabrieli* 2008).

HCl, HF and CH4 historical concentrations were reconstructed from Alpine and polar ice cores (*Eichler*, *Schwikowski* et al. 2000; *Legrand*, *Preunkert* et al. 2002).

Even organic remains (vegetal, animal) have been dated through 14C analysis (*Jenk*, *Szidat* et al. 2007; *Jenk*, *Szidat* et al. 2009) while reconstruction of past climate through pollen and bacteria trapped in ice have been attempted (*Liu*, *Reese* et al. 2005) but only on Andinian ice cores.

1.2 SITE CHARACTERISTICS

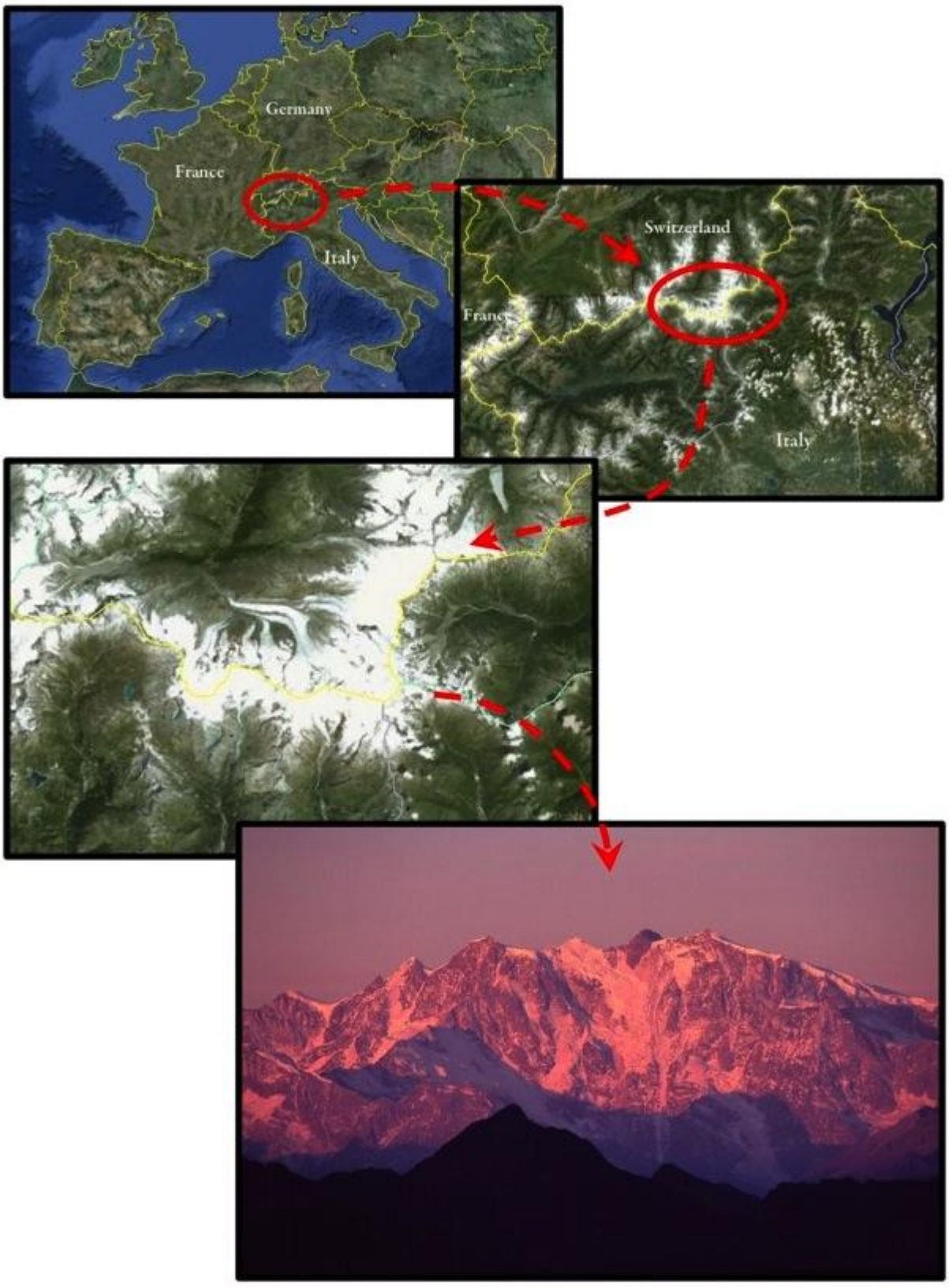

Figure 1: Monte Rosa geographical location

The Monte Rosa massif is located in the Pennine Alps, which is shared by Italy (Aosta Valley and Piedmont regions) and Switzerland (Valais canton).
It is the biggest massif of the Alps and the second highest (Punta Dufour 4634 m a.s.l.). It includes more than 20 peaks over 4000 m a.s.l. and about 10 glaciers, both on Italian and Swiss sides.
Colle Gnifetti (4450 m a.s.l.) is a mountain saddle of the massif, between Punta Gnifetti-Signalkuppe (4554 m a.s.l.) and Punta Zumstein-Zumsteinspitze (4563 m a.s.l.). (*Wedepohl* 1995)
The border between Italy and Switzerland runs between these two peaks and the saddle is the uppermost accumulation area of the Grenzgletscher (that means "border glacier").

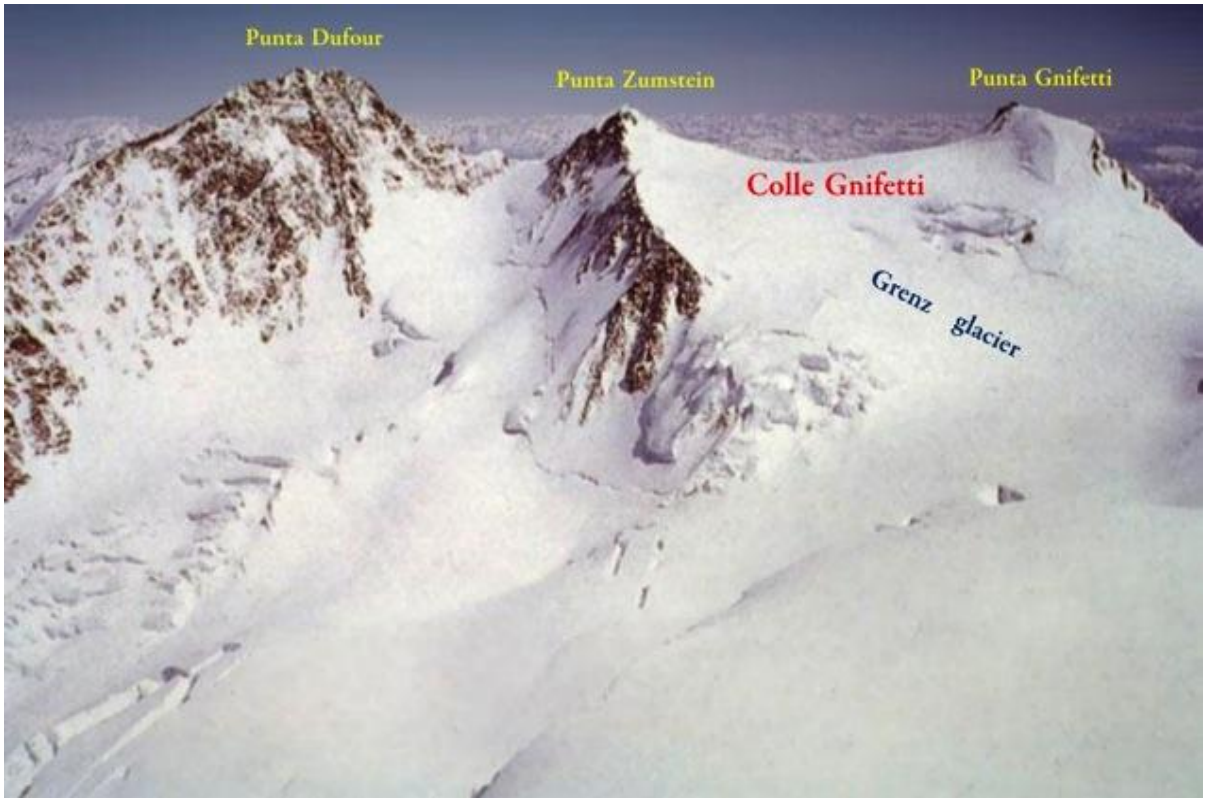

Figure 2: the three peaks (Dufour, Zumstein and Gnifetti) and the saddle of Colle Gnifetti (south western side)

The saddle is well over 4200 m a.s.l., the local critical limit above which glaciers are not yet significantly affected by melting processes, that is why there is basically no percolation, but only occasional melting and refreezing within the summer layer (*Eichler*, *Schwikowski* et al. 2000). The peculiar position of this massif, at the heart of Europe among long term heavy industrialized countries such as Germany, Italy, France and Switzerland, allows these glaciers to be good record sites for human historical pollution.

Figure 3: view of the north eastern side of the saddle

The snow depositing on the saddle tends to slide down the north eastern cliff (see figure 3) or to flow down the less steep south western slope, into the Grenz glacier. Due to the uneven steepness of the saddle, the snow/ice flows downhill with different velocities, as shown in figures 4 and 6. (*Lüthi* and *Funk* 2000)

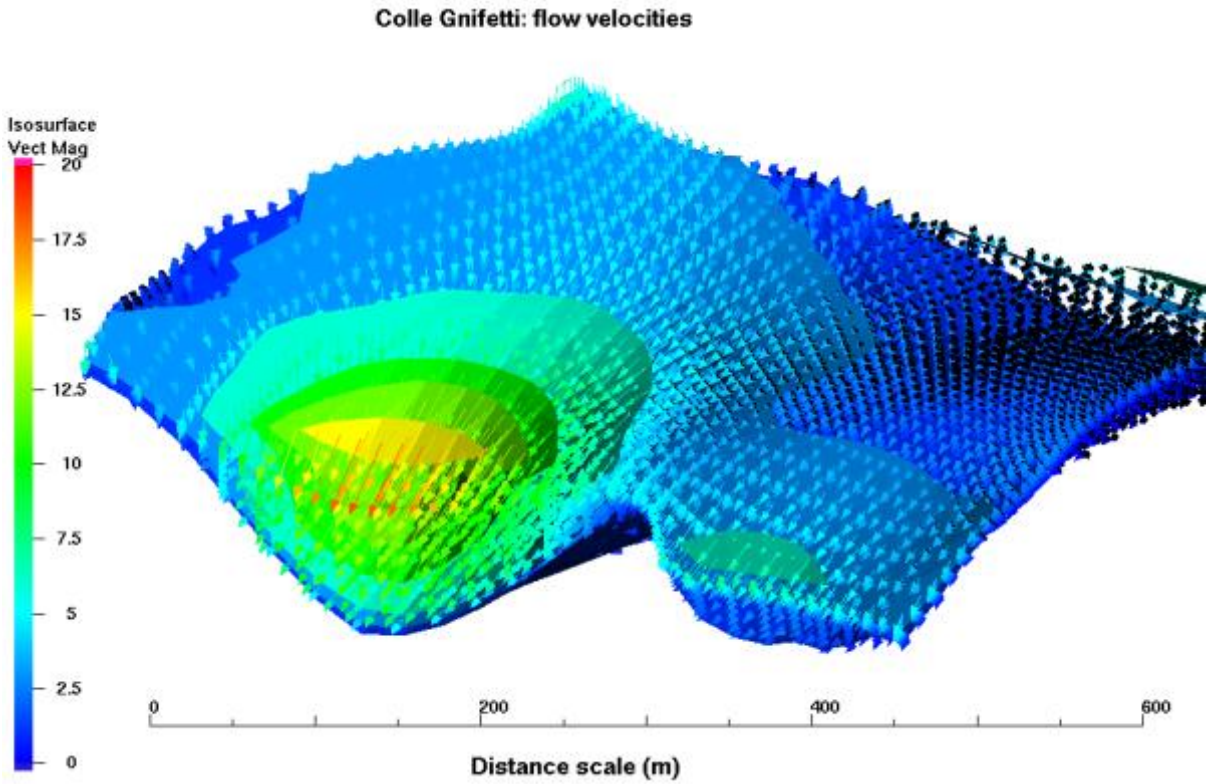

Figure 4: snow flow velocities model of Colle Gnifetti (*Lüthi* and *Funk* 2000)

The CG11 core was drilled in August 2011, at the coordinates 45°55'30''N 07°55'46''E, 4454 m a.s.l.. A snow layer of ca. 210 cm was first removed with the excavation of a trench.

The CG11 drilling site is close to other previous drilling sites (see figure 5), in particular CG03 (two cores 81 and 82 m long) and CG08 (a 10,5 m long core).

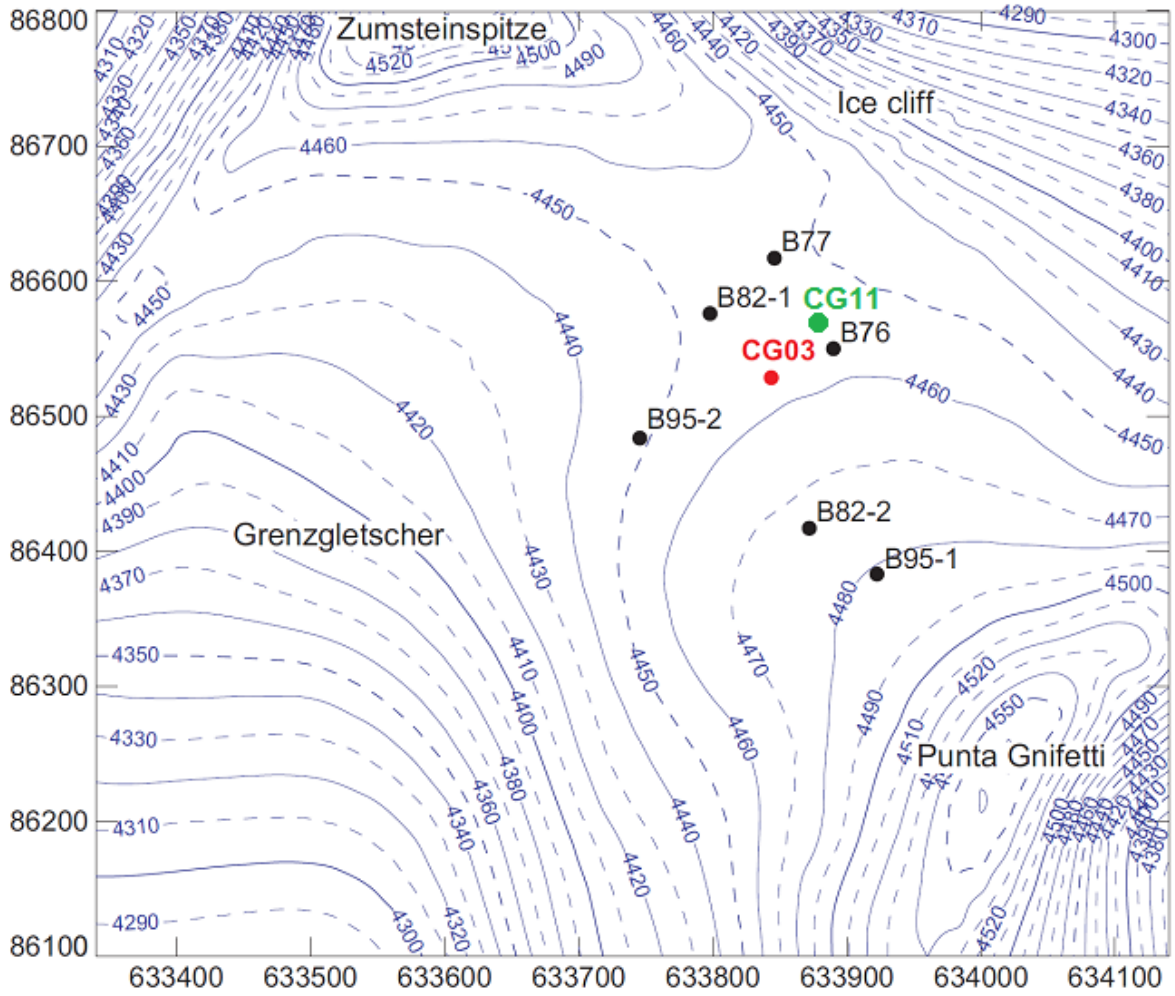

Figure 5: surface elevation of Colle Gnifetti. The coordinates are in the MN03 Swiss system. Adapted from (*Sigl* 2009)

The choice of this location was driven by the flow model of the saddle (figure 4 and 6): this model determined a clear flow direction at this place, with an estimated layer thickness of at least 14 m, reaching back in time more than 5 centuries at least (*Lüthi* and *Funk* 2000).

This because the average accumulation rate of Colle Gnifetti is relatively low (<0,5 m weq/year), due to its exposed position and wind erosion, and therefore reflects only about 10% the mean precipitation rate measured further downglacier (*Alean*, *Haeberli* et al. 1983); this phenomenon means that Colle

Gnifetti cores can cover a significant span of time even when they are not very deep.

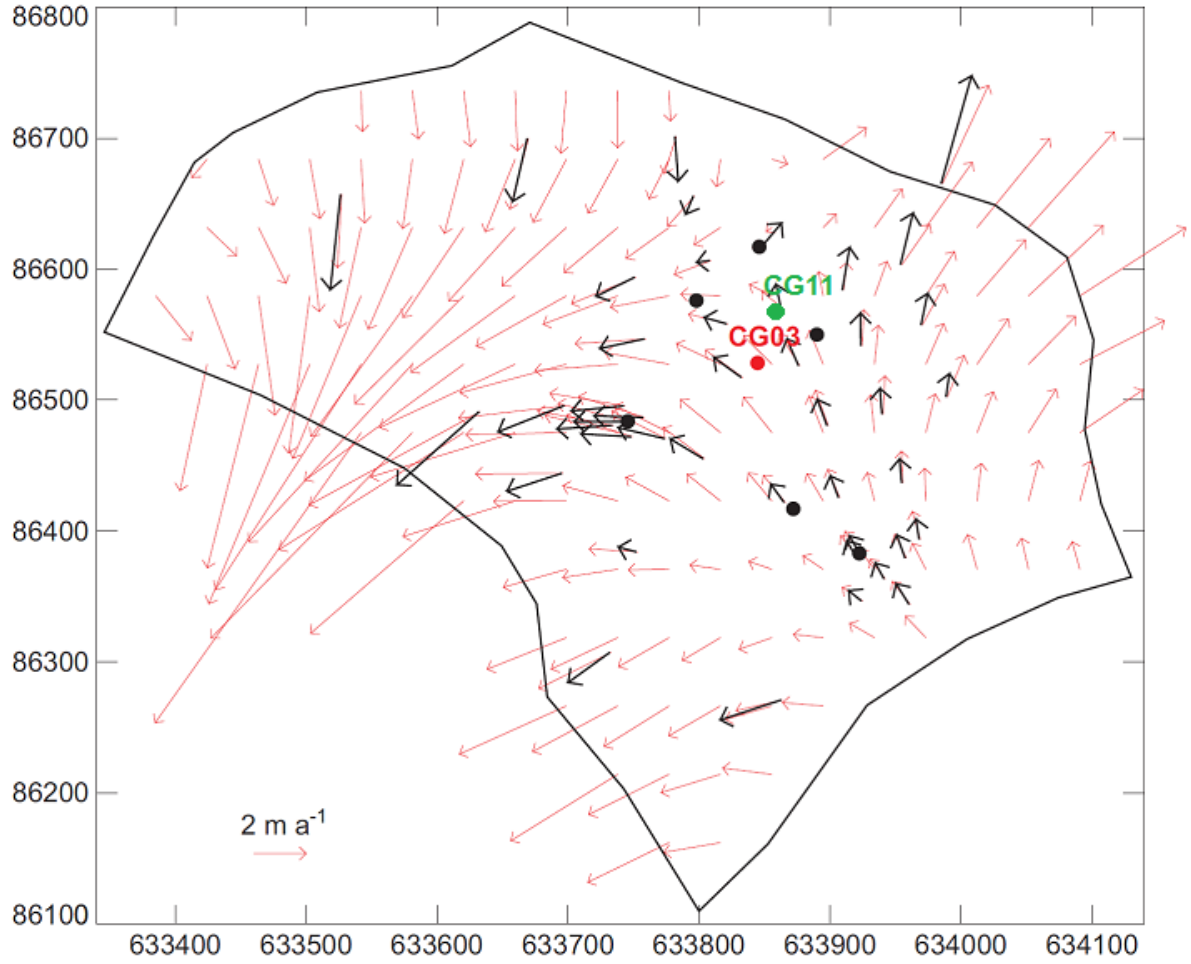

Figure 6: the flow model of the Colle Gnifetti saddle.
Adapted from (*Lüthi* and *Funk* 2000)

Also the fact of being on the NW side of Punta Gnifetti and not too close to the centre of the saddle (and to the other peak, Zumsteinspitze), allows the snow flow of this location to have only one source basin (the Punta Gnifetti itself) and therefore minimise the possible mixing of upstream effect (see figure 7) (*Eisen*, *Nixdorf* et al. 2003)

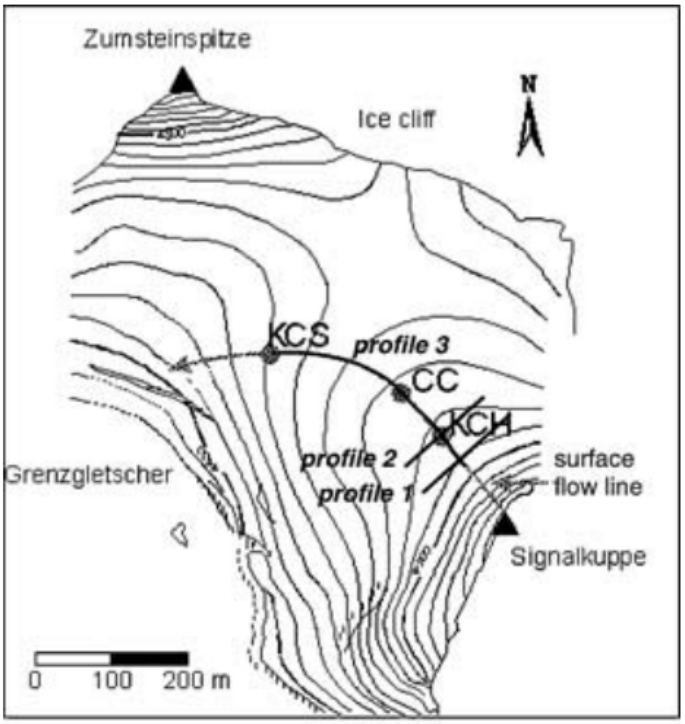

Figure 7: a study to determine the flow model of CG through ground penetrating radar (GPR) (*Eisen*, *Nixdorf* et al. 2003); the boreholes are located on the south-eastern side of the saddle, following the topography and avoiding the snow flow contribution of peak Zumstein

1.3 HISTORY OF ICE CORE DRILLING ON COLLE GNIFETTI

The Monte Rosa massif has a long history of core drilling.

The first expedition dated back to 1894 when a team from the University of Turin (Piero Giacosa, Lorenzo Scofone and Carlo Viziale) collected samples of water, ice and snow in the area of the Lys glacier. Their analyses and conclusions were astonishingly good, given the poor means and techniques of those years.

Giacosa also wrote "La differenza fra la chimica di ghiacci provenienti da località vicine, […], dimostra con argomento chimico che il ghiacciaio non è una massa omogenea […] ma un miscuglio irregolare di filoni di varie nevi che, per origine ed età diverse, devono necessariamente avere composizione varia (the different chemical composition of ice retrieved from neighbouring areas […] demonstrates chemically that the glacier is not an homogeneous mass […] but a mix of various snow veins that, having different origin and age, must necessarily be different in composition)", defining in this way an approach to glaciology that will be resumed only many years later. (*Giacosa* 1896)

After the 1976 a few deep ice core and some shallow firn core drilling expeditions followed (see table below for deep cores)

SITE	CORE	DEPTH (m)	DATING HORIZONS	ACCUMULATION RATE (cm w.eq. yr^{-1})	REFERENCES
B76 B77		33 65	^{3}H, ^{210}Pb, **SD** 1936	30-35	(*Oeschger* 1977) (*Gaggeler*, *Von Gunten* et al. 1983)
B82-1	Blue core Red core	109 124	^{3}H **SD** 1977, 1936, 1901 **V** 1912, 1883, 1815, 1783 ^{3}H **SD** 1977, 1947, 1936, 1901 **V** 1783(?)	30-40 No data	(*Döscher*, *Gäggeler* et al. 1996) (*Häberli*, *Schmid* et al. 1988) (*Schotterer*, *Oeschger* et al. 1985)
B82-2	CC	66	^{3}H **SD** 1977, 1936, 1901 **V** 1912, 1883, 1815, 1707, 1460, 1396, 1260	24	(*Keck* 2000)
B95-1	KCH	61	^{3}H **SD** 1977, 1936, 1901, 1863, 1830 **V** 1707	25	(*Keck* 2000)
B95-2	KCS	101	^{3}H **SD** 1977, 1936, 1901 **V** 1784, 1770, 1731, 1707, 1660, 1660, 1600, 1550, 1460, 1396, 1389, 1260, 943	52	(*Keck* 2000)
CG03	1 2	82 81	^{3}H, ^{14}C, annual layer counting **SD** 1977, 1947, 1936, 1901, 1863 **V** 1912, 1815, 1783 Not analysed	45	(*Sigl* 2009) (*Bolius* 2006) (*Jenk*, *Szidat* et al. 2009) (*Gabrieli* 2008)
CG08	1	10,5	^{16}O, annual layer counting	46	Not published
CG11		**11**	**annual layer counting**	**41**	**this work**

Table 1: ice core characteristics of 8 deep ice/firn cores drilled at Colle Gnifetti plus the shallow coring of this work
SD=Saharan Dust inputs – V = Volcanic inputs

1.4 DECONTAMINATION TECHNIQUES FOR ICE CORES

Researchers studying ice cores have always had to deal with the problem of accidental contamination due to various factors, among which there are the coring device and the transportation of the ice core.
Decontamination can be achieved through the rinsing of the external surface the core with de-ionized water or mechanically.
In the mechanical procedure, normally the core is first processed with a band saw that removes the most external layers and often obtains various sections that can be used for different kinds of analysis. All the operations are carried out in clean rooms kept at -15/-20°C, on LDPE surfaces with LDPE gloves.
The second stage decontamination involves the removal of the external layer (or layers) of the obtained section. This can be achieved in various modalities. Wagenbach and Munnich use a microtome knife, removing only one external thin layer (5-10 m) on a Colle Gnifetti core of 1988 (*Wagenbach*, *D.* et al. 1988);
Lavanchy and Gäggeler remove two layers (ca.5 mm) with a scalpel, analyse both the second layer and the core for heavy metals (*Lavanchy*, *Gäggeler* et al. 1999);
Planchon uses a more elaborate sequence in which a first external 50 mm layer was removed with the use of special stainless steel chisels which were initially designed for the chiselling of deep Antarctic ice cores, and horizontal subsamples were then severed from the main ice block with newly acid cleaned chisels and then placed in double acid rinsed LDPE bottles (*Planchon*, *Boutron* et al. 2001).
Ice core decontamination protocols have been studied to possible future decontamination of extra-terrestrial ice, starting from the know-how already acquired for Antarctic ice cores (*Christner*, *Mikucki* et al. 2005): the core has a first external layer removed mechanically, scraped with an acid rinsed mechanical blade; then a second layer is removed by washing with deionized water and ethanol while a third layer is removed by melting.
A really elaborated and time consuming procedure for blades and surfaces decontamination was developed in (*Vallelonga*, *Van de Velde* et al. 2002): “Lab ware was made from low-metal content plastics such as LDPE, FEP and PFA, the only exception being the chisels, which were machined from type 316L stainless steel. The plastics were cleaned in stages, beginning with a rinse in chloroform then aqua regia, followed by successively longer leaches in successively more dilute and higher purity acid baths. LDPE bottles were used for handling samples during aliquoting and storing samples prior to measurement. […] a 500ml bottle

was rinsed and filled with 0.1% UP nitric acid and left to stand at room temperature for 1 month. The solution was then analysed and the bottle was rinsed and refilled with freshly prepared 0.1% UP nitric acid. This process was repeated a number of times. All decontaminations were carried out in the ACRCHEPA module inside a cold room using a lathe, although one artificial ice core was decontaminated at LGGE. This lathe can hold ice/firn cores up to 12 cm in diameter and 85 cm long. Individuals wore Tyvek coveralls and shoulder length polyethylene gloves. A total of 3–4 h was typically required to obtain 3–4 veneer layers and an inner core. Wide-mouthed LDPE bottles containing the chiselled ice samples were sealed in acid cleaned polyethylene bags and stored frozen until aliquots of the sample were prepared. Following a decontamination, the apparatus was cleaned in preparation for the next sample. The scoops and inner core tongs were sequentially immersed in three heated HNO_3 (AR grade 3%, 15min; UP 0.5%,24 h; UP 0.5%, 4 days) acid baths. Components of the lathe were sequentially immersed in two unheated HNO_3 baths (AR grade 5%, 24 h; UP 0.5%, 4 days).The stainless steel chisels were initially cleaned for 15 minutes in an unheated HNO_3 (AR grade 5%) bath, then immersed for 24 h in a heated HNO_3 (UP 0.5%) bath before being stored in a second heated HNO_3 (UP0.5%) bath for 5 days. Following the aliquoting of samples, the wide-mouthed LDPE bottles were rinsed, filled with UP HNO_3 (0.1%) and left on a warm pad until the next decontamination, the day prior to which they were rinsed and preconditioned with UPW".

It must be noticed that this elaborate technique was thought and developed for Antarctic ice cores, which need higher decontamination standards than Alpine ice core.

In the CG03 and other works of Gabrieli (on Alpine ice cores) were used stainless steel blades, rinsed with HNO_3 to remove two/three external layers, preparing the core for a Continuous Flow Analysis (CFA), a method that was not used in this work because of the relative low density of the CG11 superficial core. (*Gabrieli* 2008; *Gabrieli*, *Vallelonga* et al. 2010).

Given the huge amount of time needed and the over efficiency of the technique mentioned above, even when simplified, when applied to Alpine ice cores (as seen in the works of Gabrieli), this study has tested a new simplified method for the decontamination of an Alpine ice core, involving ceramic knives and simple acetone-deionized water rinsing. The method has the indubitable advantages of

being simpler and faster than the one described above while it maintains a very acceptable efficiency, at least for superficial Alpine ice cores.
The method is described in the "Samples Preparation" paragraph.

1.5 THE CG03 CORE STUDY

The present study is focusing on a previous 2008 study performed by dr. Jacopo Gabrieli (*Gabrieli* 2008) of the Environmental Sciences department of Ca' Foscari university of Venice. That work focused on an ice/firn core retrieved from the same Colle Gnifetti saddle in 2003 by a Swiss/Italian team led by M.Schwikowski; the core analysed (CG03 – see map above) was 81,9 m long (125 sections) and reached the bedrock.
The core was first brought to the Paul Scherrer Institut (Villigen, Switzerland), where it was prepared for the analysis: with a commercial band saw, proceeding in a similar way as descripted for this core (CG11) at the paragraph "Samples preparation", the core was cut into several slices; part of them was then sent (in 2007) to the Ca' Foscari Environmental Science department.
The core was analysed with the use of ICP-Mass Spectrometry, ICP-Optical Emission Spectroscopy for inorganic trace elements and some isotopes of particular interest such as ^{2}H, ^{3}H,^{14}C, ^{16}O, ^{18}O, ^{239}Pu, ^{206}Pb, ^{207}Pb and ^{208}Pb ; ion-chromatography was used to determine PAHs concentrations.
The present study can also be seen as a partial (only inorganics have been analysed) continuation of the work on the CG03 core, where trace elements concentration profiles, obtained through Continuous Flow Analysis (CFA), were reported only until 1993, due to the inadequacy of the CFA technique when dealing with the less compact surface layers of the core.
Many of the procedural choices (as, for example, the cutting instrument and methods, the choice of Ba as comparing element for the Enrichment Factor estimation) taken in this study are directly derived from the method applied for the CG03; this because there is an effort to render this work as comparable as possible with the previous one.
The data were first divided into two sets (pre and post Industrial revolution) and statistically analysed through Principal Component Analysis: in the post industrial revolution set the subgroups of Pb, Zn, Cu, Cd and Bi were distinctly separated from U and other elements.

All the elements, both common crustals and TE/heavy metals, showed a marked seasonal variation with summer concentrations ranging from 25 to 150 times the winter values. This phenomenon (clearly defined in the high-resolution crustal series) was later used for the annual layer counting during the dating procedure. In particular, the behaviour of Pb was carefully investigated, outlining a series of highs and lows related to corresponding historical periods (Roman, high and low medieval ages, industrial revolution, etc.) and, more recently, a peak around 1970s and a decreasing trend starting in 1975, due to new antipollution policies. For Uranium was identified a strong increase from the 1910s, a peculiar peak at the end of WW2 and a steady increasing trend until the end of the 1970s. In the 1980s, U concentration started to decrease until reaching almost levels of the beginning of the XX century.

1.6 GEOLOGY OF THE AREA

The whole Alpine system was generated with the closure of the great Tethys Sea started around 150 million years ago, in the Jurassic.

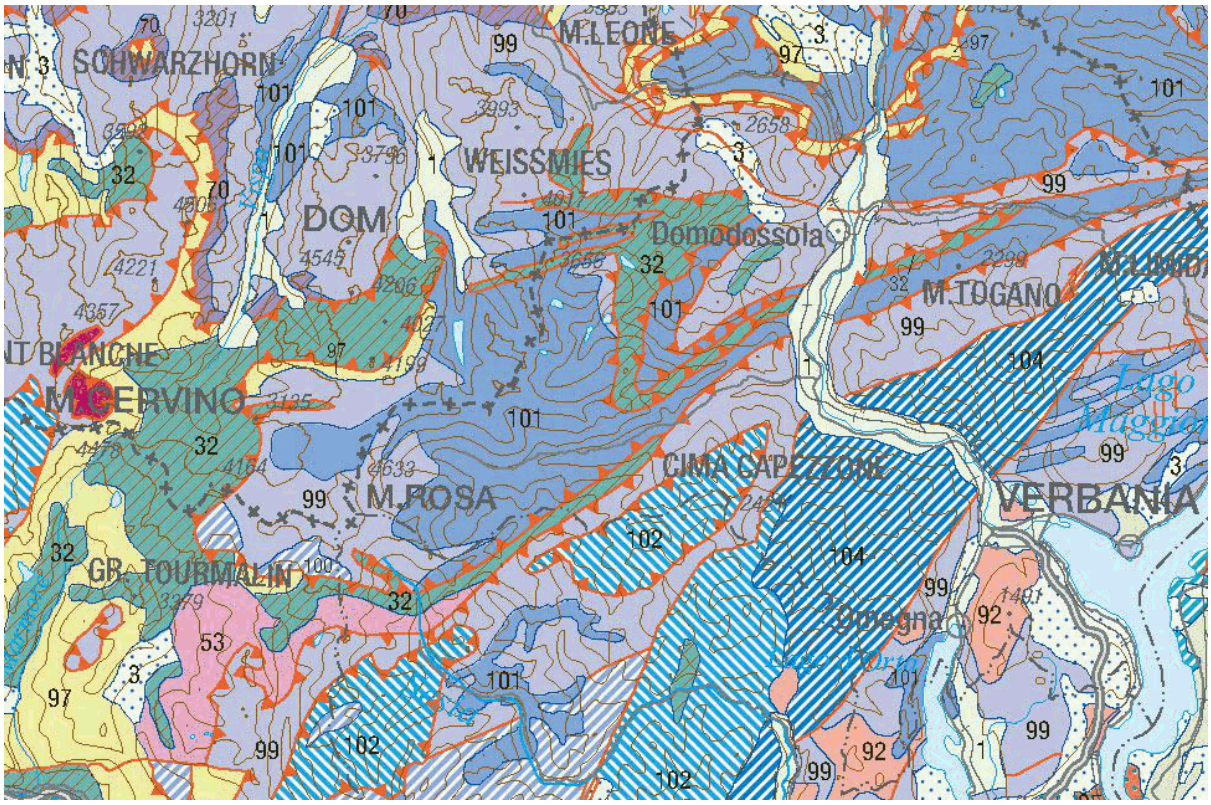

Figure 8 : geological map of the monte Rosa massif area; in blue (101) the European formations, in green (32) the oceanic Tethydian formations, in lilac (99) the African formations (Carta Geologica d'Italia 1:1000000, *ISPRA-2011*)

The Alps were the result of this huge compression movement and, therefore, the origin of their layers is not homogeneous but there are formations that can be traced back to all the plates involved in the movement: African, European, Tethydian, Adriatic, Cimmerian et cetera.
The monte Rosa massif is almost entirely composed of ancient European layers. In fact it appears like an island of the European formation surrounded first by the old Tethys ocean formation and then by the ancient African continental formation.
The European plate encompasses also the Gran Paradiso massif, the Ruitor, the Gran San Bernardo and the Monte Bianco. The monte Rosa massif is indeed a late Palaeozoic pluton (around 350 million years old) intruded in the ancient European crust and it is part of the pennidic formations.
In particular, its peaks, from monte Castore to punta Gnifetti, are formed of gneisses and granites of European origin. These high-pressure gneisses represent the basement of the European margin of the alpine Tethys.

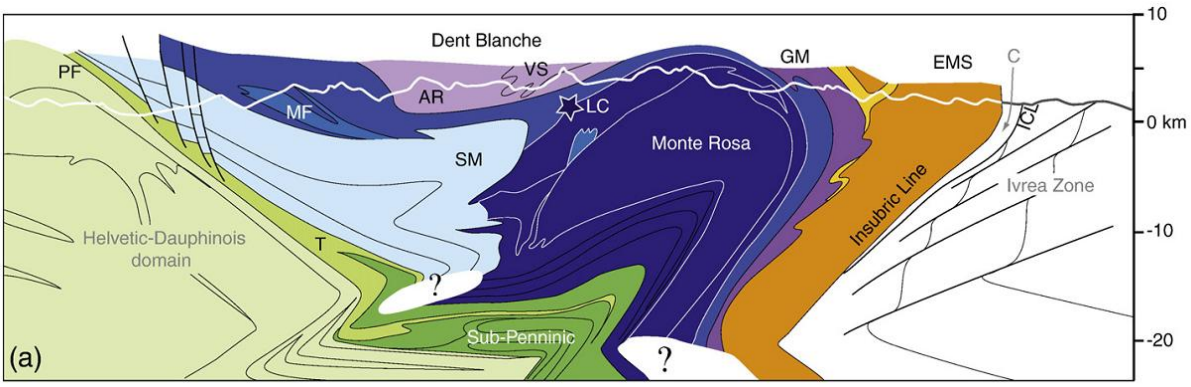

Figure 9: geological cross section of the monte Rosa massif (*Beltrando, Compagnoni et al.* 2010); AR: Arolla series; C: Canavese Zone; EMS: Eclogitic Micaschists Complex; GM: Gneiss Minuti Complex; ICL: Internal Canavese Line; LC: Lago di Cignana UHP Unit; MF:Mont Fort Unit; PF: Pennidic Front; SM: Siviez–Mischabel Unit; T: Tarentaise–Sion–Courmayeur Unit; VS: Valpelline series.

On the other hand, the surrounding formation represents the ancient oceanic floor of Tethys and it mainly consists of ophiolites; these are typical oceanic floor rocks, with high percentages of iron and magnesium in minerals such as olivine, chlorite, pyroxene, hornblende and asbestos.
In figure 10, it is possible to see the lithological composition of the area of colle Gnifetti; it is mainly paragneiss (derived from sandstone metamorphism) and orthogneiss (granite metamorphism). The main minerals constituting these rocks are listed in the table below.

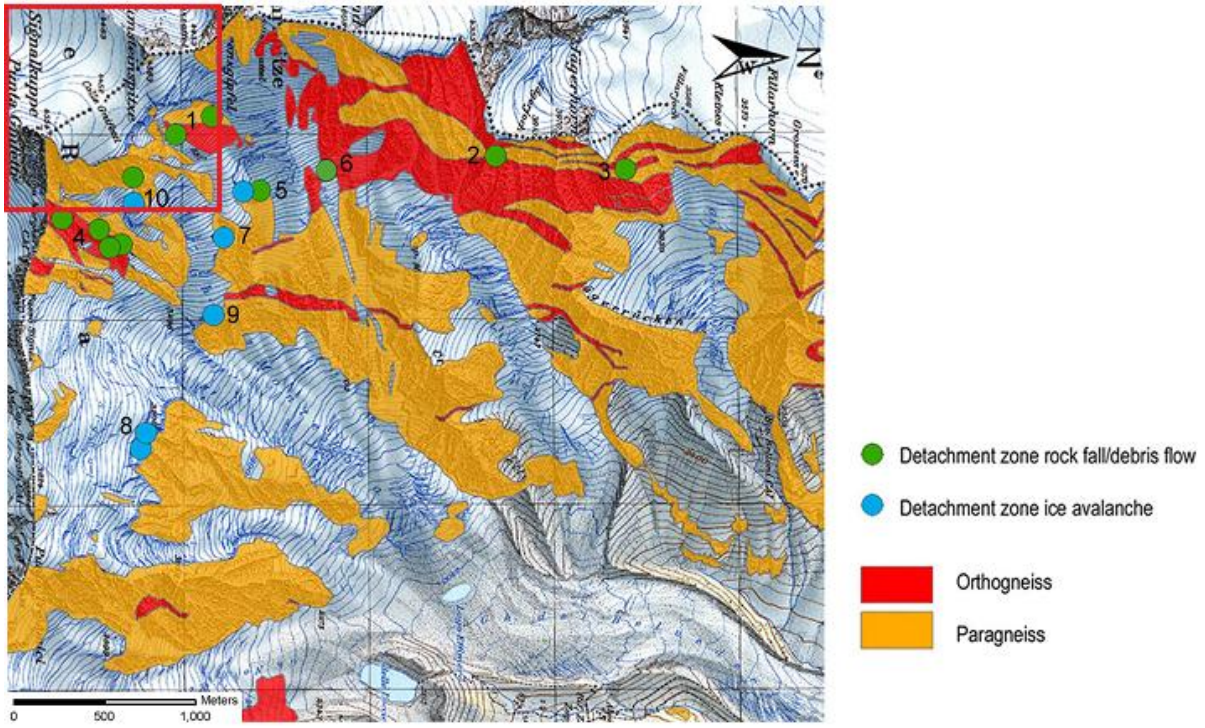

Figure 10: distribution of two different kind of gneisses of the uncovered areas on the monte Rosa NE slope. The red square encircles the Colle Gnifetti area. Adapted from (*Fischer* 2006)

It is highly probable that, there is a higher deposition of dust of those minerals constituting the surrounding peaks and slopes. This phenomenon is especially high in summer, when the movement of rock dust and particulate, provided mainly by the erosion and ablation operated by ice and snow in winter, is much more intense due to the rising height of the boundary layer and to the absence of the snow cover. The analysis of the different elements concentration could then partially reflect (only if the results of the statistical analysis of crustal elements are clear enough, that is not the case of this study) the crustal composition of the underlying and surrounding geological formations.

	Ba	Na	Mg	Ca	Fe	Al	K
ALBITE		x				x	
BIOTITE			x		x	x	x
MUSCOVITE						x	x
MICROCLINE						x	x
GENERIC FELDSPARS	x	x		x		x	x
GENERIC OPHIOLITES			x		x	x	

Table 2: main constituting elements of the main components of gneisses (orange) and ophiolites (green)

Later, in chapter 3 (Results and discussion), when the high resolution dating based on crustal elements will be examined and before the enrichment factor will be applied it would be good to take into account also this lithological characterization of the area.

1.7 MINERAL AEROSOL AND ENRICHMENT FACTOR

The transport of particles from Earth surface to the atmosphere is caused by air masses movements; winds and streams must be strong enough to win the friction bounding the particles to the ground. The main natural source for these particles can be of local origin (the bare peaks surrounding the glacier) or very distant origin such as deserts, similar barren lands in arid continental regions, forests (*Gabrielli*, *Cozzi* et al. 2008); the other main inputs are volcanoes, especially explosives ones, erupting huge amounts of ash, and sea salt spray. There is also a secondary extra-terrestrial input, especially for elements such as Pt or Ir. (*Gabrielli*, *Barbante* et al. 2004)

The Enrichment Factor (EF) is defined as the concentration ratio between a particular trace element and normally Ba or Al (or other elements deriving mainly from soil and rock particulate). This ratio is normalized to the same concentration ratio characteristic for the mean upper continental crust.

$$EF = \frac{\frac{[X]_{ice}}{[RE]_{ice}}}{\frac{[X]_{UCC}}{[RE]_{UCC}}}$$

In the equation, [X] and [RE] are the concentration in ppm of the trace element and of the reference element; UCC means Upper Continental Crust; in particular an EF higher than 1 means there is enrichment.

Given that it is a mean value for the whole upper continental crust, it is necessary to admit some uncertainty. Applying an uncertainty interval of ±10 means that for values ranging from ≈0,1 and 10 times the mean value, the source is always crustal. Over a factor 10 contribution from other sources is considered pronounced while over 100 it is considered strong (*Ferrari*, *Clotteau* et al. 2001)

(this is the same uncertainty interval adopted in the previous work on the core CG03 (*Gabrieli* 2008)).

The following table (*Wedepohl* 1995), indicates the average concentrations for 77 elements in the upper continental crust and can be used to estimate the natural background in processes where natural and anthropogenic inputs are mixed.

	UC	LC	UC/LC		UC	LC	UC/LC		UC	LC	UC/LC
Si	303480	271330	1.1	**Ce**	65.7	53.1	1.2	**Yb**	1.5	2.5	0.60
Al	77440	82120	0.94	**Ni**	18.6	99	0.19	**U**	2.5	0.93	2.7
Fe	30890	57060	0.54	**Nd**	25.9	28.1	0.92	**Br**	1.6	0.28	5.7
Ca	29450	48600	0.61	**La**	32.3	26.8	1.2	**Ge**	1.4	(1.4)	1.0
Na	25670	21200	1.2	**Cu**	14.3	37.4	0.38	**Be**	3.1	1.7	1.8
Mg	13510	31550	0.43	**Co**	11.6	38	0.31	**Mo**	1.4	0.6	2.3
K	28650	13140	2.2	**Y**	20.7	27.2	0.76	**Eu**	0.95	1.6	0.59
Ti	3117	5010	0.62	**Nb**	26	11.3	2.3	**Ta**	1.5	0.84	1.8
C	3240	588	5.5	**Li**	22	13	1.7	**I**	1.4	0.14	10
P	665	872	0.75	**Sc**	7	25.3	0.28	**Ho**	0.62	0.99	0.63
Mn	527	929	0.57	**Ga**	14	17	0.82	**W**	1.4	0.6	2.3
S	953	408	2.3	**Pb**	17	12.5	1.4	**Tb**	0.50	0.81	0.62
Ba	668	568	1.2	**B**	17	5	3.4	**Tl**	0.75	0.26	2.9
F	611	429	1.4	**Th**	10.3	6.6	1.6	**Lu**	0.27	0.43	0.63
Cl	640	278	2.3	**Pr**	6.3	7.4	0.85	**Sb**	0.31	0.30	1.0
Sr	316	352	0.90	**Sm**	4.7	6.0	0.78	**Cd**	0.102	0.101	1.0
Zr	237	165	1.4	**Hf**	5.8	4.0	1.5	**Ag**	0.055	0.080	0.69
Cr	35	228	0.15	**Gd**	2.8	5.4	0.52	**Bi**	0.123	0.037	3.3
V	53	149	0.36	**Dy**	2.9	4.7	0.62	**Se**	0.083	0.170	0.47
Rb	110	41	2.7	**Sn**	2.5	2.1	1.2	**In**	0.061	0.052	1.2
Zn	52	79	0.66	**Cs**	5.8	0.8	7.3	**Hg**	0.056	0.021	2.7
N	83	34	2.4	**As**	2.0	1.3	1.5				

Table 3: Element concentrations (ppm) in the Continental Upper Crust (UC) and Lower Crust (LC) (*Wedepohl* 1995)

1.8 TRACE ELEMENTS EMISSIONS

1.8.1 NATURAL SOURCES

Natural emissions of trace elements derive from mineral aerosol, volcanic activity and sea spray. A smaller (but consistent) amount comes from biogenic activity such as forest fires. In table 4 are shown the mean annual emissions from natural sources for trace elements.

Source	As	Cd	Co	Cu	Cr	Mn	Ni	Pb	Se	V	Zn	Hg
Atmospheric dust	0.24	0.25	4	12	50	425	20	10	0.3	50	25	0.03
Volcanoes	7	0.5	1.4	4	3.9	82	3.8	6.4	0.1	6.9	10	0.03
Forest fires	0.16	0.01	–	0.3	–	–	0.6	0.5	–	–	0.5	0.1
Vegetation	0.26	0.2	–	2.5	–	5	1.6	1.6	–	0.2	10	–
Sea spray	0.14	0.002	–	0.1	–	4	0.04	0.1	–	9	0.02	0.003

Table 4: Calculated worldwide annual emissions of trace elements from major natural source categories to the atmosphere in 10^3 tons (*Pacyna* 1986)

Volcanic emissions contribute for 40-50% of Cd and Hg and 20-40% of Cr, Cu, Ni, Pb, As, Sb emitted from natural sources (*Nriagu* 1979). Active volcanoes, especially explosive ones, can emit huge amount of particles and compounds into the stratosphere, from where these emissions can travel all around the world in some weeks and affect the global climate for years (*Rampino* and *Self* 1993); passive volcanoes too can have feeble (compared to active ones) but stable emissions of gases.

Sea spray, produced by evaporation of braking waves at the ocean surface, it is an important source of some crustal elements: mainly Na and Cl, some mixed cations (K, Na, Mg, and Ca) sulphate and $NaNO_3$ (*Li*, *Anderson* et al. 2003) and of some trace elements such as V and Hg (*Raynaud* 2003).

Next to it there are biogenic activity emissions; biogenic activity can be terrestrial, aquatic, or simply biomass burning like forest fires. Elements like Pb, Cd, Bi, U, Zn, Cu, Mn, Cr and V are present in most plants tissues in ppb or ppm concentrations. Savannahs account for more than 70% of biomass burning, along with forest; when the vegetable tissue burns, it releases into the atmosphere gases and compounds containing also the elements mentioned above. (*Kaufmann*, *Till* et al. 1992). Trace elements can also be contained in complexes formed with compounds emitted into the atmosphere by plants such as particulate carbon, non-methanated hydrocarbons (NMHC) like terpenes and

isoprenes, sulphur compounds (DMS); this is called secondary aerosol. This kind of aerosols is formed by chemical reactions and condensation of atmospheric gases and vapours. "The sulphur cycle dominates the tropospheric secondary aerosol budget. In pre-industrial conditions, it is mainly linked to marine biogenic activity, which produces large amounts of gaseous dimethylsulfide (DMS). Once in the atmosphere, DMS oxidizes primarily into sulphuric acid, ultimately present in the atmosphere in the form of fine aerosol droplets." (*Raynaud* 2003).

1.8.2 ANTHROPOGENIC SOURCES

An emission factor is used to calculate the anthropogenic source strength for atmospheric emissions of different metal compounds; for the fact that most of the attention has been put on SO_2 and NOx emissions, national inventories lack a global assessment for trace elements and metal in particular.

Various authors have tried to make compilations for global metal emissions (*Lantzy* and *Mackenzie* 1979; *Nriagu* 1979; *Weisel* 1981); there is some uncertainty due to the sparsity of the sources. In the table below (*Pacyna* 1986) there is the probably first comparison of trace metals estimated global anthropogenic emissions from natural sources.

Trace metal	Anthropogenic emissions	Natural emissions: median values	Anthropogenic/natural emission ratios
As	5.0	12.0	0.42
Cd	3.0	1.3	2.3
Cr	14.7	44.0	0.33
Cu	25.9	28.0	0.93
Hg	2.2	2.5	0.88
Mn	11.0	317.0	0.03
Mo	2.6	3.0	0.87
Ni	95.3	30.0	3.2
Pb	119.3	12.0	9.9
Sb	1.6	2.4	0.67
Se	4.6	9.3	0.49
V	240.0	28.0	8.6
Zn	57.0	45.0	1.3

Table 5: A comparison of estimated global anthropogenic emissions of trace metals in the mid-1990s with emissions from natural sources (emissions in 10^3 tonnes/y) (*Pacyna* and *Pacyna* 2001)

In table 5 (*Pacyna* and *Pacyna* 2001) is shown a comparison of estimated global anthropogenic emissions of trace metals in the mid-1990s with emissions from natural sources; it is easy to see how the anthropogenic emission often match, if not exceed, the natural emissions. The fact that this is an average global esteem must be taken into account: this means that in most populated areas (the most sensible areas) it is likely that the anthropogenic emissions greatly exceed the natural ones.

In table 6 (*Pacyna* and *Pacyna* 2001) are reported worldwide emissions of trace metals from major anthropogenic source categories to the atmosphere in the mid-1990s.

Source category	As	Cd	Cr	Cu	Hg	In
Stationary fossil fuel combustion	809	691	10 145	7 081	1 475	
Vehicular traffic						
Non-ferrous metal production	3 457	2 171	—	18 071	164	45
Iron and steel production	353	64	2 825	142	29	—
Cement production	268	17	1 335	—	133	—
Waste disposal	124	40	425	621	109	—
Other					325[a]	
Total	5 011	2 983	14 730	25 915	2 235	45
1983 emission[b]	18 820	7 570	30 480	35 370	3 560	25

Mn	Mo	Ni	Pb	Sb	Se	Sn	Tl	V	Zn
9 417	2 642	86 110	11 690	730	4 101	3 517	1 824	240 084	9 417
			88 739						
59	—	8 878	14 815	552	466	319	—	77	40 872
1 060	—	36	2 926	7	7	—	—	71	2 118
—	—	134	268	—	3	—	—	—	2 670
511	—	129	821	272	24	115	—	23	1 933
11 047	2 642	95 287	119 259	1 561	4 601	3 951	1 824	240 255	57 010
38 270	3 270	55 650	332 350	3 510	3 510	3 790	5 140	86 000	131 880

Table 6: Worldwide emissions of trace metals from major anthropogenic source categories to the atmosphere in the mid-1990s (in tonnes/year) (*Pacyna* and *Pacyna* 2001)

a – emission of Hg from gold production

b – Nriagu and Pacyna (1988)

1.8.3 EUROPEAN TRACE ELEMENTS EMISSION INVENTORIES

As mentioned above, a reference point to which compare any study on polluting emissions is the basic need for attribute any useful sense to the results of these studies.

That is why, during the 1970s, after the big economic boom and at the beginning of scientific and public environmental concern, researcher started to gather data all around the continent (actually almost only in the western block until the fall of the wall) to create inventories of various trace elements emissions.

The first important work of this kind was presented in 1979 by Pacyna (*Pacyna* 1984) (*Pacyna*, *Semb* et al. 1984); different emission sources for 15 main trace elements were considered and the data were obtained from statistical estimations of consumption of fuels, ores, et cetera and production of various goods. While this first work was focused on Europe, a second work by Nriagu and Pacyna (Nriagu and Pacyna 1988) constitutes the first worldwide estimation of annual input into soil, water and air of 16 trace elements.

Later, other works from the same group of researchers highlighted the input amounts and sources for more than 15 trace elements, refining the previous estimations and defining some trends by comparison with them (*Pacyna*, *Scholtz* et al. 1995) (*Pacyna* and *Pacyna* 2001).

During the 1990s the UNECE EMEP project (European Monitoring and Evaluation Program) took off; this is a system that gathers the national emissions inventories of several European countries for trace elements emitted by anthropogenic sources (www.emep.int). This project rose from the increasing awareness of health and environmental risks coming from this kind of pollution and the realisation of its trans boundary character.

A partial (Pb, Ni, Cr, As, Cd) comparison between EMEP data and independent sources was performed by a new study of Pacyna (*Pacyna*, *Pacyna* et al. 2007); the study concludes that there is an underestimation in EMEP data, by a factor ranging from 1,4 to 3,0.

More recent studies were performed by Berg and Hovmand (*Berg*, *Aas* et al. 2008) (*Hovmand*, *Kemp* et al. 2008) but these work are focused particularly on the Scandinavian area and therefore less interesting for a whole European point of view. At the present moment the most complete and reliable source available on trace element inputs characterisation remains the various work of Pacyna and the EMEP inventory.

1.9 WINDS, AIR MASSES AND BOUNDARY LAYER

An analysis of wind patterns involving the drilling site area was performed with the HYSPLIT MODEL tool of NOAA (National Oceanic and Atmospheric Administration). Each of the line in the plots in figures 11 and 12 describes a wind pattern directed to colle Gnifetti; the interval between each pattern is 24 hours for a total of 10 days per image. Two periods, January-February and July-August, being averagely the coldest and warmest periods of a year, were chosen as most representative of the winter-summer configurations of the boundary layer. Figure 11 describes the wind patterns for the January-February period 2005: it is clear how in winter the major direction of winds to colle Gnifetti can be tracked back to Atlantic and Central Europe. Germany and France seem to be the two most important source areas for most of the possible particles arriving on the monte Rosa.
Figure 12 instead describes the wind patterns for the period June-August 2005. If compared with the winter interval it is possible to see a partial shift to central-eastern and southern Europe of the wind patterns.
It must be noted that only the 2005 Jan-Feb and Jul-Aug wind patterns were analysed; the year 2005 was chosen because it is the central year of the CG11 time span (1997-2011) but clearly it is only an example and cannot be taken as definitive model for the whole interval.

A simplified meteorology of the western Alps defines SE, SW and W fronts to be the main cause of winter precipitations while convective flow systems are the main cause for summer precipitations (*Kappenberger* 1997).
A key role is played by the boundary layer (BL) that is defined as that part of troposphere in direct contact with soil, influenced by the presence of Earth surface and with a response time to atmospheric forcing that remains within the hour; it has a variable height from the ground and it is calmer and warmer than the free troposphere above. The height of the boundary layer can vary from area to area with season and time: the seasonal inversion shift can range from few tens to thousands of metres. This layer is a barrier difficult to penetrate for any kind of substance emitted at ground level such as combustion particulate as much as soil particulate; these tend to be confined in the BL and almost never pass to the free troposphere.

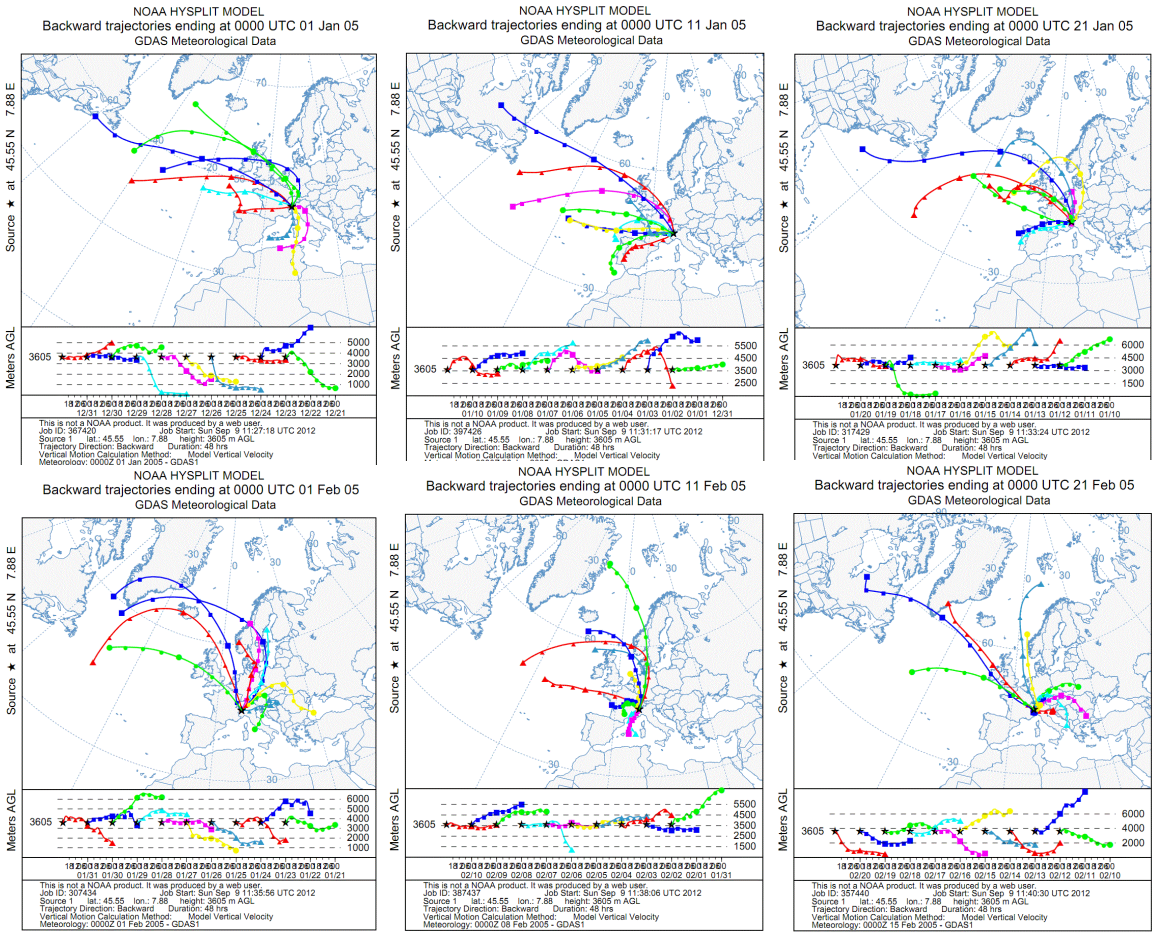

Figure 11: air mass back trajectories (NOAA Ready) reaching Colle Gnifetti during to the period January-February 2005. The back trajectory resolution is 24 hours. Each plot represents a 240 hours series.

The transport and dispersion of low altitude emission sources gases and aerosol are strongly influenced from the various local features of the boundary layer and the dynamics of the temperature inversion. A BL that is relatively low and stable for several days can strongly increase the concentrations of pollutants from anthropogenic source due to relatively small volume in which they are trapped.

On the other hand, especially in summer, when the BL tends to rise, the vertical mixing increases and both the natural and anthropogenic gases and aerosol are free to reach massively higher locations such as, in this case, Colle Gnifetti; they reach high altitudes carried by the winds and included in the precipitation, in fact that the main cause of summer snowfalls are convective storm systems through which the pollutants can move from the bottom of the valleys to glaciers.

There is a thermal inversion immediately above the BL and often even within the BL itself. Temperature ranges are quite wide, as well as humidity ranges; often the winter solar radiation at medium latitudes is not strong enough to warm the ground and so the temperature inversion can linger for several consecutive days,

strictly limiting the transport of any kind of particle to higher sites (*Kappenberger* 1997).

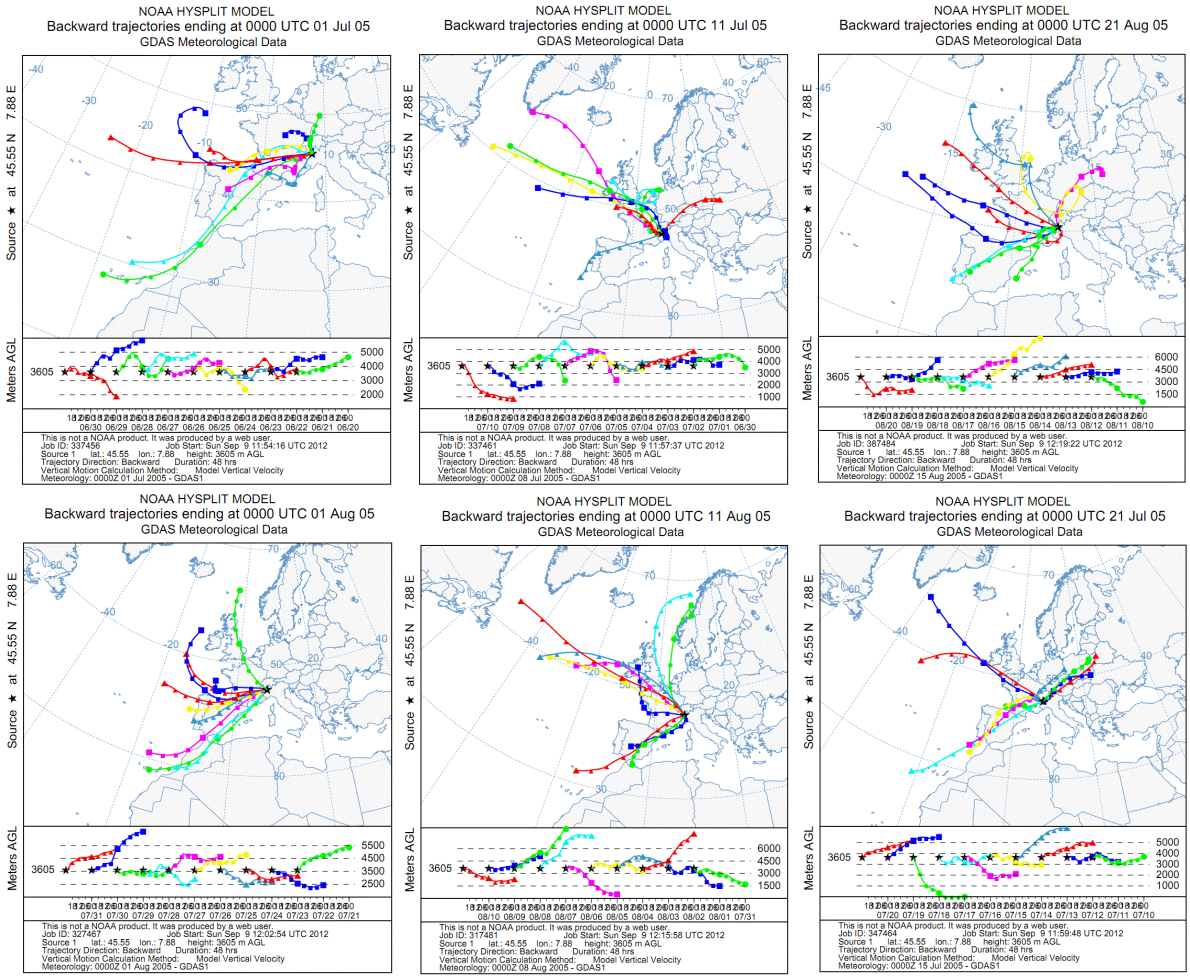

Figure 12: air masses back trajectories (NOAA Ready) reaching Colle Gnifetti during to the period July-August 2005. The back trajectory resolution is 24 h. Each plot represents a 240 hours series.

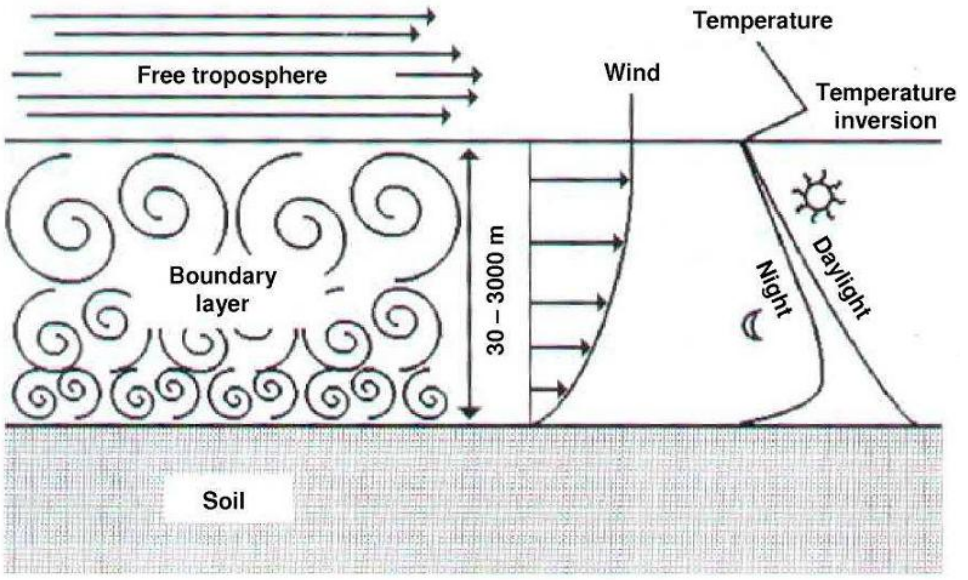

Figure 13: schematic representation of the boundary layer and its temperature inversion

2. INSTRUMENTATION AND METHODS

2.1 INDUCTIVELY COUPLED PLASMA MASS SPECTROMETRY

ICP-MS is a very powerful analytical tool.
It has been on the market since 1983 and it continues to evolve. It is now one of the most used and appreciated instrument for chemical analyses all around the world.
Its stronger points, compared to other spectrometric techniques, can be summarized as:

- relatively brief analysis time coupled with a high reliability
- very low detection limits (around one part per trillion – ppt or even less) for most of the elements of the periodic table
- a wide analytical working range (nine orders of magnitude)
- isotopic capability
- rapid multielement ultratrace analysis capability

The samples, previously adequately prepared, are pumped into a nebulizer, then atomized and ionized through a plasma torch. The non-charged particles are then skimmed off the main ion flux and ions are then divided on the basis of their different mass to charge ratio. A detector transforms these information into energy pulses, gathered from the computer.
The following paragraphs will briefly describe the main components of the ICP-MS systems, focusing on the two instruments used in this study.

2.1.1 SAMPLE INTRODUCTION SYSTEM

The sample is usually in a liquid state. If it is not, it must be prepared as close as possible to a liquid state and great care must be put on the size of the possible particles, to avoid clogging the introduction system.
This is composed of two main components:

- **nebulizer**
- **spray chamber**

of which exist man different designs.
The sample can enter the nebulizer in two ways: directly, because of a negative pressure difference between the two ends of the nebulizer itself or be pumped through a peristaltic pump.

This last system, that is the one adopted in both the instruments used in this work, guarantees a constant flow regardless of the density or the viscosity of the different samples. The peristaltic pump is normally a rotating cylinder composed of many mini-rollers, around which the sampling tube is clipped.
The liquid sample flow is then joined to a carrier gas flow (usually Ar, ≈1l/min) that increase the pressure in the nebulizer and push the sample out of a small orifice, generating a spray. There are various kinds of nebulizer, which can be summarized in:

- concentric
- V-flow
- Babington

Both the Agilent 7500 (called Q2 from now on) and the ThermoFinnigan Element2 (E2 from now on) mount a **concentric nebulizer** one (1-3ml/min).

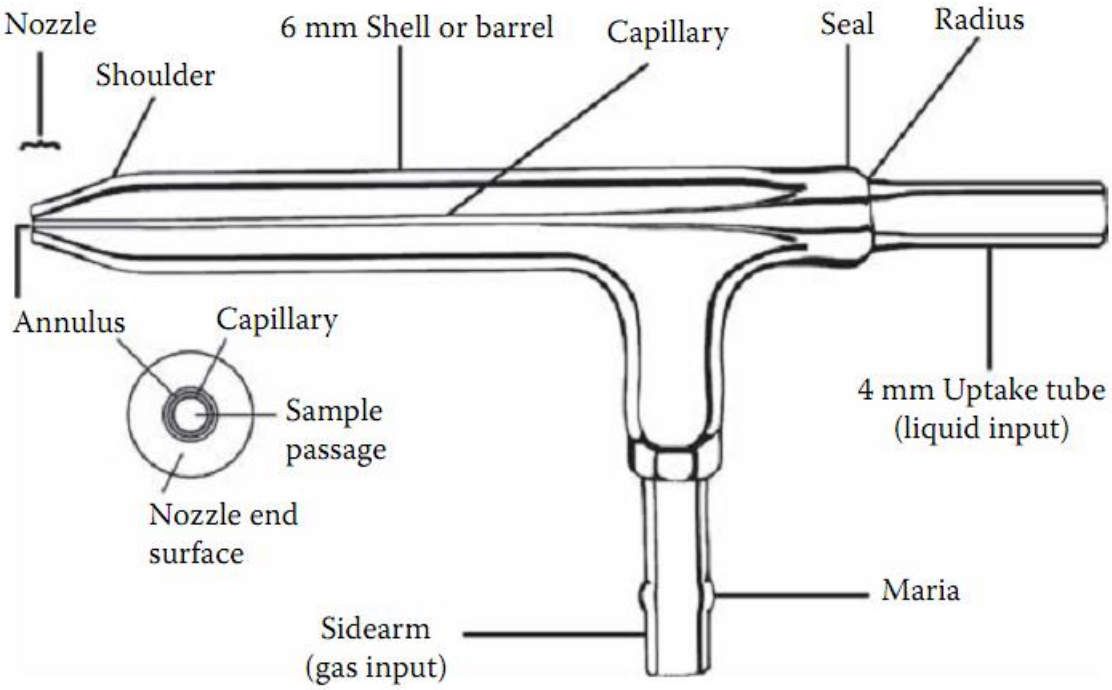

Figure 14: schematics of a concentric nebulizer (courtesy of Meinhard Glass Products)

From the nebulizer the sample is then sprayed into a **spray chamber**, which has two main function: to smooth the possible irregular pulses of the nebulizer and to make a selection of the droplets based on their size.
The selection is normally made by gravity given the difference in weight of the various particles. Only the finest droplets are able to continue their journey to the plasma torch. This because larger droplets could bring too much matter on the ionizing system, overloading it.

Spray chambers usually are externally cooled to minimize the amount of solvent going into the plasma and to ensure a thermal stability of the sample. They can be divided in two main types: **Scott double pass** (Q2) and **cyclonic** (E2).

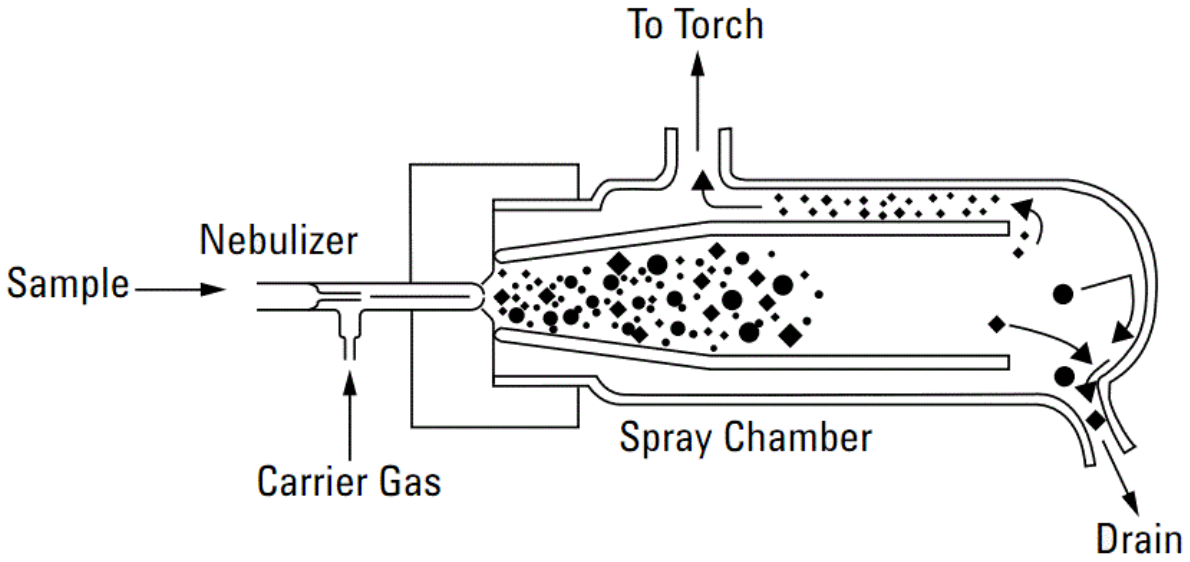

Figure 15: scheme of a Scott double pass spray chamber

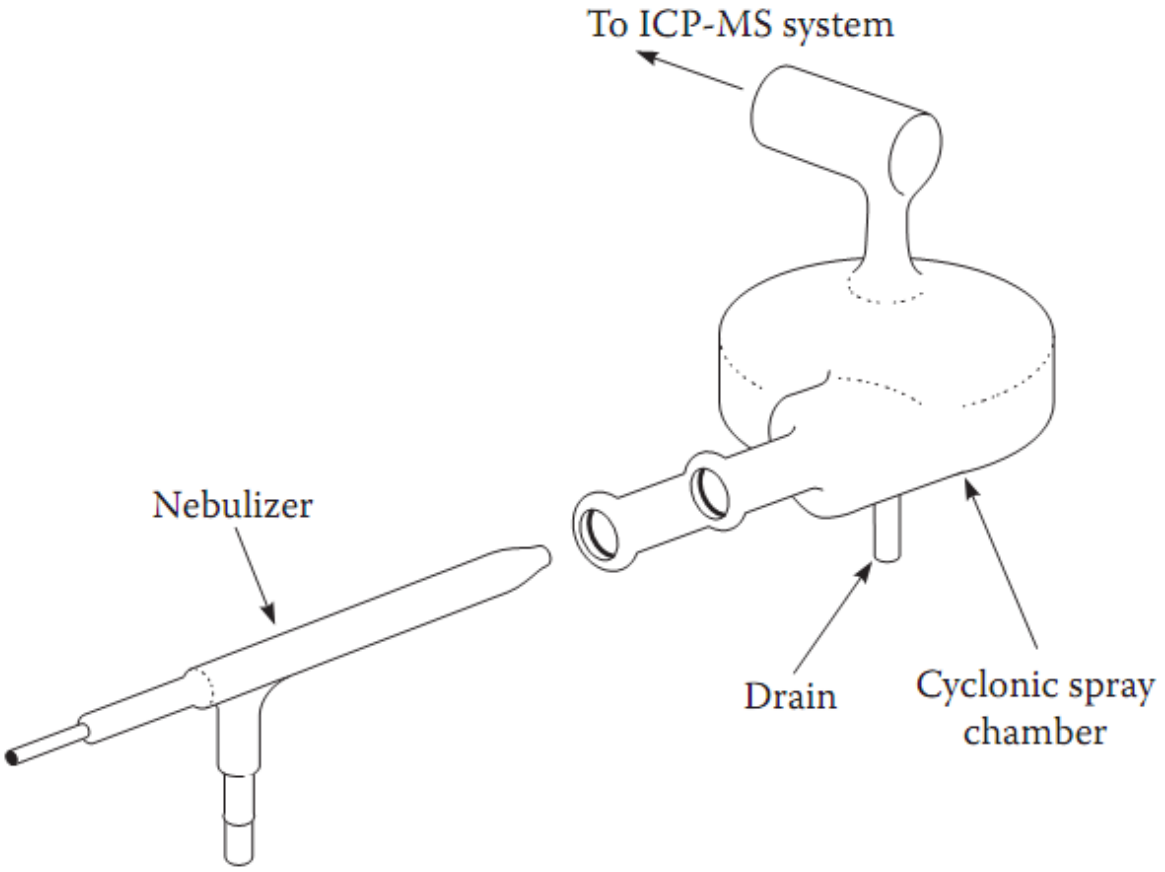

Figure 16: scheme of a cyclonic spray chamber (From S. A. Beres, P. H. Bruckner, and E. R. Denoyer, Atomic Spectroscopy, 15[2], 96–99, 1994.)

2.1.2 PLASMA SOURCE

The plasma source of the instrument is composed of two main parts: a quartz (or other heat resistant materials) concentric pipes torch around which runs a radio frequency coil.

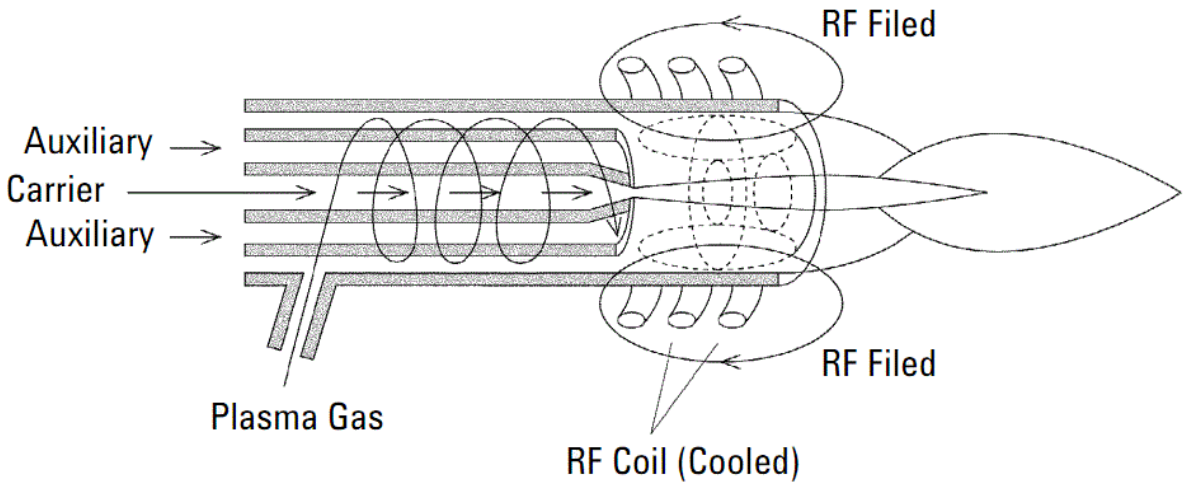

Figure 17: schematics of a plasma source of a ICP-MS

As shown in figure 17 there are three concentric tubes in the torch. In the most external passes a flow of plasma gas, usually Ar at ≈12-17L/min; in the middle tube there is the auxiliary gas flow (still Ar, ≈1L/min), that is used to change the position of the base of the plasma relative to the tube and the injector.

The central tube is where there is the sample injector. The sample passes, already nebulized, among the carrier gas coming from the spray chamber. Around the end the torch is surrounded by the RF coil (usually copper). This coil is powered between 750-1500W and generates an alternating current that oscillates within the coil; the frequencies used are normally 27 or 40 MHz. This oscillation creates a very strong magnetic field. The ionization of the gas is triggered by a high voltage spark: electrons are stripped from some Ar atoms, caught in the field and accelerated, they collide with other Ar atoms, in a cascade process that produces the plasma and also affects whatever is in it (the sample), that gets vaporized, atomized and ionized.

The plasma can reach up to 10000 K but normally remains between 6000 and 8000 K.

2.1.3 INTERFACE REGION

The interface region is quite a critical point of the whole instrument. The sample introduction system and the ICP-torch work at atmospheric pressure while the mass analyser sector requires a vacuum environment.
The flow of ionized gas (and sample) is then forced to pass through two "cones", the only opening to the internal vacuum chamber. The first is called "sampler cone". This is a nickel cone (mounted on a copper water-cooled disk) with an orifice of 1 mm in diameter that allows only a central fraction of the ionized flow to pass to the intermediate region kept at 2-3 Torr by a rotary vane pump, while the rest of the flow is diverted on the sides. The flow has then an expansion due to the pressure gap.

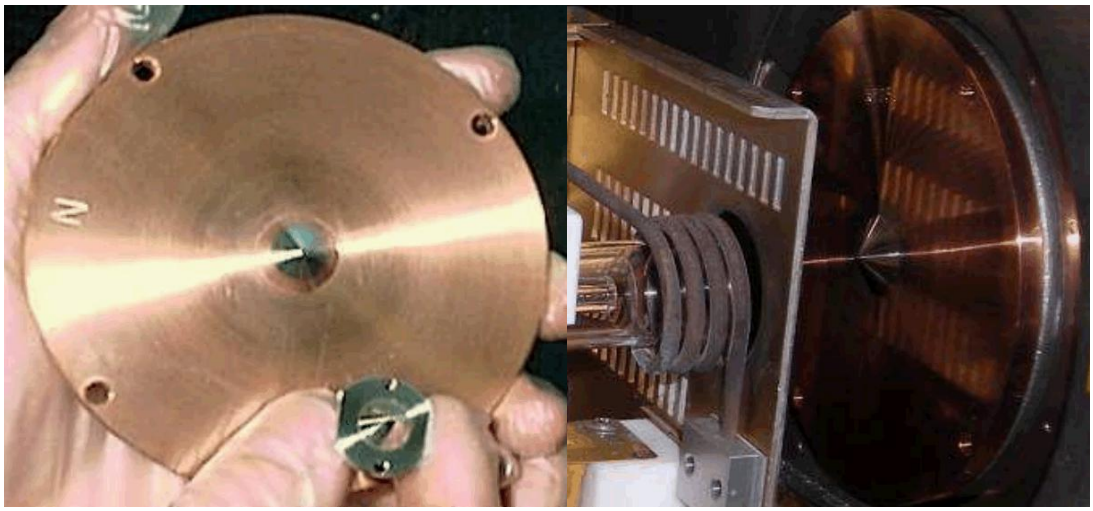

Figure 18: the sampler cone in the copper plate and the skimmer cone (small one)
Figure 19: the ionized flow, originating from the torch, passing through the sampler cone

Then again the flow is forced to pass through a second orifice, the "skimmer cone", that leads to the vacuum area (10^{-3} – 10^{-4} Torr). This cone is sharper and with a smaller orifice than the sampler cone (0,4 mm); it can be Nickel or sometimes Platinum, depending on the analytical necessities. The flow expands (and its density decreases) again. The vacuum is generated and kept by a turbomolecular pump. The effect of this pressure drop is that the electrons, due to their smaller mass, diffuse further than the cations, resulting in a positively charged ion beam.
The whole process is shown in figure 20.

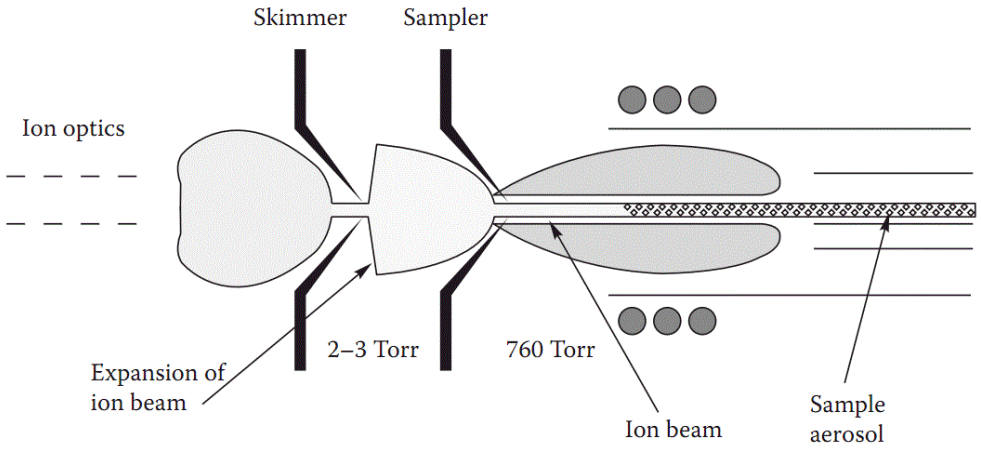

Figure 20: schematics of the interface region

2.1.4 ION LENSES

After the interface region the ion beam enters the vacuum region. Here it encounters a system of electrostatic plates called "ion lenses". The function of these lenses is to separate the positive ions, that will be then analysed, from the other components of the beam such as photons, neutrals and all non-ionized material. To achieve this task the metal plates, that have a small orifice through which the beam will pass, are placed off-axis respect the setting in beam. The whole flow would then be stopped if the plates were not electrified. The electromagnetic field generated deflects only the positive ions into the orifice, thus obtaining an almost pure positive ion beam and leaving all the interfering material behind.

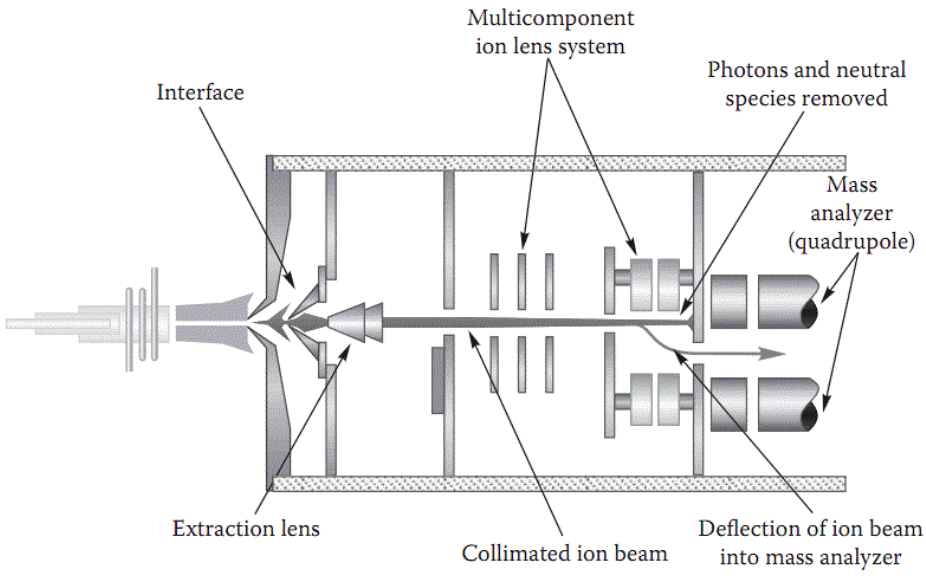

Figure 21: schematics of the ion lenses system

Designs can differ among different instruments but the principle remains the same.

2.1.5 COLLISION/REACTION CELL

After the ion optics normally the beam reaches into the mass analyser. However, in some instruments (among which the Q2) there is another component in between: a collision/reaction cell. The main task of this device is to reduce further the various kinds of interference and to do so it acts directly on the ion beam working in three main modalities such as neutral mode, collision mode and reaction mode.

It is composed of in a stainless steel vessel that contains 4, 6 or 8 rods (quadrupole, hexapole or octopole) that operate in a RF mode, which are used to focus the ion beam. The whole cell is pressurized with a gas (the collision or reaction gas) coming from a conduit. In the Q2 we have a octopole and He/H_2 collision/reaction gases.

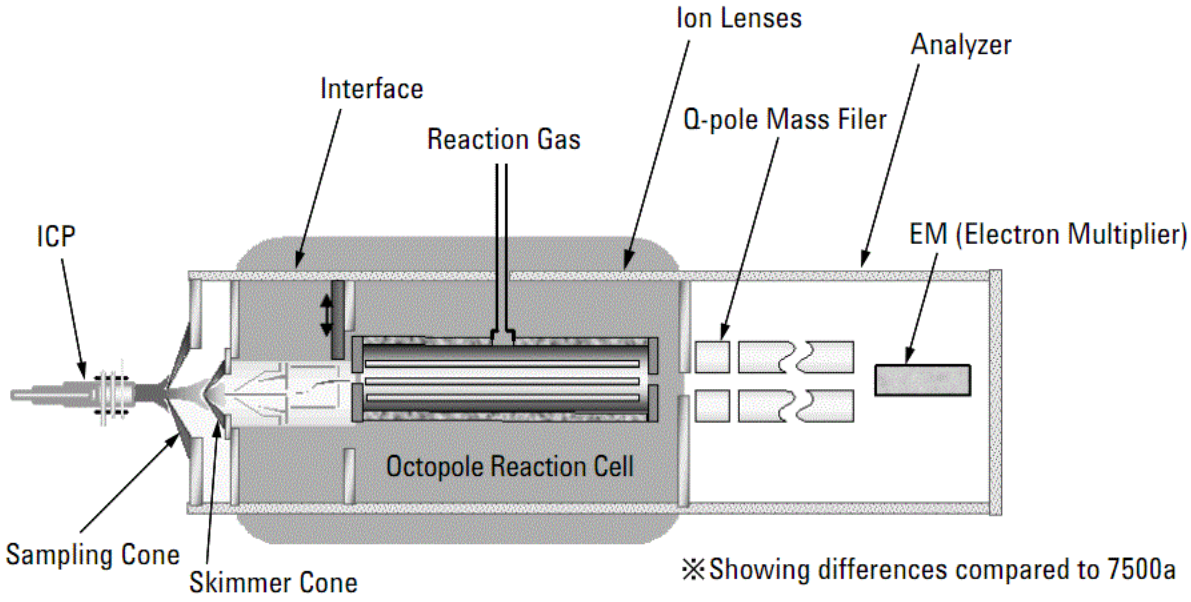

Figure 22: position of the collision/reaction cell

Various processes can happen in a collision/reaction cell. The molecule of the gas can collide and slow down only (or almost only) the interfering molecules or can react only with them to create a heavier (and slower) compound that will not exit the cell, or again can modify the status of the ion avoiding interference of isotope of different elements but with identical mass number and so on. Some of these processes are listed below.

- Charge/electron transfer
  (e.g. $H_2 + {}^{40}Ar^+ \rightarrow Ar + H_2+$ while $H_2 + {}^{40}Ca^+ \rightarrow {}^{40}Ca^+ + H_2$ – no reaction)
- Proton transfer
- Hydrogen atom transfer
- Molecular association reaction
- Collisional fragmentation
- Collisional retardation
- Collisional focusing

Of course the modality to use (collision or reaction) and the choice of the gas will always depend on the kind of analyte in exam and the kind of interference to minimize, lowering the detection limit for that species.
It is important to point out that the use of the collision/reaction cell, especially in collision mode, eliminates most of the interference but, on the other hand, also the analyte signal will be reduced.

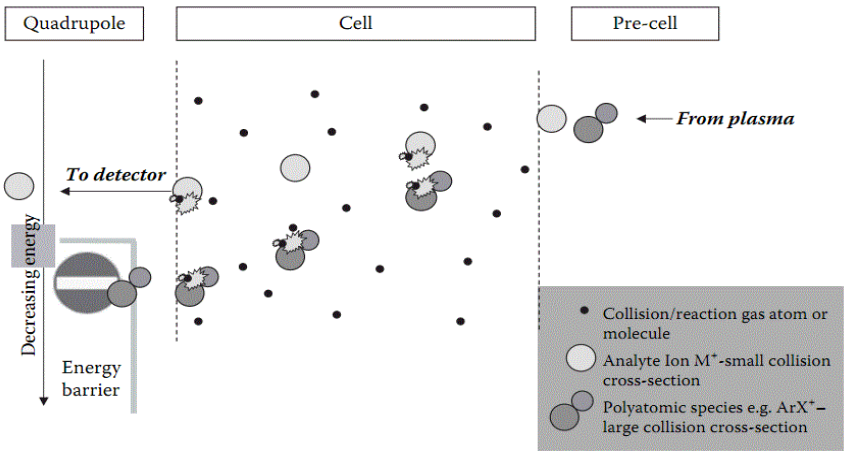

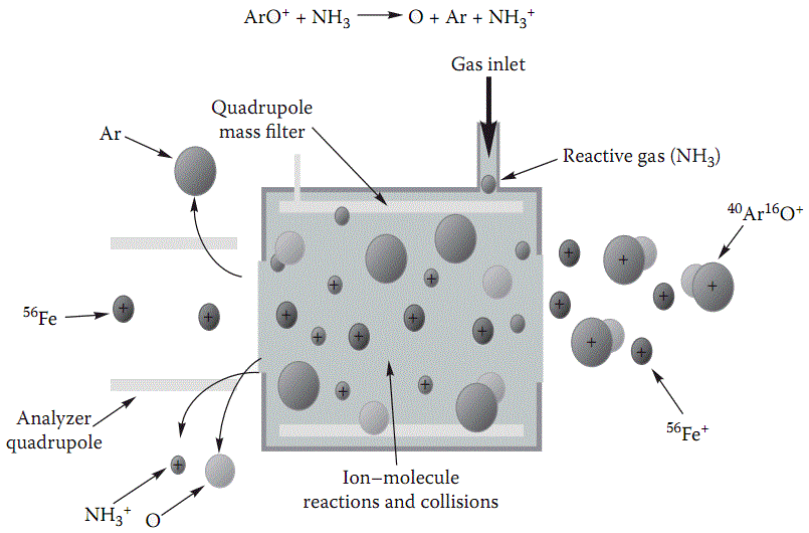

Figures 23 and 24: example of collision and reaction modes

2.1.6 MASS ANALYSER

There are essentially four types of mass analysers: quadrupole mass filter, double focusing sector field, time-of-flight and collision-reaction cell. Each has strong and weak points, depending on the main purpose for which the instrument is used. Here will be briefly described the quadrupole system (Q2) and the sector-field (E2).

2.1.6 QUADRUPOLE MASS FILTER

A quadrupole is a mass filtering device composed of four parallel metal rods through which pass AC and DC at RF. AC is positive and out of phase for the two pairs of rods while the DC is alternatively negative and positive for the two pairs. This creates a dynamic hyperbolic electric field that must be travelled across by the ion beam to reach the detector. Only the ions that will have a stable trajectory through the quadrupole will be detected and that depends on their interaction with the generated field. This process is very selective because each ion has a different mass to charge ratio and so most of the ions will have an unstable trajectory, except one or two, given a particular voltage setting of the rods. Furthermore the quadrupole voltages can be adjusted very quickly to scan a mass range of 0-300 amu in a tenth of a second even if normally the instrument takes a couple of minutes to scan for 20-25 elements in duplicate, for a higher accuracy.

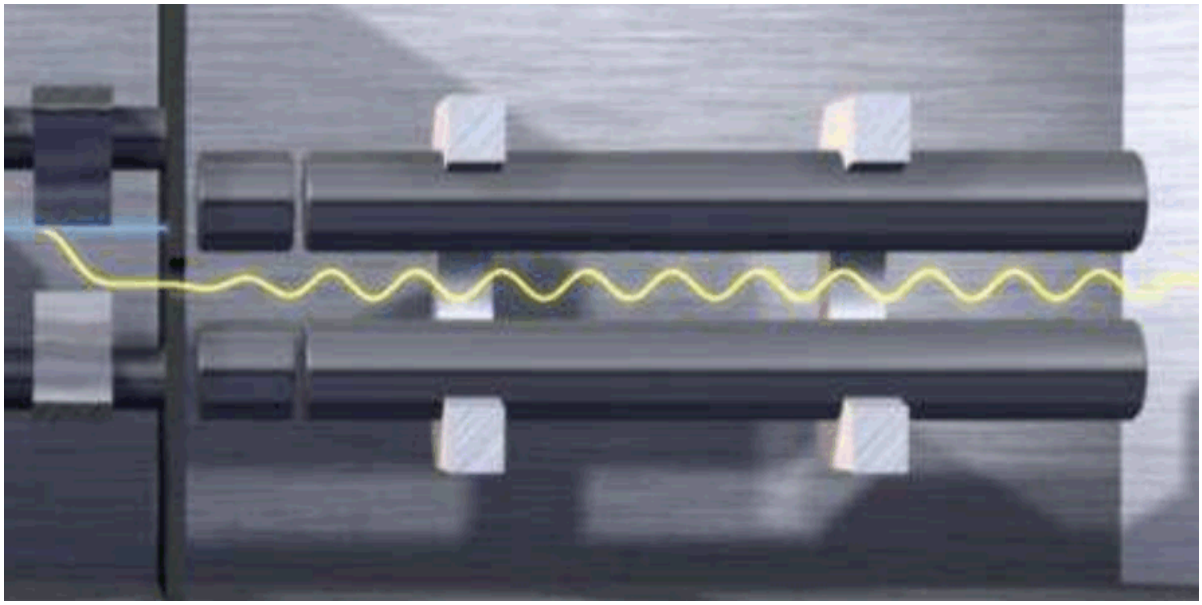

Figure 25: graphical representation of a quadrupole mass analyser

2.1.7 SECTOR-FIELD

Two devices compose the sector field mass analyser: an electromagnet or magnetic sector (MS) and an electrostatic sector (ES), often but not always in this order.

The MS is an analyser that can detect different ions on the base of the different curve trajectories they will have in the magnetic field given their mass to charge ratio. Ions from the oncoming beam have a certain kinetic energy $1/2mv^2=eV$. The analyser magnetic field of intensity H acts on the ions as a force $F = Hev$ that changes their trajectory in a curve with radius r so $Hev = mv^2/r$. From these three equations come the relation between the curvature radius and the mass of the ion $m/e = H^2r^2/2V$.

By itself the MS is a low-resolution analyser but its resolution increases when coupled with the electrostatic sector in the double focusing sector field.

The ES is a device used to divide ions with different kinetic energy. It is not a mass analyser because it does not separate ions on the basis of their mass to charge ratio (what the MS does). The ions pass between two charged curved condenser plates: the ions with the right amount of kinetic energy are able to pass while the others hit one of the two sides of the device and stop there.

The double focusing sector field is not so common as the quadrupole system but its resolution is definitely higher.

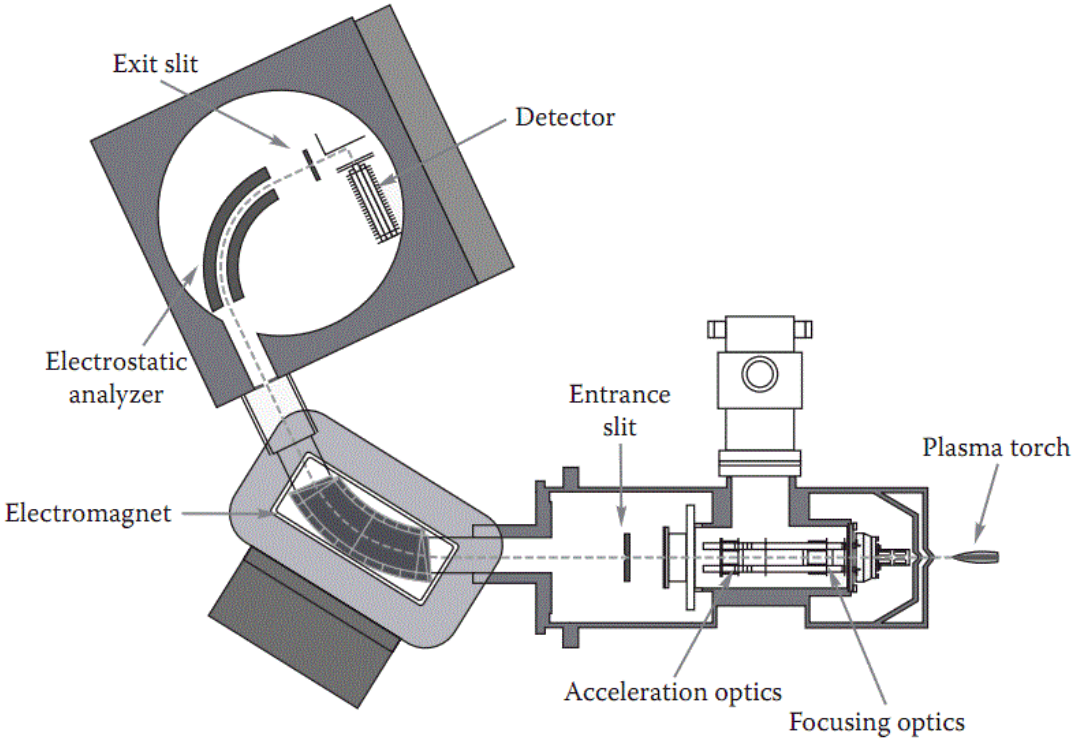

Figure 26: schematics of a double focusing sector field analyser

2.1.8 DETECTOR

Once the target ions have been separated in the mass analyser they have to be counted and this is the task of the detector. In most ICP-MS the detectors are electron multiplier.

An EM still operates in the vacuum area of the instrument and can be composed by a sequence of dynodes or a continuous dynode, charged negatively, where the positive ions strike and release some electrons. These electrons will strike other dynodes (or another part of the dynode) and release other electrons in a cascade process. The result is a discrete pulse of millions of electrons generated by a single charged ion.

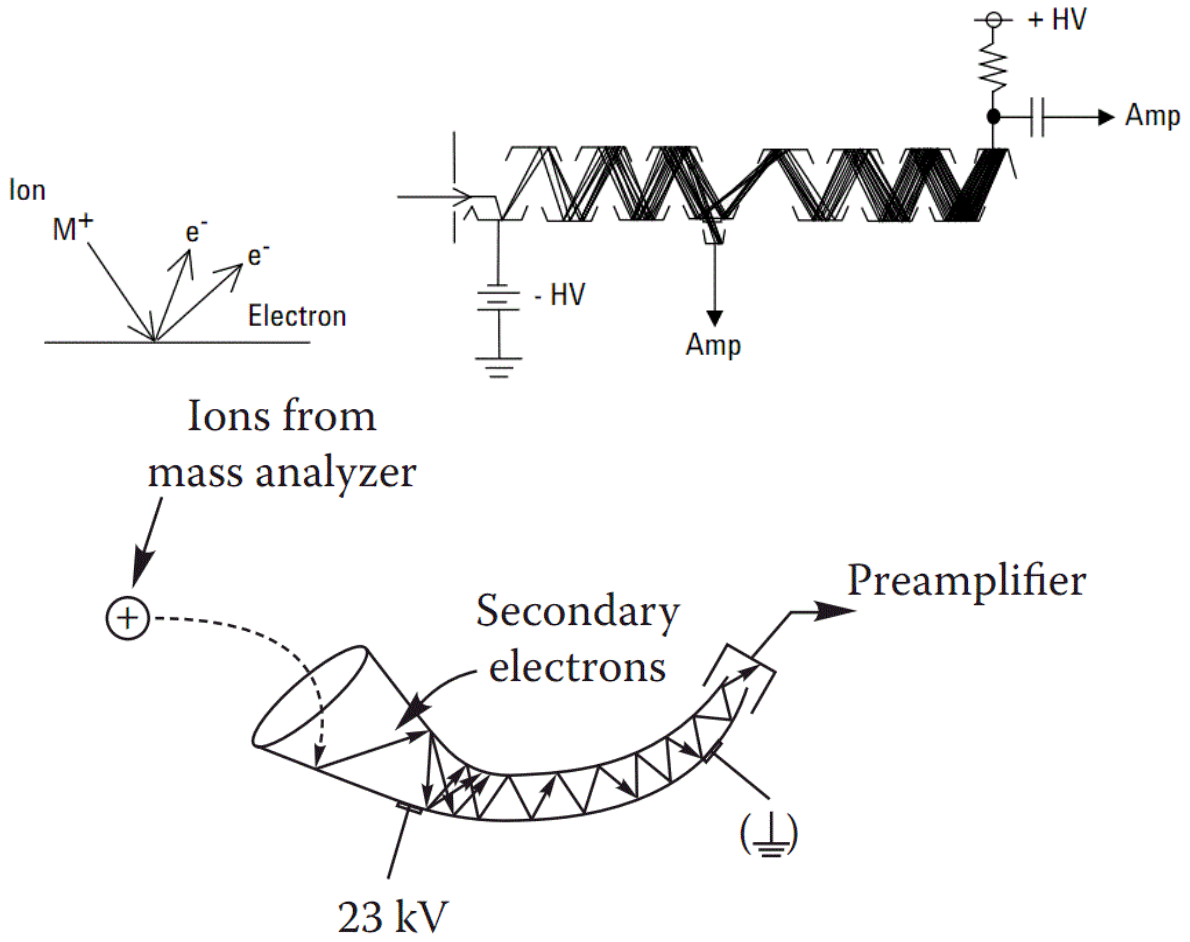

Figure 27: schematics of the functioning of an ion detector

The pulse is then collect by a preamplifier and send to a digital electronic counter that will count only values over a certain threshold to discriminate between real ion pulses and background noise. The accepted pulses are then processed by the data system of the instrument.

2.1.9 RESOLUTION

The resolving power of a ICP-MS is defined as the capacity to distinguish two contiguous peaks of a mass spectrum. IUPAC defines the resolution R, necessary to distinguish between a peak A and a peak B, as

R = M/ΔM where **M** is the mass to charge ratio of peak A and **ΔM** is the difference between the two m/z values of peak A and B.

There are various ways to define the smallest gap that allows distinguishing two different ions; the two most common methods for MS are:

- **Peak width** – where the value ΔM is given by the width of the peak measured at a specific fraction of its height (for example 0,5%, 5%, 10%, 50%)
- **Valley height** – where ΔM is defined as the interval between two peaks of the same intensity where the valley height is lower than a certain fraction of the height of the whole peak

Q2 (as most quadrupoles) is able to distinguish integer masses (R ≈ 300 - 400) while the E2 (and sector fields in general) can reach up to an R ≈ 10000, that make possible to tell apart even different analytes with the same nominal mass (that is why there is no need for the universal cell).

2.1.10 INTERFERENCES

ICP-MS suffers, as other analytical techniques, from various interference issues. These can be divided in non-spectral and spectral interferences.

The first kind, called also "matrix effect" it is pretty common but can be fairly diminished by diluting the sample, changing the sample introduction system or using an appropriate internal standard.

More serious are the spectral overlaps; these kind happens when a ionic species in the plasma has the same m/z value of an analyte ion. There are four categories of these interferences: isobaric ions, polyatomic ions and refractory oxide ions.

Isobaric species are two elements which isotopes have essentially the same mass; in case of quadrupoles the isobaric species are the one which isotopes differ of less than one unit; for DF-SF the difference in mass gets reduced to fraction of units. This kind of overlap often occurs with the most abundant isotope of a species and so with the most sensible; it can be solved taking in account that there are fixed ratio of abundance between the various isotopes of

the same species (for example: $^{40}Ca^{+}$≈97% $^{41}Ca^{+}$≈2,1%) and measuring the relative peaks. With the correct abundance table, nowadays every ICP-MS software can execute the adequate corrections.

Polyatomic interferences occur when the interaction between the analyte and the matrix (or atmosphere) species produce polyatomic ions; some of these can overlap to the analyte peaks having the same m/z ratio and need a good blank to be distinguished or, in worse cases the analyser is compelled to use another isotope of the analyte.

Polyatomic Species	Interfered Analyte
$^{12}C^{15}N$, $^{12}C^{14}NH$	^{27}Al
$^{38}Ar^{1}H$	^{39}K
^{40}Ar	^{40}Ca
$^{35}Cl^{16}O$	^{51}V
$^{35}Cl^{16}O^{1}H$	^{52}Cr
$^{36}Ar^{16}O$	^{52}Cr
$^{40}Ar^{12}C$	^{52}Cr
$^{38}Ar^{16}O^{1}H$	^{55}Mn
$^{40}Ar^{16}O$	^{56}Fe
$^{40}Ar^{16}O^{1}H$	^{57}Fe
$^{40}Ar^{35}Cl$	^{75}As
ArAr	^{80}Se

Table 7: most common polyatomic interferences

The most serious interference occurring in ICP-MS is due to oxide and hydroxide formed with the analyte itself interacting with the matrix components, the solvent and plasma gases. Their peaks tend to overlap with the peaks of the analyte. Most of the research has been aimed to reduce the oxide and hydroxide interferences, given that their formation depends on some experimental variables such as the speed of the injecting flow, the RF power, the distance between the sampler and the skimmer cone in the interface, the size of their orifice, the plasma gas composition, the elimination of oxygen and the solvent removing process. All these variables can be adjusted prior to each analysis.

2.2 INSTRUMENT SETTING UP

2.2.1 ICP-QMS (Q2)

The quadrupole mass spectrometer used is a Agilent 7500, with a concentric nebulizer and a Scott double pass spray chamber, water cooled at 2°, while the plasma operated at 1500W. Quadrupole focus and bias and octopole parameters varied for the different configuration of the universal cell (without, reaction mode with H_2 and collision mode with He).

PARAMETER	NO REACTION	H_2	He
PLASMA CONDITIONS			
RF Power	1500 W	1500 W	1500 W
Carrier Gas Flow	1,24 L/min	1,24 L/min	1,24 L/min
Nebulizer Pump	0,1 rps	0,1 rps	0,1 rps
S/C Temp.	2°C	2°C	2°C
ION LENSES			
Extract 1	0 V	0 V	0 V
Extract 2	-155 V	-155 V	-155 V
QP Focus	5 V	-8 V	-10 V
QUADRUPOLE PARAMETERS			
AMU gain	121	121	121
AMU offset	125	125	125
QP bias	-1 V	-16 V	-16 V
OCTOPOLE PARAMETERS			
OctP RF	170 V	180 V	180 V
OctP bias	-6 V	-20 V	-20 V
REACTION CELL			
Reaction mode	OFF	ON	ON
H_2 Gas flow	0 mL/min	2 mL/min	0 mL/min
He Gas flow	0 mL/min	0 mL/min	4 mL/min

Table 8: ICP-QMS (Q2) main setting parameters

The commercial tuning solution used contained Lithium (m/z=7), Yttrium (m/z=89) and Thallium (m/z=205). Cobalt (m/z= 59, used for the tuning in place of Li for the collision/reaction mode) was added to the original solution at the same concentration of the other elements listed above.

2.2.2 ICP-SFMS (E2)

The sector field mass spectrometer used is a Thermo-Finnigan "Element 2", with a concentric nebulizer and a cyclonic spray chamber. The plasma operated at 1400 W. A solution of ^{115}In 1 ppb was used for the tuning process. All the main setting parameters can be found in table 9.

PARAMETER	VALUE
RF Power	1400 W
GAS FLOW	
Cool	16,00 L/min
Auxiliary	0,960 L/min
Sample	0,996 L/min
Additional	0,000 L/min
Additional	0,000 L/min
ION LENSES	
Extraction	-2000,00 V
Focus	-854,0 V
X-deflection	-0,90 V
Y-deflection	-5,43 V
Shape	110,0 V
HIGH RESOLUTION LENSES	
Quad 1	1,86 V
Focus Quad 1	-13,38 V
Quad 2	10,93 V
INTENSITY (Low resolution)	
Conc. [In]	1 ppb
Counts	$2{,}5 \cdot 10^6$ cps

Table 9: ICP-SFMS (E2) main setting parameters

2.3 STATISTICAL ANALYSIS TOOLS

The software used for the analysis is XLSTAT, a statistical integration pack for Microsoft Excel.

The first step was to ask the programme to describe and visualise the raw data sets; this is achieved with the use of boxplots (displaying the median, the 1st and 3rd quartiles, the minimum and maximum values and possible outliers) and histograms of the population distribution.

The two main tools that have been used to analyse the data were Explorative Factorial Analysis (EFA) and Principal Component Analysis (PCA). At a first glance it was clear that both sets of data did not have an acceptable normal distribution (see figure 28A) and so, even if the EFA and PCA tool have already an embedded normalization function, another kind of normalization was attempted. That is why a variable normalization was applied to both the data set; one of the two kinds of standardization used is called "Box Cox" in the XLSTAT package, where it is defined as a transformation "to improve the normality of the sample: XLSTAT accepts a fixed value of lambda, or it can find the value that maximizes the likelihood of the sample, assuming the transformed sample follows a normal distribution". The Lambda (that can be set by the user or searched and optimized by the programme, is an exponent (ranging from -5 to +5) to which all the data should be raised to achieve a transformation into a "normal shape" (see figure 28B).

Actually the Box-Cox does not look exactly for a normal curve but tends to minimize the standard deviation; that is why the resulting datasets should always be tested for normality.

In this study case the box-cox turned out to be enough to achieve a dataset acceptably normalized only for the Q2 high-resolution crustal dataset.

This transformation into a gauss like pattern is the basic condition to obtain, through a following analysis, principal components that are truly independent between each other. The EFA and PCA tools already perform an automatic pre-normalization of the data, but other "manual" standardizations were attempted before the use of EFA and PCA, to compare to different outcomes.

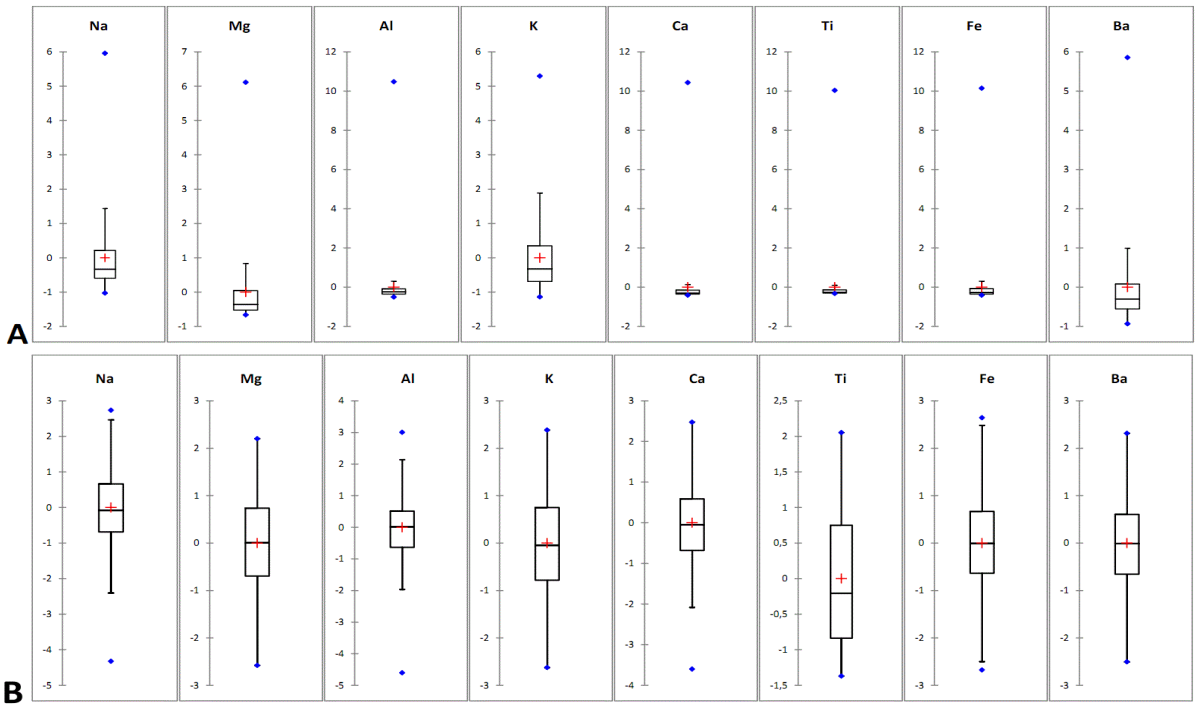

Figure 28: boxplots of the high-resolution crustal elements analysed with the Q2 before (A) and after (B) the normalization with the Box-Cox

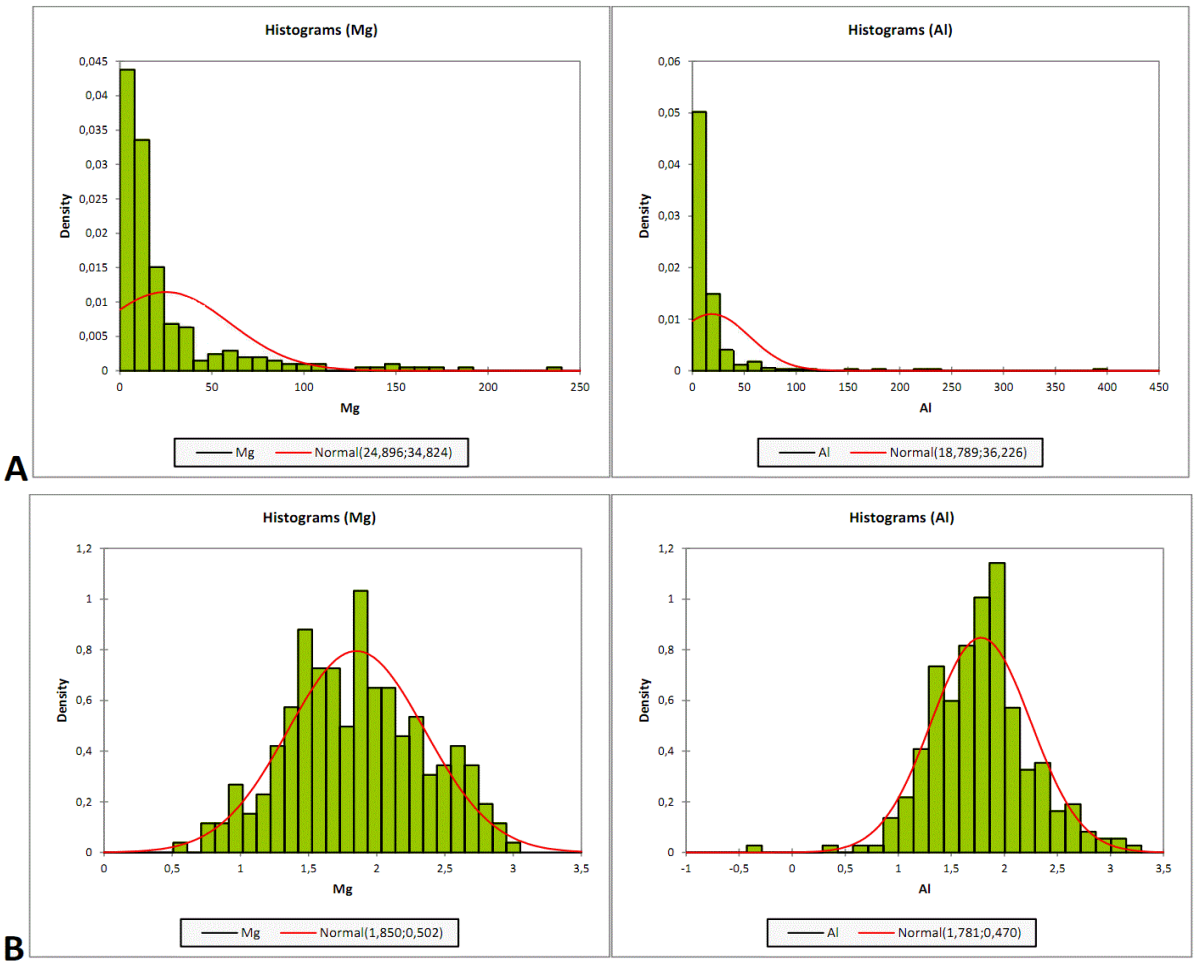

Figure 29: the histograms of two of the elements analysed with the Q2 (Mg-Al) showing the approximation of the normal curve before (A) and after (B) the Box-Cox normalization

Another common standardization technique was used in this case: a “coding by rank” application. This is a simple function of almost every statistic programme that allows ranking all the data of a population with n samples: every entry has a relative rank position determined by its relative value in the same population from 1 to n. This kind of data standardization creates a normalised population but it is not parametric which means that the real values are not mathematically changed in any way but the transformation is temporary and operates only on an internal property already present in the population.
This system was used on both the high-resolution crustal dataset (Q2) and the low-resolution trace elements dataset (E2) (while the box-cox was used only in the Q2 dataset because, when applied to the E2 dataset, it clearly led to a useless distribution after the EFA and the PCA were performed and was therefore rejected).

2.3.1 PRINCIPAL COMPONENT ANALYSIS (PCA) AND EXPLORATIVE FACTORIAL ANALYSIS (EFA)

When dealing with a lot of measurements and variables and a clear graphical representation is not available, it could be difficult to perceive immediately the information stored in the data. That is why we must rely on particular statistic tools when dealing with high dimension datasets; Explorative Factorial Analysis and Principal Component Analysis are multivariate statistical technique that allow to simplify the visualization of results and obtain more information from the data.
EFA and PCA are similar but not identical tools. Their main differences rely on a different approach to the “inherent error” of the measurement (which EFA takes into account while PCA does not) and to the fact that EFA assumes that there is an underlying causal relation between the variables while PCA it is only a variable reduction technique.
"*Calculations for both PCA and EFA involve matrix algebra as well as matrices of Eigen vectors and Eigen values. Any explanation of this would be quite involved and not particularly enlightening for most readers of this column, so suffice it to say that both PCA and EFA depend on calculating and using matrices of Eigen vectors and values in conjunction with a matrix of the correlation coefficients all of which are based on the variables being studied. The difference between PCA and EFA in*

mathematical terms is found in the values that are put in the diagonal of the correlation matrix. In PCA, 1.00s are put in the diagonal meaning that all of the variance in the matrix is to be accounted for (including variance unique to each variable, variance common among variables, and error variance). That would, therefore, by definition, include all of the variance in the variables. In contrast, in EFA, the communalities are put in the diagonal meaning that only the variance shared with other variables is to be accounted for (excluding variance unique to each variable and error variance). That would, therefore, by definition, include only variance that is common among the variables." (*Brown* 2009)

These tools can identify patterns in the data, the interrelation among the various groups of variables, and express them in a way to highlight similarities and differences.

The starting data are transformed into new variables called "principal components" or "latent variables" which reduce the complexity of the original data matrix, allowing the evaluation of the correlations between the variables while visualising the samples.

A basic condition for EFA and PCA is that the dataset on study must have a sufficient internal correlation (that is why, in the programme, these tool already perform a data standardization by themselves even if sometimes it is better to adjust the data "manually" prior the application of these tools).

The first step is calculating the coefficients of linear correlation between every variable. The second step involves the extraction of the factors: correlation matrix, eigenvectors and eigenvalues; the ratio of each eigenvalue by the sum of m eigenvalues corresponds to a percentage explanation factor of the variance of the standardized data.

The eigenvector with the highest eigenvalue is the "principal component" of the data set; the calculated factors are then arranged according to decreasing importance (the capability to explain the total variance of the original data. Interpretation will be normally based on only the first two or three factors (for PCA) (which explain almost all the possible variance) while the others are disregarded.

The newfound eigenvectors can be then used as orthogonal axis for a new representation in bidimensional plots of the original data, which coordinates have been transformed through the correlation coefficients between variables and corresponding factors.

Another advantage of these techniques is that after the patterns are found, it is possible to compress the data conserving most of it even reducing the number of dimensions involved.

2.3.2 AGGLOMERATIVE HIERARCHICAL CLUSTERING (AHC)

AHC is the third and last statistical tool that was used in this work to analyse the datasets. The AHC first it returns a bar chart with the level of dissimilarity of the possible nodes of observations, then it creates a dendrogram that groups all the different observations on the basis of similarity. The programme recognises the point when dissimilarity starts to be too strong and marks that with a truncation line. All the groupings above that line are to be considered already homogenous.

2.4 PHYSICAL PROPERTIES OF THE CG11 ICE CORE

The core has a diameter of about 80 mm and a length of about 10,8 m. Due to the characteristics of the sampling instrument it has been divided into 21 “tubes” numbered from 1 to 20 (with a 19B). Physical features detectable to a naked-eye analysis were noted on the field and also later, when the core was processed in the laboratory: it was possible to distinguish the various snow/firn sequence (sometimes quite clearly, sometimes not), thick and thin ice lenses (alone or in groups) and dust layers. The only observed dust layer was found at a relative depth of ca. 9,70 m, probably corresponding to the peak of Ca of 1999 (see core profile). A full profile of the CG11 core, derived from these data, can be found in the attachments; of course it has been assumed that, due to the nature of the sampling instrument, there has been a partial loss of material between the tubes. A density/depth profile of the core has been calculated and it is shown in the analysis section.

2.5 SAMPLES PREPARATION - ICE/FIRN CORE PROCESSING

The whole 11 m core was in fact divided into 21 sections named “tubes”; their length ranged approximately from 100 mm to 700 mm. Each of these sections were stored and then processed separately in a cold room at a temperature of -20°C.

The external layers of the tubes had been contaminated during the drilling, cutting and storage processes. That is why a decontamination procedure was needed. When dealing with ice, deionized water rinsing of the external surface is one of the most common method for decontamination but in this case we were dealing with firn and its high porosity make this method counter-productive. The alternative was then to remove mechanically the contaminated layers.

A modified commercial band saw with a stainless steel blade was used to remove the external more contaminated layers and reach the inner core, following the cutting scheme reported in figure 30.

The saw working surface, where the sections are placed to be cut, is a polyethylene worktop; at right angles with it there is an adjustable polyethylene guide. Both the blade and the polyethylene surfaces were thoroughly cleaned with acetone before each use. In addition, polyethylene gloves were used to carry out every procedure.

Each section had a diameter of ca. 80 mm. Two first cuts of 15 mm were used to remove the external contaminated layers, obtaining a section C as in figure.

A following 40 mm cut selected the central section F, from which all the analysed samples were derived. The squared core of section F (section H) was then obtained with another 40 mm cut; **section H** was the one selected for **heavy metals analysis** (and therefore underwent a second decontamination process, described in the next paragraph) through ICP-MS and for Black Carbon analysis through Single Particle Soot Photometer SP2 .

All H cores were then divided, if necessary, in sections not longer than 340 mm, to avoid later problems during chiselling due to their fragility.

The remaining, more external, **section G**, was then cut twice to obtain a 20x20 mm **section L** that would have been analysed for the high-resolution **crustal elements** used for the **dating process**; section L was then divided into 40 mm long parallelepipedic sections.

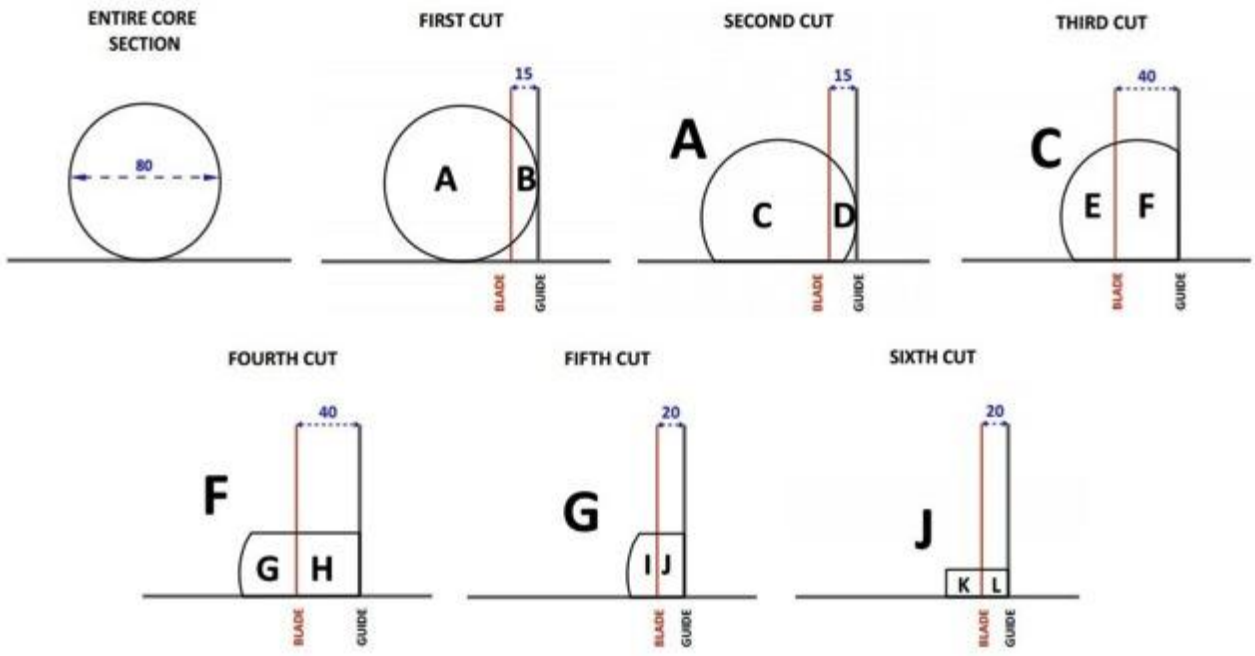

Figure 30: scheme for the CG11 core cutting. Section H is used (after chiselling) for Trace Elements analysis through icp-ms and for Black Carbon analysis through SP2.
Section L is used for dating through Trace Elements by icp-ms at the Ca' Foscari university and through δ18O and δD analysis by SIRMS at the PSI of Villigen (CH)

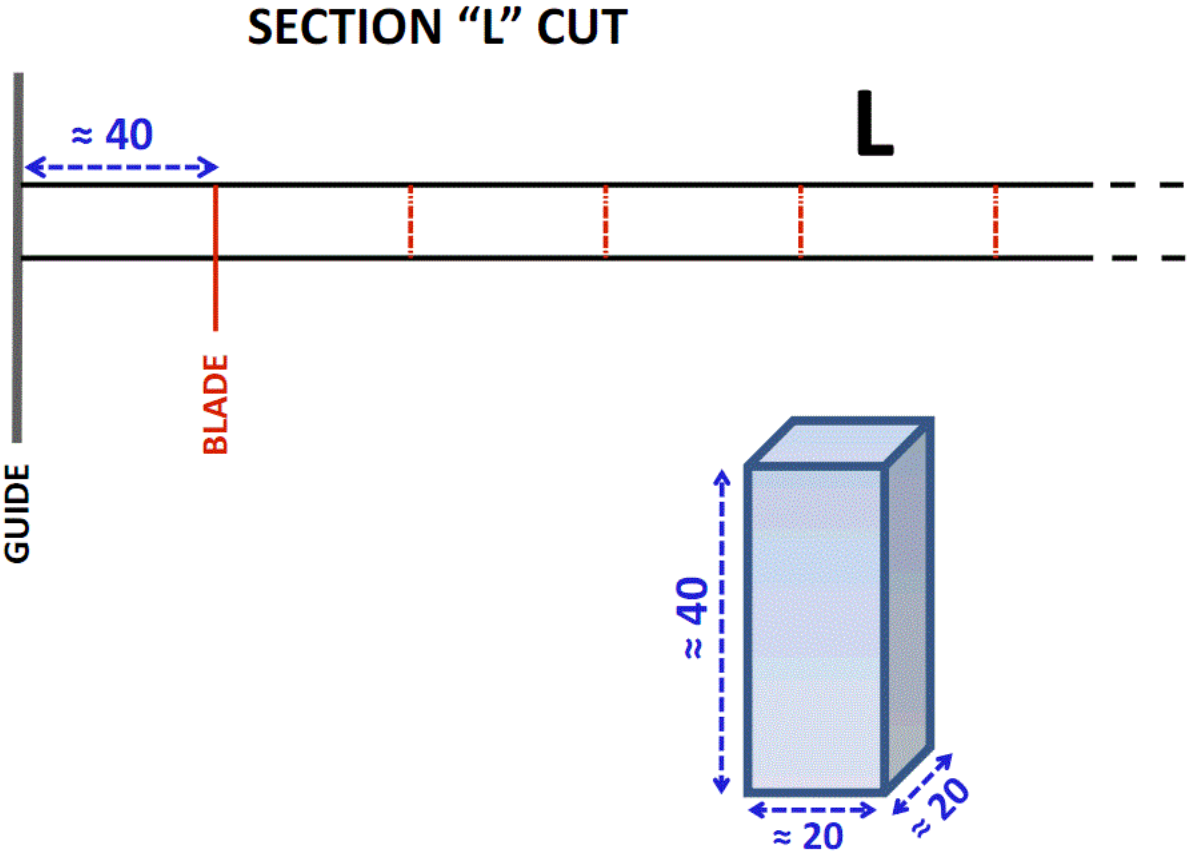

Figure 31: cutting sequence of section L for high resolution - all measures are in mm

2.5.1 CHISELING

All the operations were carried out in the cold room, at -20°C, under a laminar flow bench (class 100) and wearing polyethylene gloves.
Each section derived from section H (in figure 36) was placed into a polyethylene turning lathe with two cylindrical heads. Each head has a 40x40x15 mm square indentation in which the section was inserted.

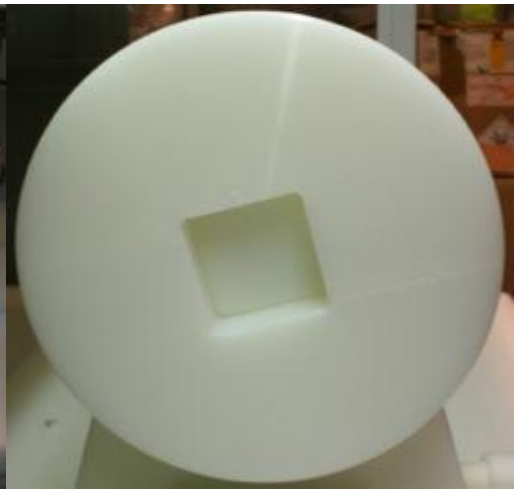

Figure 32: polyethylene turning lathe used to hold and turn the firn sections to chisel
Figure 33: particular of the lathe head with a square indentation to insert the firn section (ca. 1cm deep)

The chiselling process was carried out with ceramic knives (figure 34). Each knife was carefully cleaned with acetone and deionized water prior each use and then placed in a polyethylene bag that had been previously washed with deionized water.
The ceramic knives were used to scratch out the surface layers of the firn section on its four sides; the scratched material was collected in a low density polyethylene scoop (figure 35).

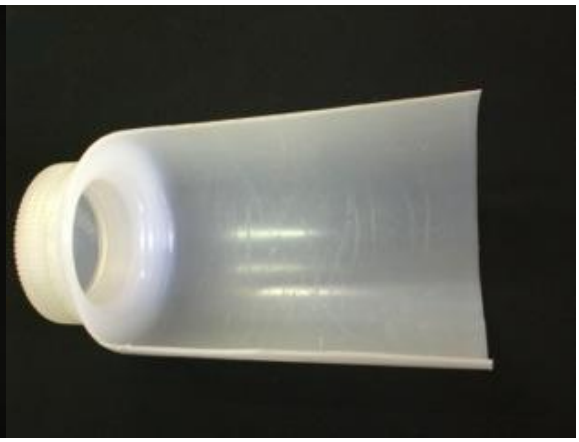

Figure 34: ceramic knives of three different sizes used to chisel the firn
Figure 35: polyethylene scoop used to collect the chiselled firn

Every section was scratched three times, each time with a different knife. The knives and the scoop were used to remove only one external layer each time and then cleaned again with acetone and deionized water before the next use. The final inner core was not collected with the scoop but directly inside the polyethylene bag, avoiding any contact with its surface. The only things that actually touched the core were the 3rd cut knife and the inside of the bag.
At the end of the process we had four samples for each section:

a – 1st layer (the most external)

b – 2nd layer

c – 3rd layer

d – the inner core

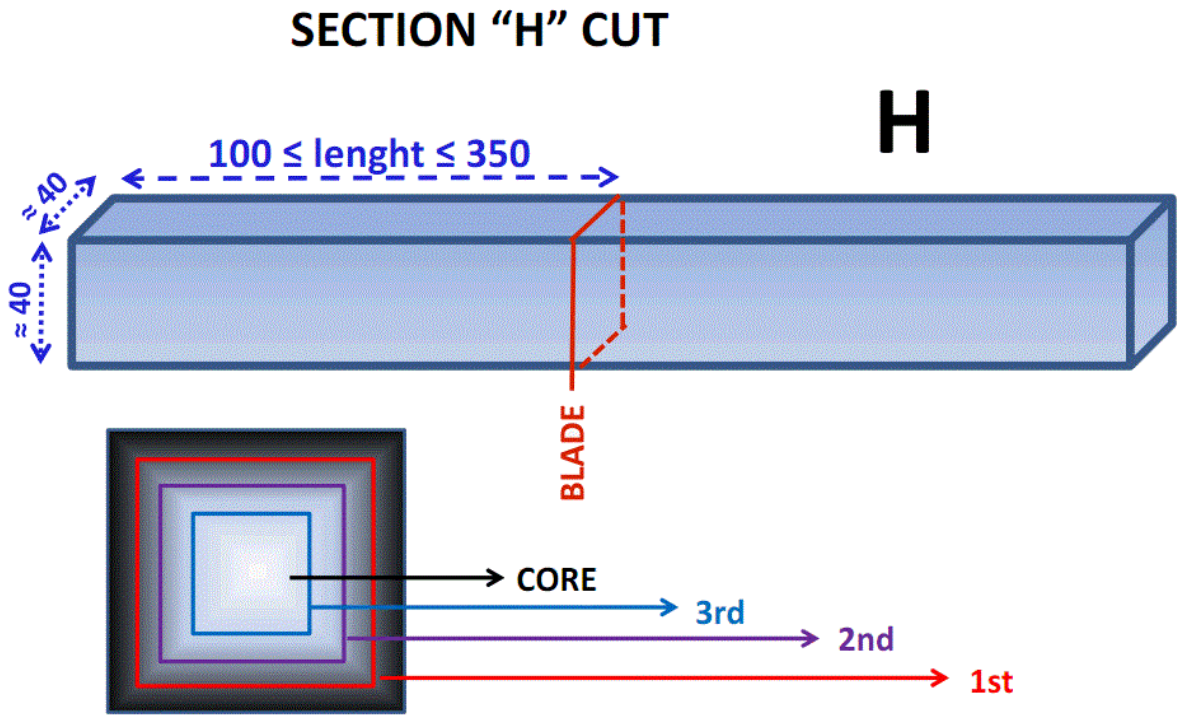

Figure 36: operations sequence for chiselling of section H

All these samples were stored in sealed polyethylene bags and kept frozen in the cold room until the following melting operation.
During this procedure there is a high risk of carrying the contamination from the outer to the inner layers; thus all the removed layers (and not only the inner core) were analysed separately and their values compared to assess the presence of accidental contamination. The use of some procedural blanks was another factor used to better estimate the possible presence of contamination of the inner core and so test the reliability of the whole process.

Due to the nature of the chiselling process, involving the turning lathe with the indentations, the resolution of the analysis cannot be higher than 15-20 cm at maximum, therefore the record obtained is relatively coarse (*Candelone*, *Hong* et al. 1994) (especially when compared with the high-definition (4 cm intervals) crustal profiles used for the dating process.

2.5.2 SAMPLES MELTING

All the melting operations were performed at room temperature (ca. 20°C) in a ppb clean room, in a laminar flow cabinet and wearing polyethylene gloves.
The 20x20x40 mm samples meant for HD crustal elements analysis for the dating process were extracted from their polyethylene bags and placed in polyethylene vials to melt.
The samples obtained from the chiselling of the 40x40 mm sections were instead simply let to melt in their sealed polyethylene bags. The melting water obtained was used to prepare two vials per each sample: one for black carbon analysis and one to be analysed in Venice for TE through ICP-MS. This last sample was acidified at 2% in mass with ultra-pure HNO_3.
Both melting operations and melting water subdivision in vials were achieved in a matter of 5-6 hours. All the samples were then frozen again until the moment of the analysis.

3. RESULTS AND DISCUSSION

3.1 CALIBRATION AND QUALITY CONTROL

3.1.1 ANALYTICAL RANGE AND BLANKS

The raw data of the ICP-SFMS analysis, which were given in counts, had to be translated into concentrations through a calibration procedure. Blanks, CRM and standards were used to achieve the calibration. Given the different order of magnitude of the concentrations of the main crustal elements (Ca, Na, K, Ti, Fe, Al, Mg, Ba), a different set of standards and blanks was used for this group of elements.

Element	Analytical Range (µg/L)	BLANK (counts)	σ BLANK (counts)	SLOPE	σ SLOPE	R^2
Li	0,0005 - 1,5	2477,5	4,8	419624	6048	0,9996
Be	0,001 - 0,15	323,3	6,38	50780	773	0,9993
Rb	0,0005 - 1,5	5422,1	12,56	1289062	16482	0,9990
Sr	0,005 - 8,5	56936,3	4,17	1583444	37312	0,9978
Ag	0,0005 - 0,15	678,1	6,79	389726	4748	0,9994
Sn	0,0005 - 1,5	2827,4	10,34	415210	3252	0,9996
Cs	0,0005 - 0,5	518,5	21,49	1849056	2346	1,0000
Tl	0,0005 - 0,5	333,2	51,74	1170002	7673	0,9998
Pb	0,005 - 8,5	28894,5	10,01	1135788	28106	0,9976
U	0,0005 - 0,5	341,6	46,76	1723613	17618	0,9995
Bi	0,0005 - 0,5	951	6,72	1535570	5908	0,9999
Cd	0,005 - 0,5	1458,9	6,07	184564	17665	0,9820
V	0,001 - 8,5	153,1	20,81	53390	1953	0,9934
Cr	0,001 - 8,5	455,2	7,82	39986	386	0,9994
Mn	0,15 - 8,5	3075,6	3,39	45280	631	0,9994
Co	0,0005 - 1,5	156,9	11,07	67075	3554	0,9862
Ni	0,15 - 8,5	1054,4	3,4	11554	120	0,9998
Cu	0,15 - 8,5	3291,8	6,66	25166	3619	0,9797
Zn	0,001 - 8,5	4784,4	4,57	275	27	0,9902
Ga	0,001 - 1,5	96,2	19,95	36564	430	0,9993
As	0,15 - 1,5	81,1	13,41	165	7	0,9961

Table 10: analytical range, blank level and regression parameters for the calibration of the trace elements analysed through ICP-SFMS

In particular the calibration procedure involved the use of eight standards with concentrations ranging from 0,0005 to 8,5 µg/L for trace elements and heavy metals while for the main crustal elements, six standards, of which only the first

three were used for the ICP-SFMS crustal data calibration, ranging from 7 to 1200 µg/L (see following paragraph).
Zn and As values were later disregarded because their calibration results were completely out of scale compared to the standards and were not satisfactory, even after several adjustments; they were therefore considered unreliable and omitted.

Element	Analytical Range (µg/L)	BLANK (counts)	σ BLANK (counts)	SLOPE	σ SLOPE	R^2
Ba	7 - 120	115588	6	3443574	202657	0,9965
Na	30 - 470	360652	3	30197	454	0,9998
Mg	30 - 470	60769	9	19549	297	0,9998
Ca	70 - 1200	17004	14	1390	20	0,9998
Ti	7 - 120	490	16	3650	353	0,9908
Fe	7 - 120	202122	5	35522	4307	0,9855
Al	7 - 120	294076	2	36740	1726	0,9978
K	30 - 470	18228	12	1821	13	0,9999

Table 11: analytical range, blank level and regression parameters for the calibration of the main crustal elements analysed through ICP-SFMS

Some procedural blanks were also obtained to test the efficacy of the decontamination procedure (par. 2.5): the cleaned knives were briefly rinsed with deionized water, the water passed first to the scoop and then then collected into pre cleaned bags and frozen for some days; the analyses of these blanks were performed along with the other external layers samples (analysed with the Q2). Their values, for every element analysed, were always lower than the one of any other sample, revealing practically no contamination of any kind that could be traced back to the materials and instruments.

3.1.2 STANDARDS AND CERTIFIED REFERENCE MATERIAL (CRM)

CRMs are materials with the values of specific properties (in this case "concentration") that are homogenous and well stabilised so that they can be used for calibration operations or methods evaluation.
CRMs and multistandards are prepared under strictly controlled conditions, ensuring the stability of the concentration values for the indicated length of time; their properties are certified with technically valid procedures, while homogeneity and stability are documented.

The same CRMs and multi standards have been used for both the Q2 and E2 analysis to evaluate the instrumental accuracy

The TMRAIN-95 is a CRM of the National Water Research Institute of Canada; its elemental composition and concentration can be viewed in table 12.

Analyte	Value (µg/L)	Uncertainty (±2 STDs)	E2 values (µg/L)
Al	1,7	± 0,91	3,31
Sb	0,35	± 0,1	
As	1,07	± 0,25	2,34
Ba	0,73	± 0,15	0,36
Be	0,27	± 0,061	0,55
Bi	0,63	± 0,26	0,44
Cd	0,48	± 0,12	0,5
Cr	0,79	± 0,17	0,81
Co	0,22	± 0,037	0,22
Cu	6,2	± 0,93	5,83
Fe	24,2	± 3,64	21,98
Pb	0,29	± 0,093	0,29
Li	0,39	± 0,078	0,32
Mn	6,1	± 0,78	5,80
Mo	0,17	± 0,1	
Ni	0,8	± 0,17	0,77
Se	0,74	± 0,29	
Sr	1,7	± 0,26	1,59
Tl	0,33	± 0,072	0,37
U	0,25	± 0,06	0,3
V	0,64	± 0,12	0,61
Sn	0,77	---	0,62
Ti	0,47	---	0,44
Analyte	**Value (mg/L) (background conc.)**		**E2 values (mg/L)**
Ca	0,66		0,57
Mg	0,17		0,15
Na	0,09		0,07
K	0,04		0,04

Table 12: TMRAIN-95 compositional values table (blue) as defined by the NWRI of Canada compared with experimental values of this study (values highlighted in yellow are not within the established range)

The IMS-102 of the Ultra Scientific Analytical Solutions (www.ultrasci.com) is a multi-standard solution from which the differently diluted trace elements standards were derived. It includes 29 elements (Al, As, Ba, Be, Bi, Cd, Ca, Cs, Cr, Co, Cu, Ga, In, Fe, Pb, Li, Mg, Mn, Ni, K, Rb, Se, Ag, Na, Sr, Tl, U, V, Zn) all at the same concentration value of 10,00 ± 0,05 mg/L).
A series of increasingly diluted standards were prepared starting from IMS-102 and are reported in table 13.

The main crustal elements calibration was referred to a specific series of crustal standards, prepared directly from single elements standard solutions through various dilution steps. Their composition are reported in table 14, all concentrations are in µg/L.

TE STDs	STD7	STD6	STD5	STD4	STD3	STD2	STD1	STD0
IMS-102	8,35969	1,50907	0,43438	0,15264	0,04415	0,00448	0,00090	0,00042
Sn	8,46972	1,52893	0,44010	0,15465	0,04473	0,00453	0,00091	0,00042
Ti	8,56464	1,54607	0,44503	0,15638	0,04523	0,00458	0,00092	0,00043

Table 13: concentrations of the trace elements/heavy metals standards (µg/L)

CRUSTAL STDs	STD6	STD5	STD4	STD3	STD2	STD1
Ca	50486,06	8922,50	3952,50	1180,22	204,90	76,46
Mg	19995,36	3533,82	1565,42	467,43	81,15	30,28
Na	19873,70	3512,32	1555,89	464,59	80,66	30,10
K	19895,82	3516,23	1557,62	465,11	80,75	30,13
Fe	5054,14	893,23	395,68	118,15	20,51	7,65
Al	5076,25	897,14	397,41	118,67	20,60	7,69
Ti	4899,30	865,86	383,56	114,53	19,88	7,42
Ba	5043,08	891,27	394,82	117,89	20,47	7,64

Table 14: concentrations of the main crustal elements standards (µg/L)

3.2 DENSITY PROFILE

The density profile of the CG11 core was obtained in a simple but thorough way: the three dimensions of every parcel of the core derived from the cut of the L section was carefully gauged with a calliper and weighted on a high precision electronic scale; after the volume of each parcel (that measured approximately 40x20x20 mm) was calculated, the density of each parcel was derived.

These density values were then plotted against the corresponding depth values and so the following density/depth profile was obtained. It easy to see how, with highs and lows, the density tends to increase with depth.

Once density and depth were obtained it became possible to calculate the depth in equivalent metres, simply multiplying the first by the second; the equivalent depth of the core resulted in ca. 5,75 m.

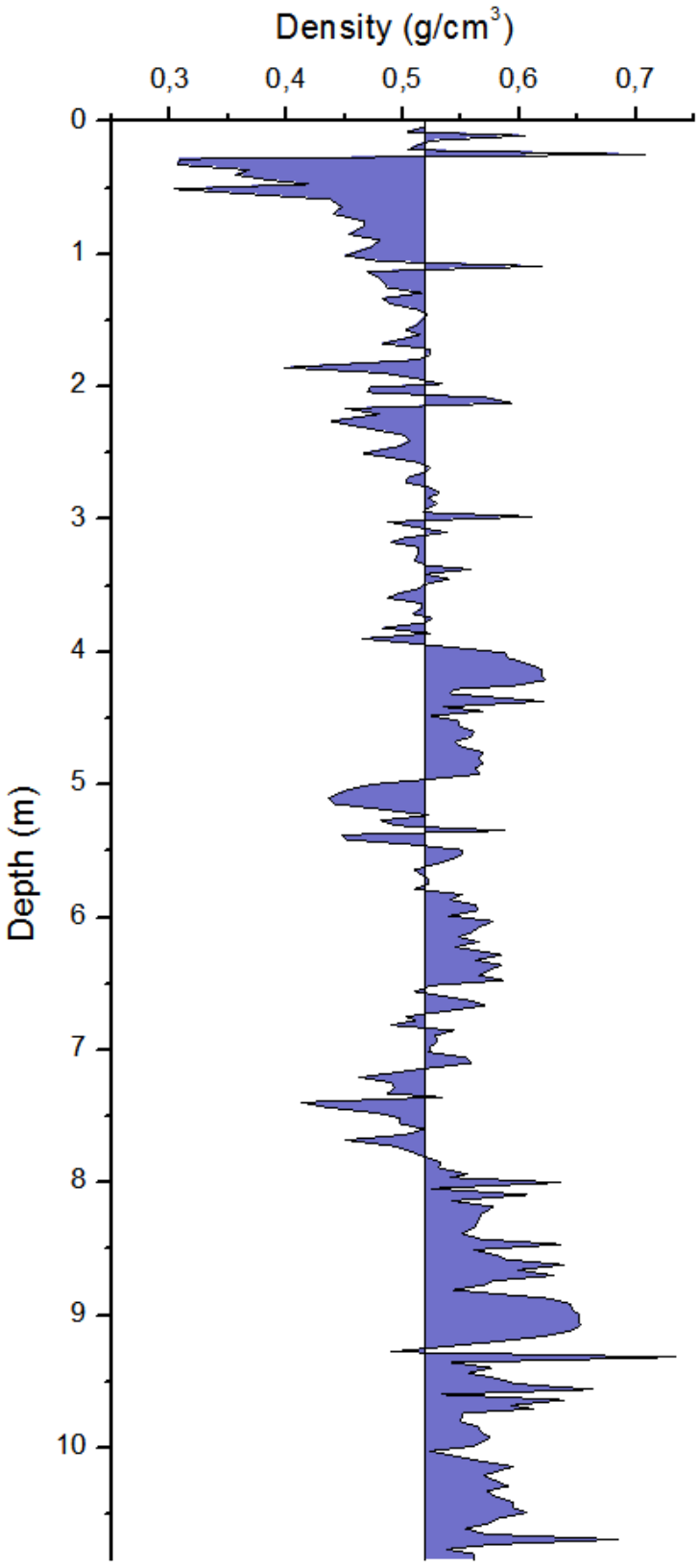

Figure 37: depth/density profile of the CG11 core

3.3 CHARACTER OF THE DATA

Altogether, almost 9000 measurements of various elements were obtained (≈2050 for high resolution crustal elements with Q2: ≈ 5200 for both crustal and trace elements with Q2 in the external layers removed after chiselling and ≈ 1900 for both crustal and trace elements with E2 in the decontaminated cores.

The Q2 analysed the samples scanning for 40 isotopes (^{7}Li, ^{9}Be, ^{23}Na, ^{24}Mg, ^{27}Al, ^{39}K, ^{43}Ca, ^{44}Ca, ^{44}Sc, ^{45}Sc, ^{46}Ti, ^{47}Ti, ^{51}V, ^{52}Cr, ^{53}Cr, ^{55}Mn, ^{56}Fe, ^{57}Fe, ^{57}Co, ^{59}Co, ^{59}Ni, ^{60}Ni, ^{63}Cu, ^{65}Cu, ^{66}Zn, ^{68}Zn, ^{69}Ga, ^{75}As, ^{85}Rb, ^{88}Sr, ^{107}Ag, ^{111}Cd, ^{118}Sn, ^{121}Sb, ^{133}Cs, ^{137}Ba, ^{205}Tl, ^{208}Pb, ^{238}U) using at least two collision/reaction cell configuration with most of them. A lot of these elements had multiple isotopes analysed (ex.: ^{43}Ca and ^{44}Ca) and almost all the isotopes were analysed with the three collision/reaction cell modalities (therefore, for example, Ca had 6 series, 3 modalities per 2 isotopes) Only one isotope series per element was kept. A selection was then operated on the basis of a confrontation between expected CRM-standard values and the experimental obtained concentration, choosing only one isotope per element and only one collision/reaction cell configuration per element, obtaining only one series per element, which was supposed to be the most accurate and representative.

The E2 scanned for almost the same group of isotopes, with only some differences: ^{7}Li, ^{9}Be, ^{23}Na, ^{24}Mg, ^{27}Al, ^{39}K, ^{44}Ca, ^{44}Sc, ^{45}Sc, ^{47}Ti, ^{51}V, ^{52}Cr, ^{55}Mn, ^{56}Fe, ^{59}Co, ^{60}Ni, ^{63}Cu, ^{64}Zn, ^{69}Ga, ^{75}As, ^{85}Rb, ^{88}Sr, ^{107}Ag, ^{111}Cd, ^{118}Sn, ^{121}Sb, ^{138}Ba, ^{205}Tl, ^{208}Pb, ^{209}Bi, ^{238}U.

The concentrations found ranged from ppm (mg/L) to ppt (ng/L); Ca, Na and other crustals were the elements with the highest concentrations whilst Tl, Cs, Ga and other trace elements had the lowest.

Values under detection limits were practically never observed if not in some low concentration standards and blanks.

In the following tables are reported the summary statistics (μg/L) for concentrations of all elements analysed with the Q2 (only high resolution crustal – 260 depth intervals, resolution ranging from 26 to 59 mm) and the E2 (54 depth intervals, resolution ranging from 75 to 330 mm).

A	max	min	mean	1st quart.	median	3rd quart.	STD
Na	679	4,6	104	46	72	125	97
Mg	237	1,7	25	7	12	26	35
Al	398	0,7	19	6	10	16	36
K	210	0,22	50	29	40	60	30
Ca	7157	5,64	275	45	85	179	659
Ti	20	1	1	1	1	1	2
Fe	210	0	8	1	3	7	20
Ba	5,4	0,4	1,2	0,8	0,9	1,2	0,7

B	max	min	mean	1st quart.	median	3rd quart.	STD
Li	1,17	0	0,06	0,01	0,02	0,06	0,16
Be	0,13	0	0,01	0	0	0	0,02
Rb	1,25	0,01	0,15	0,04	0,06	0,13	0,26
Sr	59	0	3	0	1	1	9
Ag	0,08	0	0,01	0	0	0,01	0,01
Sn	0,39	0,01	0,07	0,02	0,03	0,09	0,09
Cs	0,2	0	0,03	0	0,01	0,02	0,04
Ba	19	0	1	0	0	1	3
Tl	0,07	0	0,01	0	0	0,01	0,02
Pb	5,5	0,1	0,8	0,2	0,3	1,1	1,2
U	0,36	0	0,03	0	0,01	0,02	0,07
Bi	0,14	0	0,02	0	0	0,02	0,02
Cd	0,11	0	0,01	0	0	0,01	0,02
Na	916	5	84	15	26	47	174
Mg	1150	0	80	10	20	40	190
Ca	13500	0	700	100	200	300	2000
Ti	16	0	2	0	0	1	3
V	4,8	0,0	0,5	0,1	0,1	0,4	1,0
Cr	3,5	0,0	0,2	0,0	0,1	0,1	0,6
Mn	46	0	4	1	2	3	8
Fe	584	1	49	6	16	35	100
Co	0,87	0	0,1	0,01	0,02	0,08	0,19
Al	811	1	60	6	16	44	134
Ni	2,9	0,0	0,4	0,1	0,2	0,4	0,6
Cu	4,3	0,0	0,7	0,2	0,3	0,7	0,9
Zn	192	2	32	8	12	32	42
Ga	0,56	0	0,04	0	0,01	0,02	0,09
K	275	2	37	17	21	37	48
As	0,79	0,51	0,59	0,55	0,58	0,63	0,06

Table 15: summary statistics for all the analysed elements through ICP-QMS in high resolution (A) and ICP-SFMS in low resolution (B)

The dating of the data series has been carried out through the comparison between the CG11 data and the CG03 data an CG08 data. It is quite clear how the concentration peaks normally mark the late summer period, beginning of the following winter; this is probably due to two factors: the anthropogenic source tend to be relatively stable throughout the year, maybe peaking a bit during winter while natural sources (mainly crustal particulate) tend to be higher in this period of the year. Anyway the behaviour of these signals is strongly regulated by the seasonal changes in the mixing layer properties: the boundary layer is higher in summer and so enhances summer inputs and smoothes winter inputs.
More in detail: anthropogenic emission due to oil and coal combustion for the production (Italy still relies mostly on this kind of sources while Germany and France rely on a little more diversified energy sources) of heat and energy are supposed to be higher in winter, due to the higher demand. On the other hand soil particulate ablation and redeposition is higher during late summer when most of the snow cover has melted and there is more bare surface from which more particulate can be drawn therefore a peak in crustal elements is expected to coincide with late summer (as it was).

3.4 DATING

Dating was achieve through annual layer counting, comparing CG11 high resolution crustal element profiles with the respective profiles of previous studies, which had been already dated through ^{2}H, ^{16}O profiles and annual layer counting.

Two set of data were chosen: the CG03 profile (the work of Gabrieli of which this is a virtual partial continuation) (*Gabrieli* 2008) and the CG08 profile, (a Swiss study still not published).

For all the four crustal elements analysed that the 3 studies have in common (Ca, Na, Mg, K), were compared the concentration/equivalent depth profiles and similarities were highlighted; this served as a starting point for the dating process (an example in figure 38).

The second step was to lay all the concentration tables close to each other to highlight the peaks and the valleys, marking maximum and minimum values and define, with a certain degree of uncertainty, the season and the year of each section.

The final step was to compare data on dust layers (almost none in CG11) and the distribution of ice lenses to confirm and/or refine the dating.

The dating process did not happen to be very difficult for similarities, peaks and valleys were, most of the times quite clear.

The result placed the CG11 core in time interval going from 1997 to 2011 of which only the period 1998-2010 can be study effectively (the first and last year are incomplete).

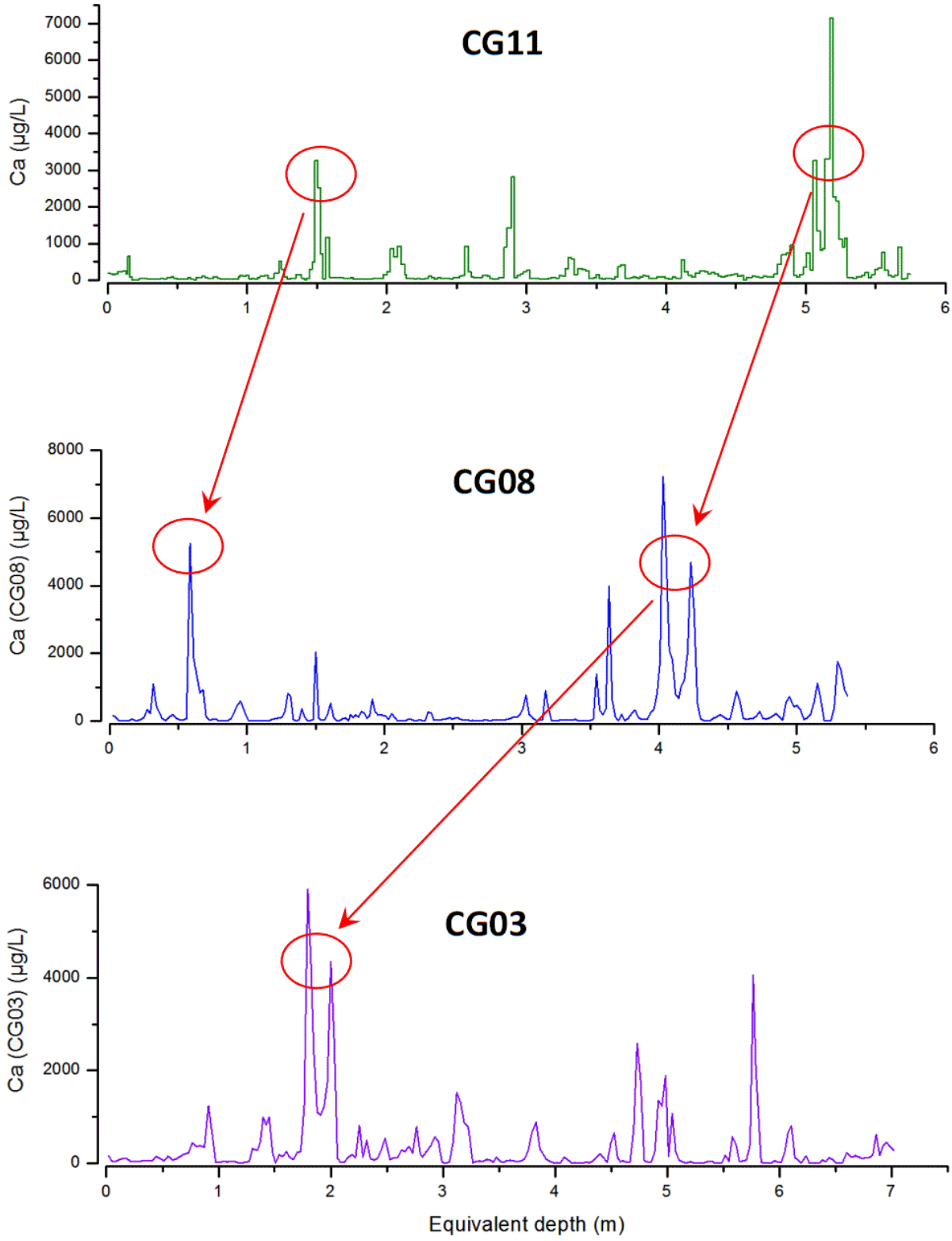

Figure 38: example of correlation between concentration/depth graphics of different studies to achieve dating of the CG11. In this example it is possible to see Ca concentration in µg/L plotted on equivalent depth in metres

Given the not perfect correspondence between the high resolution crustal elements sections (4 cm long) and the E2 trace elements sections (definitely longer), the dating process of the E2 profiles must be done through weighted means and other calculations. The results can be visualised as the example in figure 39: here is reported one high resolution crustal profile (Ca) and two E2 trace element profiles (Ba and Be) with the relative dating. All the other crustal and trace element profile are reported in the attachments.

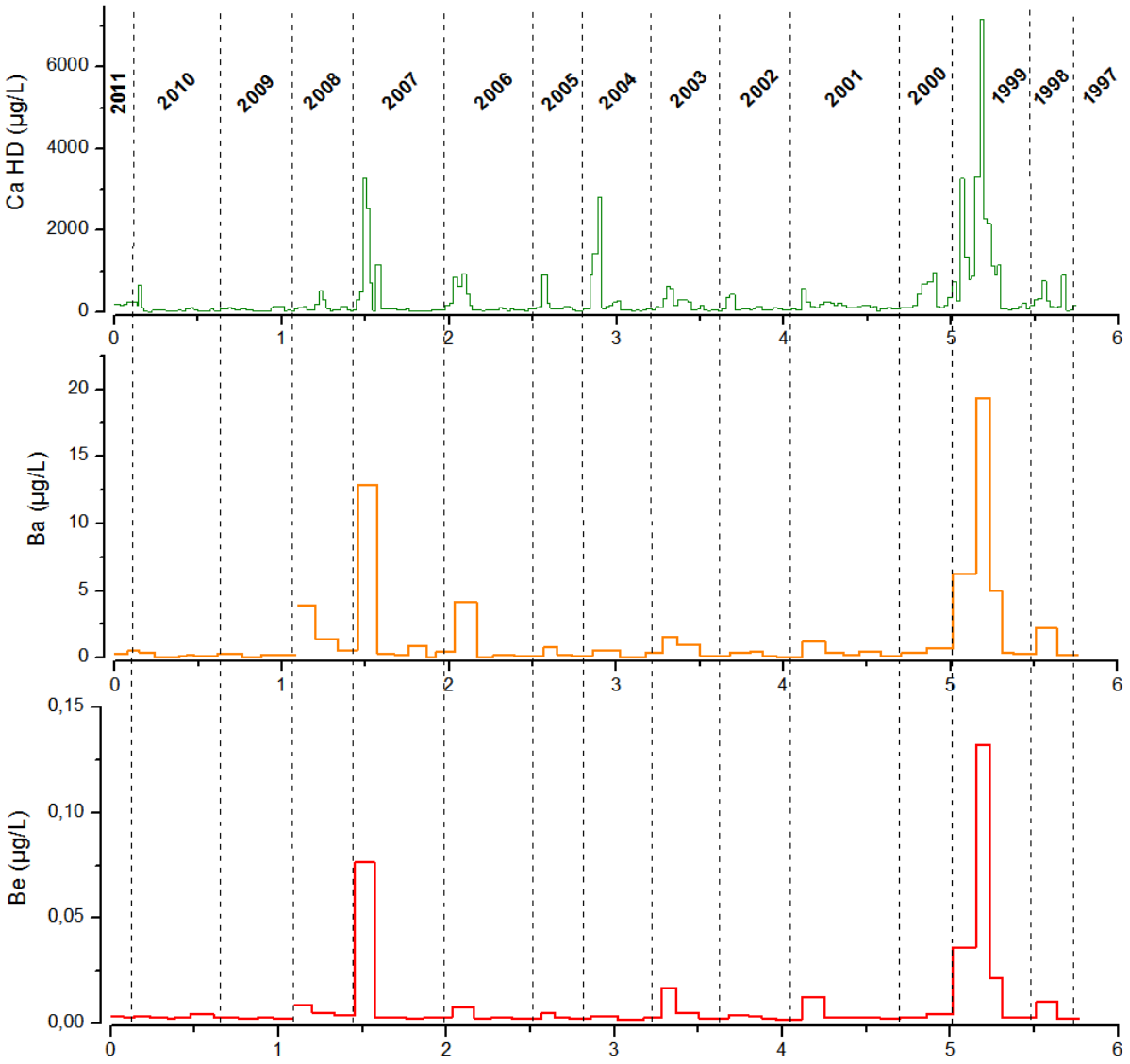

Figure 39: example of dated crustal and trace elements profiles

Once the dating process was finished, it was possible, coupling it with the equivalent depth, to calculate the mean annual accumulation and the total mean accumulation: 0,41 m w.eq./year (table 16). This value is well within the accumulation rate range estimated by Keck (*Keck* 2000)and confirmed again by

(*Eisen*, *Nixdorf* et al. 2003): decreasing from around 0,6 m w eq. at KCS borehole (see figure 7) to 0,2 m w eq. at the upper KCH positions.

year	accumulation rate (m w eq/year)	samples per year	Na (µg/L)	Mg (µg/L)	Al (µg/L)	K (µg/L)	Ca (µg/L)	Ti (µg/L)	Fe (µg/L)	Ba (µg/L)
2011										
2010	0,5	26	81	10	11	45	75	0,8	3	0,8
2009	0,42	21	38	6	13	27	62	0,7	3	1,0
2008	0,33	16	64	13	11	39	125	1,1	7	1,0
2007	0,53	27	101	32	37	47	349	2,4	20	1,4
2006	0,5	23	64	16	28	47	182	1,7	17	1,0
2005	0,28	15	88	16	9	45	148	0,9	5	1,0
2004	0,35	17	92	27	17	56	379	1,2	7	1,1
2003	0,4	19	116	23	11	45	179	0,8	2	1,1
2002	0,41	20	66	11	8	38	101	0,7	3	1,0
2001	0,63	26	66	11	8	38	101	0,7	3	1,0
2000	0,28	12	119	23	13	49	146	0,8	3	1,0
1999	0,44	19	266	85	45	86	1369	2,2	17	2,2
1998	0,23	11	117	31	13	63	286	0,9	6	1,3
1997										

Table 16: mean annual concentration values in µg/L of the high resolution crustal elements analysed through Q2

year	Ca	EF Ca	Mg	EF Mg	Na	EF Na	K	EF K	Fe	EF Fe	Al	EF Al
2011												
2010	101	11	15	4	49	6	14	2	11	1	10	0
2009	107	12	14	3	23	3	20	2	13	1	12	0
2008	897	11	76	2	70	1	42	1	65	1	86	0
2007	1121	8	167	3	177	1	57	0	92	1	120	0
2006	554	10	65	3	35	1	41	1	47	1	49	0
2005	152	10	25	4	25	2	24	2	34	2	29	1
2004	151	12	21	4	19	2	22	2	17	1	14	0
2003	437	13	45	3	50	2	39	1	25	1	44	1
2002	149	12	24	4	18	2	24	2	27	2	26	1
2001	296	14	30	3	40	2	27	1	23	1	25	0
2000	401	16	46	4	60	3	44	2	32	1	31	0
1999	3702	14	373	3	353	1	112	0	199	1	265	0
1998	625	12	58	3	63	1	33	1	4	0	38	0
1997												
year	Be	EF Be	Rb	EF Rb	Sr	EF Sr	Ag	EF Ag	Sn	EF Sn	Cs	EF Cs
2011												
2010	0	4	0,04	1	0,4	5	0	158	0,04	51	0	3
2009	0	3	0,04	1	0,4	4	0,01	306	0,03	42	0	2

2008	0,01	1	0,16	1	3,7	4	0,01	74	0,07	11	0,04	3
2007	0,02	1	0,3	1	7,3	5	0,01	37	0,09	8	0,07	2
2006	0	1	0,13	1	2,3	4	0,01	123	0,09	20	0,04	4
2005	0	2	0,08	1	0,3	2	0	129	0,06	48	0,01	4
2004	0	2	0,05	1	0,6	4	0	115	0,07	67	0,01	3
2003	0,01	2	0,17	1	1,1	3	0,01	149	0,09	34	0,02	3
2002	0	2	0,09	2	0,4	3	0,01	226	0,05	46	0,02	6
2001	0	2	0,09	1	0,8	4	0,01	204	0,06	36	0,01	2
2000	0	1	0,1	1	1,5	6	0,01	107	0,06	31	0,01	2
1999	0,04	1	0,61	1	17,4	6	0,04	69	0,19	8	0,09	2
1998	0,01	1	0,16	1	2,9	5	0,01	126	0,15	36	0,03	3
1997												

year	Bi	EF Bi	Cd	EF Cd	V	EF V	Cr	EF Cr	Ba	EF Ba	Li	EF Li
2011												
2010	0,03	758	0	109	0,1	7	0,1	5	0,2	1	0,02	3
2009	0,01	198	0	124	0,1	6	0,1	5	0,2	1	0,01	2
2008	0,01	17	0,01	32	0,4	2	0,1	1	1,8	1	0,09	1
2007	0,01	23	0,02	38	0,9	3	0,4	3	3,2	1	0,29	3
2006	0,01	57	0,01	54	0,2	2	0,1	2	1,2	1	0,05	1
2005	0,02	234	0	62	0,2	9	0,2	13	0,3	1	0,03	3
2004	0,01	241	0,01	127	0,3	12	0,1	4	0,3	1	0,06	6
2003	0,03	235	0,01	91	0,4	6	0,1	3	0,7	1	0,06	2
2002	0,01	149	0	76	0,1	5	0,1	6	0,3	1	0,02	2
2001	0,02	188	0,01	76	0,2	6	0,1	4	0,5	1	0,08	5
2000	0,02	172	0,01	132	0,4	10	0,1	4	0,6	1	0,04	2
1999	0,03	22	0,06	66	2,7	6	1,3	4	6,2	1	0,06	0
1998	0,02	86	0,02	118	0,3	4	0,1	1	1,1	1	0,01	0
1997												

year	Mn	EF Mn	Co	EF Co	Ni	EF Ni	Cu	EF Cu	Ga	EF Ga	Pb	EF Pb
2011												
2010	1	6	0,01	3	0,1	19	0,2	49	0,01	2	0,23	45
2009	1	6	0,01	4	0,2	26	0,3	75	0,01	2	0,26	49
2008	4	3	0,15	5	0,3	6	0,6	16	0,06	2	1,2	26
2007	8	3	0,19	3	0,6	7	0,7	11	0,07	1	1,07	13
2006	3	4	0,14	7	0,3	10	0,7	27	0,04	2	0,85	28
2005	2	8	0,07	11	0,3	28	0,8	106	0,03	4	0,52	59
2004	1	6	0,02	4	0,3	35	0,7	109	0,01	1	0,64	87
2003	3	5	0,11	9	0,4	19	0,9	53	0,03	2	1,08	57
2002	2	7	0,04	8	0,2	26	0,4	72	0,02	3	0,39	57
2001	2	6	0,06	8	0,3	20	0,6	63	0,02	2	0,53	45
2000	4	10	0,07	8	0,3	21	0,8	66	0,02	1	0,87	61
1999	17	3	0,39	4	1,5	9	2,1	16	0,18	1	3,14	20
1998	3	3	0,05	3	0,3	8	0,5	20	0,02	1	1,22	42
1997												

year	Ti	EF Ti	Tl	EF Tl	U	EF U						
2011												
2010	0,3	0	0	8	0,01	10						
2009	0,3	0	0	14	0,01	6						
2008	1,7	0	0,02	11	0,02	3						
2007	3,3	0	0,02	4	0,08	6						
2006	1	0	0,01	6	0,02	4						
2005	2,6	2	0	10	0,01	10						
2004	0,5	0	0,01	28	0,01	6						
2003	1,2	0	0,02	26	0,03	12						
2002	0,9	1	0	9	0,01	14						
2001	0,6	0	0,01	12	0,02	9						
2000	0,7	0	0,01	19	0,01	6						
1999	7,8	0	0,03	5	0,12	5						
1998	0,8	0	0,02	18	0,02	6						
1997												

Table 17: mean annual concentration values in µg/L of the low definition crustal and trace elements analysed through E2 and their calculated Enrichment Factors

3.5 STATISTICAL ANALYSIS

3.5.1 EFA and PCA on HIGH RESOLUTION CRUSTAL DATA (Q2)

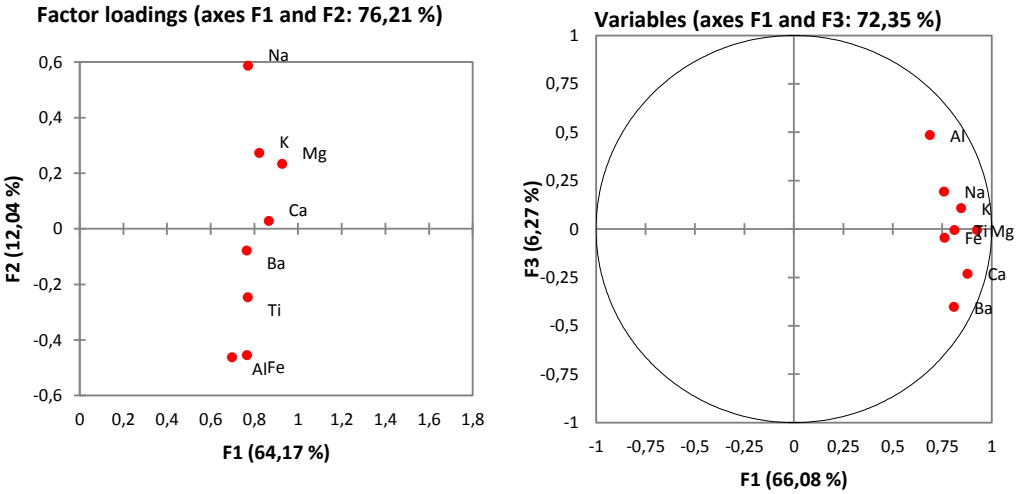

Figures 40 and 41: EFA and PCA applied on box-cox transformed Q2 data

EFA and PCA analyses plots performed on box-cox transformed and ranked Q2 data are presented in figures 40, 41, 42 and 43.

It appears that the crustal elements analysed tend to form some little subgroups such as Al-Fe-Ti, Mg-Na and K-Ca while Ba is normally left alone. These data are obviously not sufficient to point out to any kind of mineralogical source in particular; actually the only polite guess can be done with K-Ca that are well separated from Mg and Fe and could indicate a feldspar-gneiss origin and not an ophiolitic origin (see paragraph "geology of the area"). Overall, a statistical analysis of the Q2 data aimed to highlight any clear connection with the local lithology of the site, revealed itself quite inconclusive. This could be due to the previous acidification of the samples, that upset the ionic potential of the species, and to the lack of other key elements such as Cl, Si et cetera.

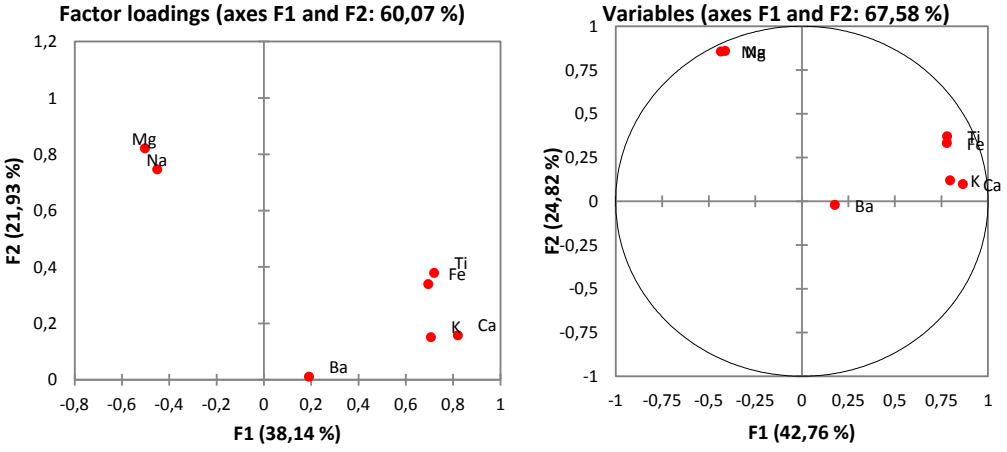

Figures 42 and 43: EFA and PCA applied to ranked Q2

3.5.2 EFA and PCA on LOW RESOLUTION TRACE ELEMENTS DATA (E2)

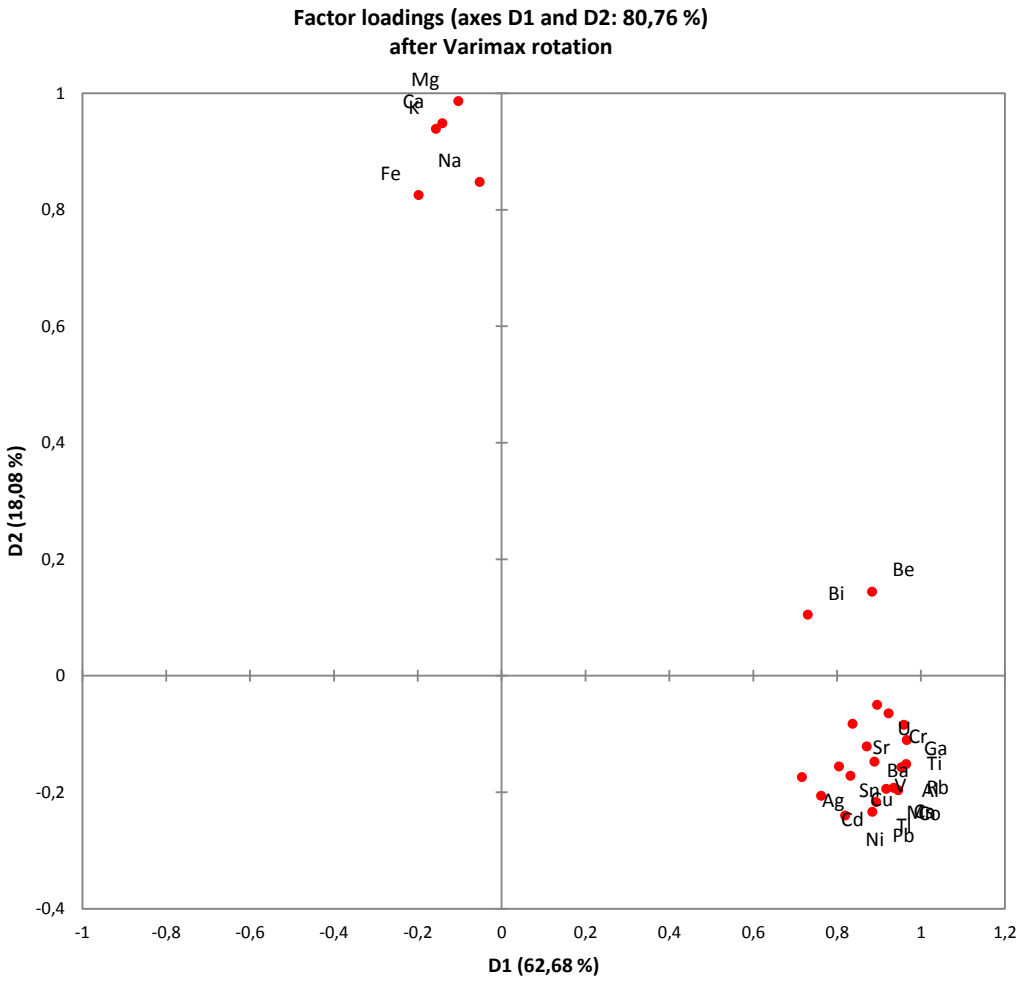

Figure 44: EFA applied on ranked E2 data

Both EFA and PCA on the E2 data here reported have been applied a first time on the raw data (relying only on the EFA or PCA auto standardization) and a second time on the ranked data.

The EFA and PCA applied on ranked E2 data (figures 44 and 45) separate quite clearly a group with the five main crustal elements (Mg, Ca, K, Na, Fe) from the rest of the crustal (Al, Ti, Ba) and trace elements.

This behaviour could be interpreted saying that the sources of the element of the first group are almost only natural (rock dust and sea sprays) but the speculation cannot be confirmed or refined because other key elements are missing (such as Cl, for example) and it does not give any other information on the data.

The respective correlation matrix and factor scores are reported in the attachments.

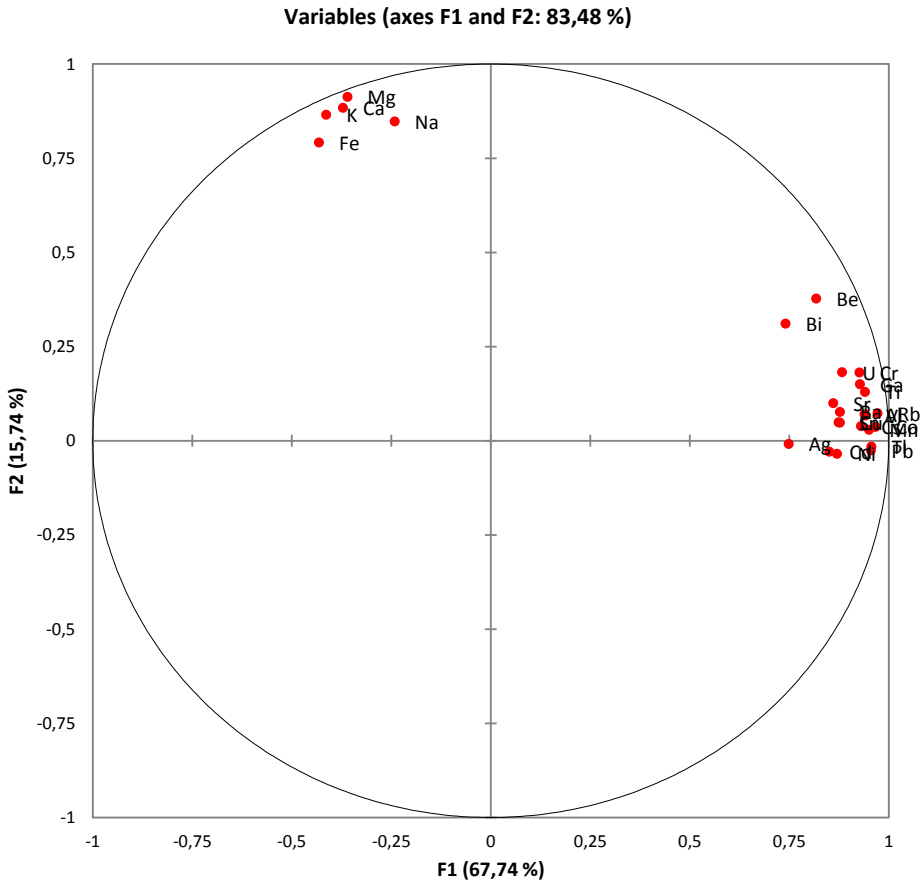

Figure 45: PCA applied on ranked E2 data

EFA and PCA applied on E2 raw data (figures 46 and 47) still bring the separation of the main crustal group but in a less visible way. Other elements patterns are highlighted. Bi, Li and Ag stand alone and seem uncorrelated with the other elements; while for Bi and Li there is few or none explanation, Ag non-correlation can be easily explain with the mineralogical characterisation of the site (see paragraph "Enrichment factor – Silver).

Another element to be quite isolated is lead, which is quite consistent with its peculiar combination of emission sources and history (see paragraph EF – lead).

A group of three elements (Tl, Cu, and Sn) is clearly detached from the main group; as a matter of fact Cu and Sn (and probably Tl) share the same emission sources and emission patterns (see par. EF).

Cd, expected to be close especially to Cu, due to their similar emission source, is found quite distant from it, at least in the F1-F2 plot; anyway F1-F3 plot bring it closer to Cu.

Within the main group it is possible to tell apart some subgroups. One of these subgroups is composed by Rb, Co and Ni, which clearly share similar emission sources and patterns (see par. on EF).

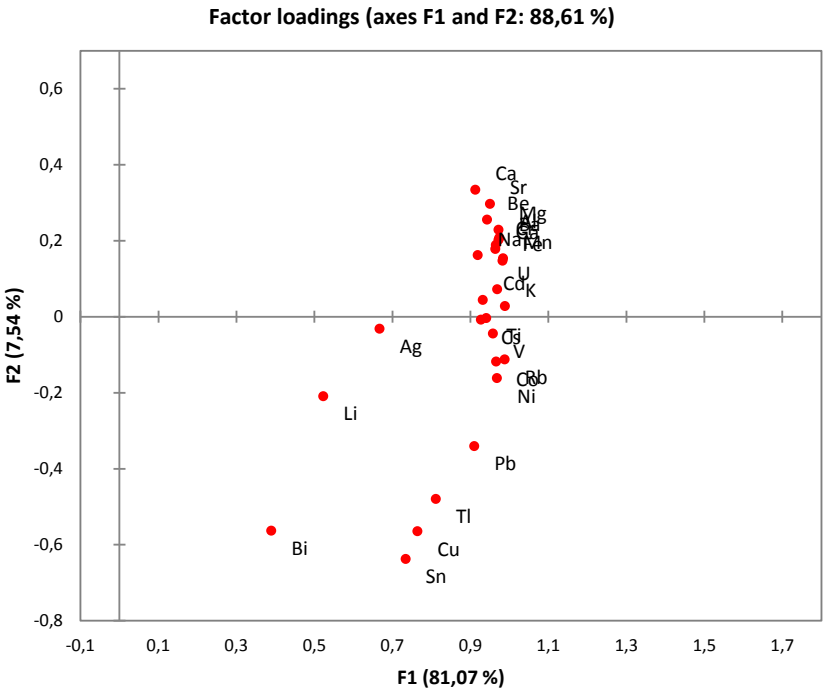

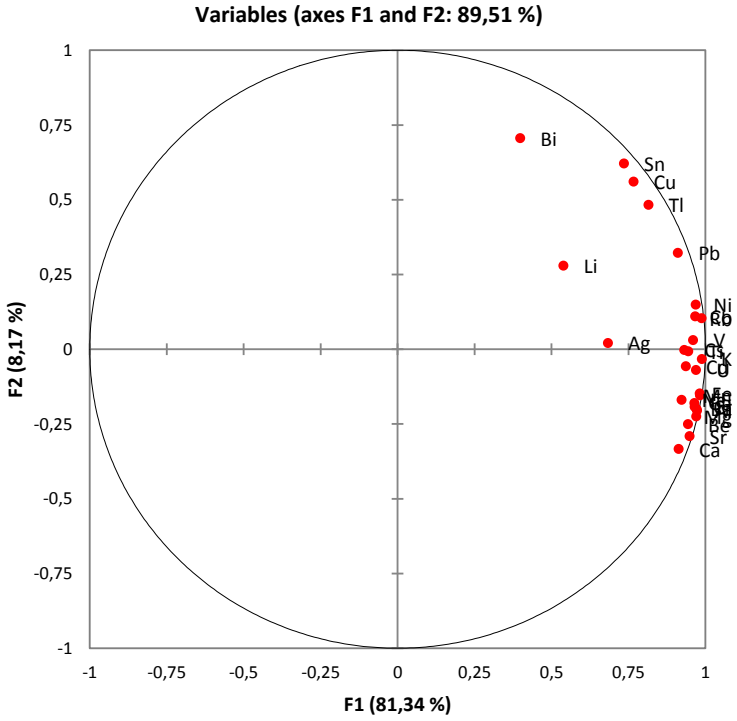

Figures 46 and 47: EFA and PCA applied to E2 raw data

U it is in the main group but relatively isolated. This is probably due to its peculiar emission sources. The fact that it is close to the crustal element group could be a hint of the fact that its anthropogenic sources have decreased in the last decades along with its EF.

All the correlation matrix and factor scores are reported in the attachments.

3.5.3 AGGLOMERATIVE HIERARCHICAL CLUSTERING (AHC) on LOW RESOLUTION TRACE ELEMENTS DATA (E2)

Agglomerative Hierarchical Clustering was applied on both raw and normalised data, virtually confirming all the previous PCA and EFA results on the same datasets.

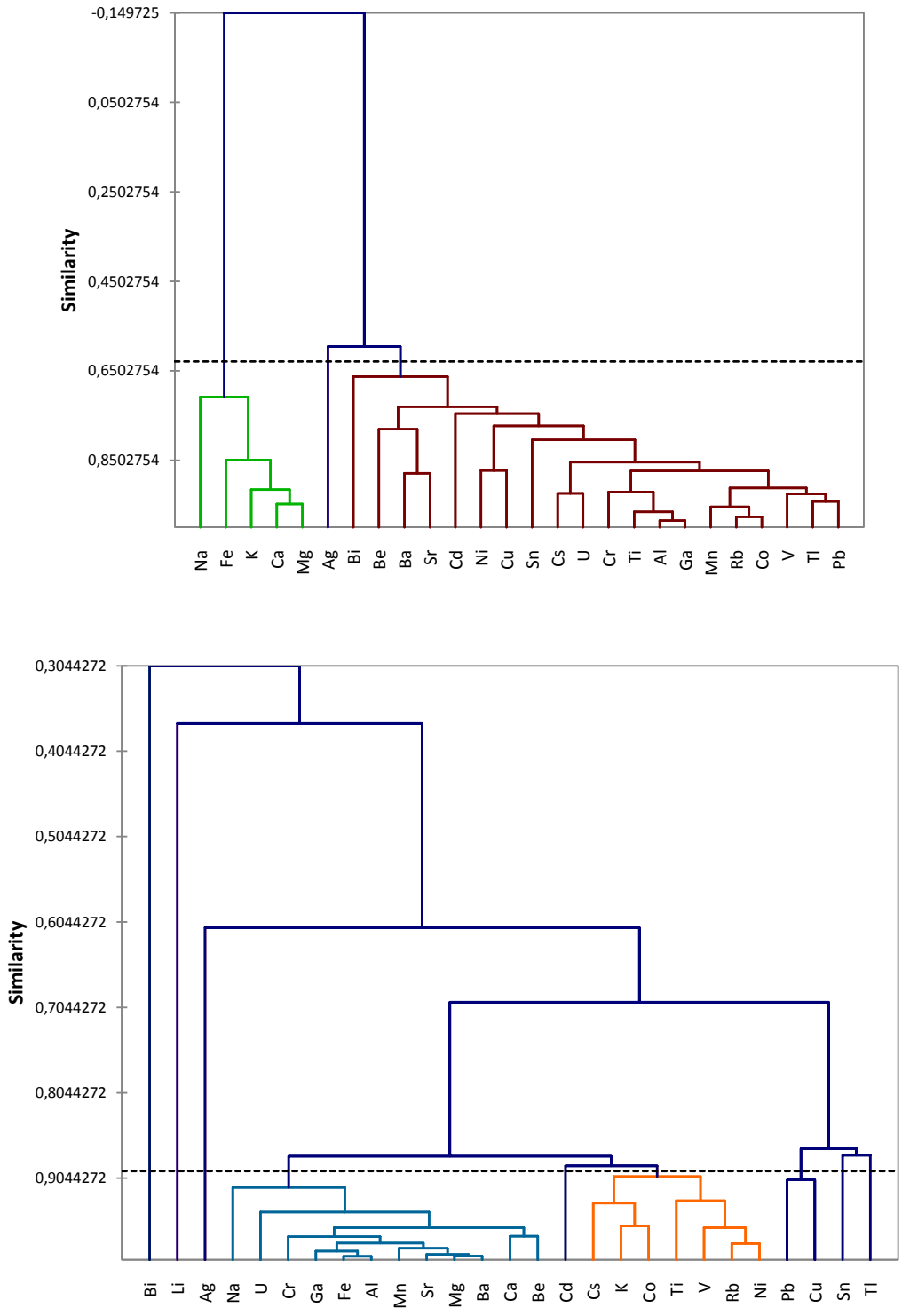

Figures 48 and 49: cluster analysis performed on raw Q2 (above) and E2 (below) data

3.6 TRACE ELEMENTS AND HEAVY METALS CONCENTRATION PROFILES AND ENRICHMENT FACTORS

A calculation of the EF was performed for all the trace elements in this study. The crustal elements of comparison was Ba and the mean Upper Crustal Concentration of various elements were taken from (*Wedepohl* 1995). An interval going from 0 to 10 was adopted to smooth the uncertainty due to the average character of the UCC data (calculated on the whole world).

In this session are discussed the concentrations profiles and the EF profiles of almost all the elements of the low-resolution analysis, starting with those element which EF resulted to be clearly over the limit of 10 and therefore have a probable strong anthropogenic source.

Time period	Concentration (ng/g)							
	V	Cu	Zn	As	Cd	Pb	Bi	U
1992 - 1990	0.251	0.167	2.11	0.052	0.0099	0.788	0.0031	0.0124
1990 - 1985	0.208	0.188	2.34	0.047	0.0263	1.061	0.0026	0.0242
1985 - 1980	0.197	0.112	1.47	0.046	0.0169	1.008	0.0029	0.0236
1980 - 1975	0.235	0.161	1.25	0.051	0.0156	1.526	0.0039	0.0284
1975 - 1970	0.189	0.274	3.13	0.072	0.0446	2.365	0.0042	0.0560
1970 - 1965	0.211	0.212	4.06	0.098	0.0432	3.091	0.0069	0.0144
1965 - 1960	0.078	0.173	8.88	0.079	0.0276	1.425	0.0059	0.0065
1960 - 1955	0.160	0.300	8.00	0.182	0.0519	2.041	0.0085	0.0096
1955 - 1950	0.081	0.112	3.97	0.111	0.0208	1.072	0.0053	0.0053
1950 - 1945	0.110	0.114	2.85	0.105	0.0147	0.854	0.0051	0.0059
1945 - 1940	0.118	0.165	2.63	0.120	0.0152	0.614	0.0070	0.0080
1940 - 1935	0.086	0.120	1.52	0.084	0.0102	0.398	0.0045	0.0058
1935 - 1930	0.062	0.086	1.32	0.096	0.0092	0.430	0.0034	0.0046
1930 - 1925	0.048	0.090	1.04	0.095	0.0084	0.432	0.0032	0.0049
1925 - 1920	0.062	0.119	0.96	0.183	0.0126	0.877	0.0062	0.0062
1920 - 1915	0.065	0.108	0.87	0.146	0.0112	0.982	0.0069	0.0065
1915 - 1910	0.137	0.094	0.79	0.118	0.0087	0.639	0.0038	0.0075
1910 - 1905	0.029	0.045	0.67	0.139	0.0073	0.457	0.0016	0.0032
1905 - 1900	0.043	0.053	1.49	0.106	0.0043	0.249	0.0015	0.0011

Table 18: concentrations (ng/g) of the trace elements analysed in CG03 for the time span 1900-1992 (*Gabrieli* 2008)

The obtained concentration data of Zn and As were excluded from the whole analysis, because when compared with CRMs and standards they were

completely out of scale, even after several changes to the calibration process, and they were therefore considered unreliable and omitted (a similar problem occurred with the Gabrieli CG03 study and it is probably due to some instrument setting or problem).
There are important differences in the character of the two studies. The CG03 study (a PhD thesis) focused also on PAHs, Pu, lead isotopes on a time scale longer than 2000 years. On the other hand the CG11 was only analysed for trace elements but, compared to CG03, more elements were taken into account, and therefore the overlapping of the two cores trace elements analysis is only partial.
In the following table are presented concentration values for the trace elements analysed in the CG03 study for the time span 1900-1992.

3.6.1 LEAD

In the following pages have been reported the EF trend graphics of only the elements of which the EF clearly exceeded the limit of 10 (marked in red).
The concentrations trend of lead seems to correlate in a good way with the previous study of Gabrieli (*Gabrieli* 2008): in the last two decades examined (1970-1990) the Pb values decrease steadily from ca. 3 μg/L to less than 1 μg/L, which is consistent with the mean of the period 1998-2010 of the CG11 core that is around 0,8 μg/L (0,6 μg/L if the unusually high values of 1999 are expunged from the calculation). While in previous centuries much of the Pb particulate was originated by mining activities, it was clear how during the XX century the primary source became coal combustion and the use of leaded gasoline. The lead pollution increased until 1975 and then started to decrease thank to the enforcement of new anti-pollution regulation. In 1998 was signed the Arhus convention, that fixed the year 2005 as the temporal limit for the use of leaded gasoline. It is possible to see the decreasing trend from 2004 to 2008 in the lead EF graphic.

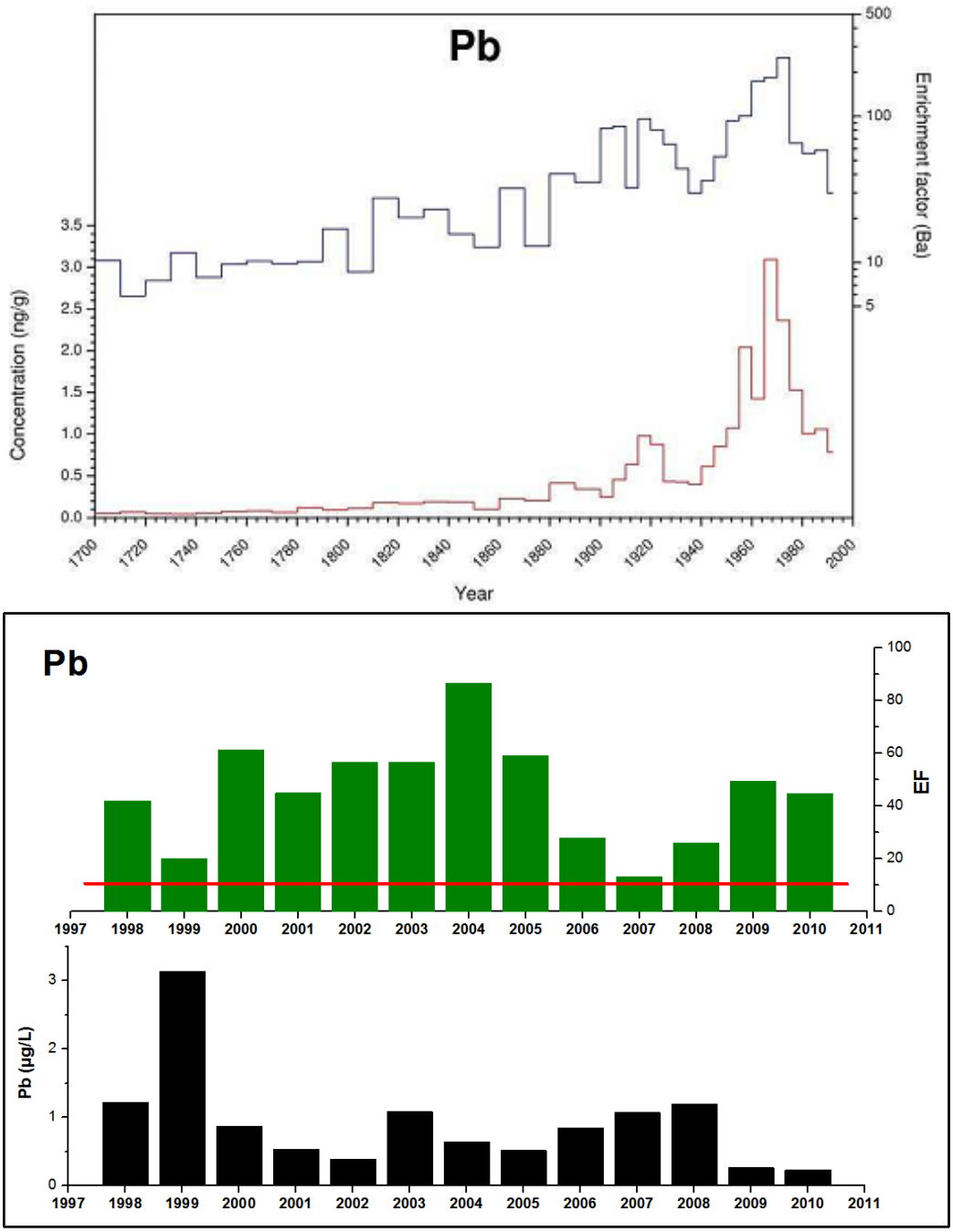

Figure 50: Pb concentrations and enrichment factors from 1700 to 2000 (CG03) (*Gabrieli* 2008)

Figure 51: Pb annual concentrations and enrichment factors from 1998 to 2010 (CG11)

The fact that 2009-2010 EF do not match this trend can be probably explained with an unusual low concentration of Ba (used as fix element for the EF calculation) which weight is enhanced by the relative short period under analysis. Also, the low Pb concentration of these last two years could be traced back to the beginning of the great international economic crisis that (among other things) marked a drop in fuel consumption.

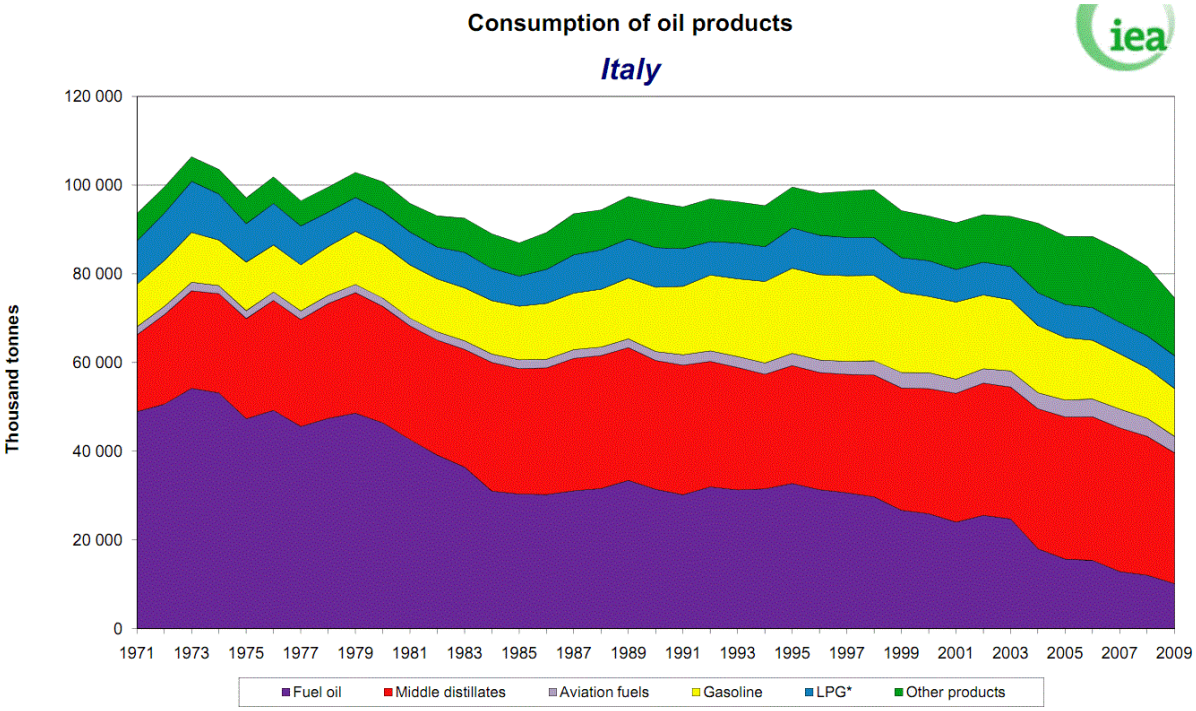

Figure 52: oil products consumption trend of Italy from the beginning of the 1970s to 2009

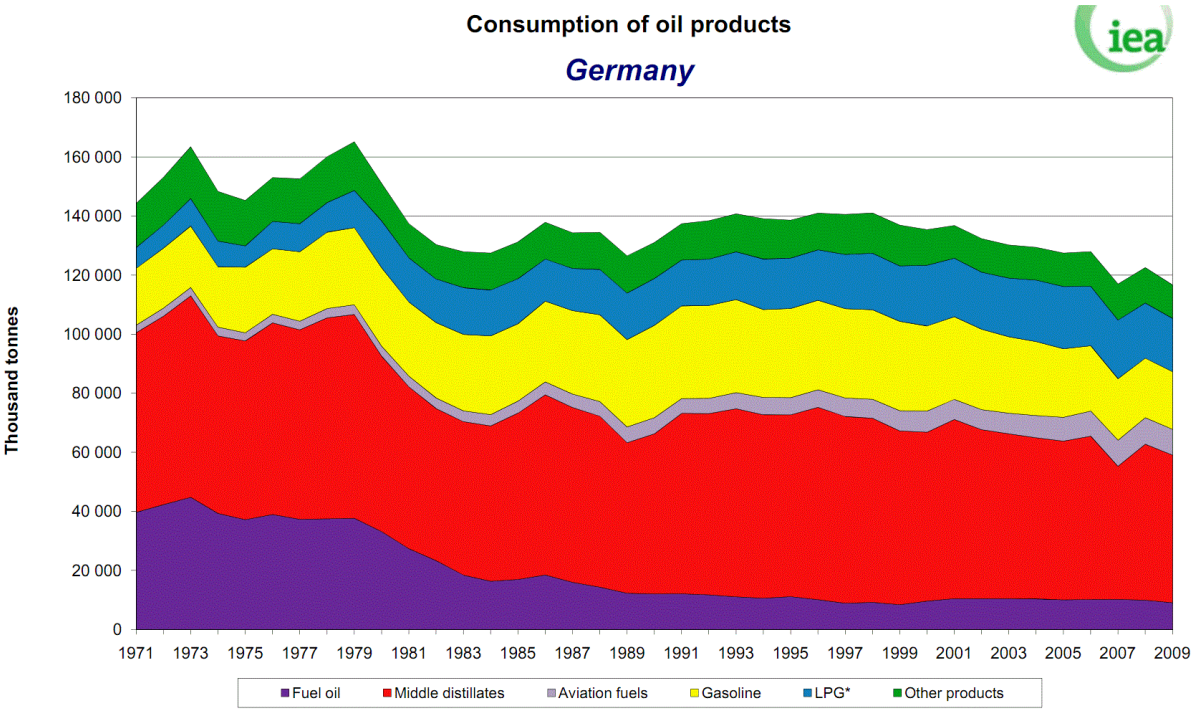

Figure 53: oil products consumption trend of Germany from the beginning of the 1970s to 2009

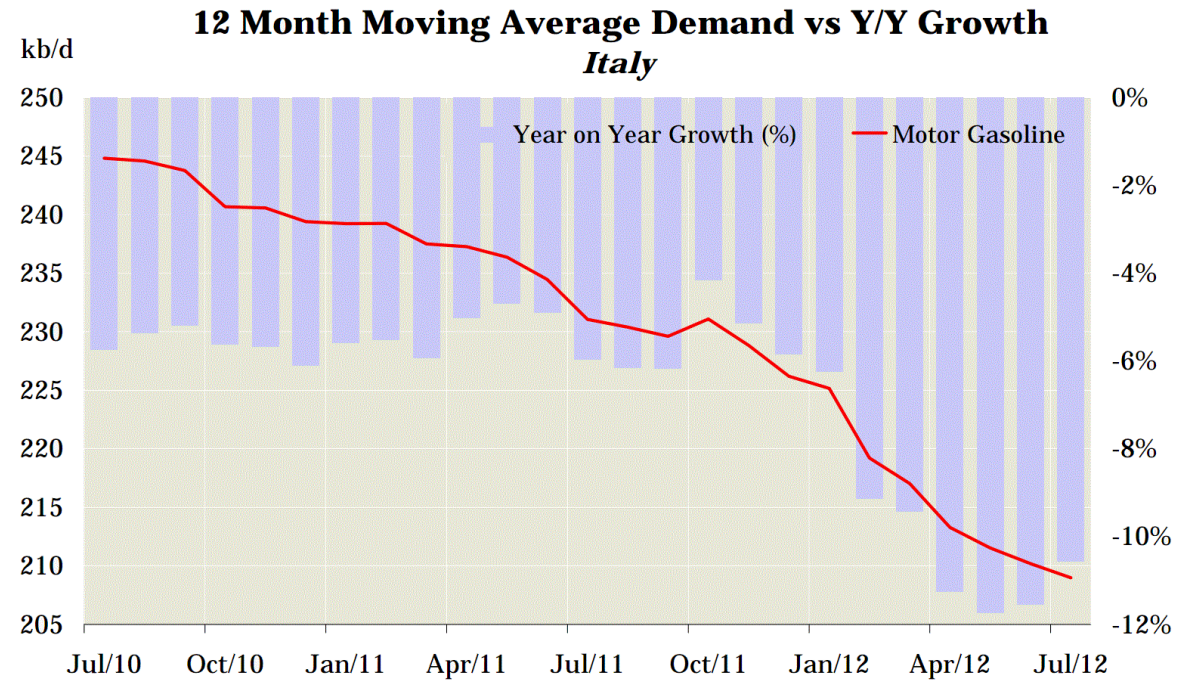

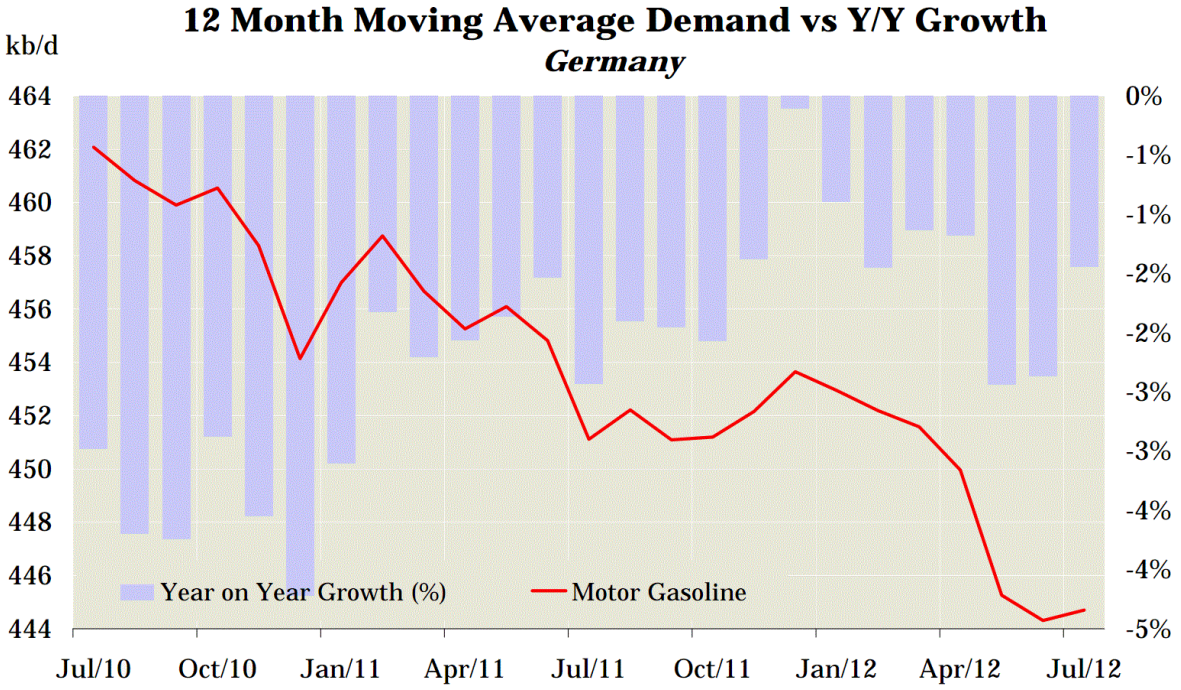

Figures 54 and 55: Italy and Germany trends of motor gasoline demand in the last 2 years. Taking previous estimations into account (figures 53 and 54), it is easy to find out that there was a strong drop in 2008 and, with highs and lows, the trend stood and still is negative in mid-2012 (source: IEA-International Energy Agency – Oil Market Report)

3.6.2 SILVER

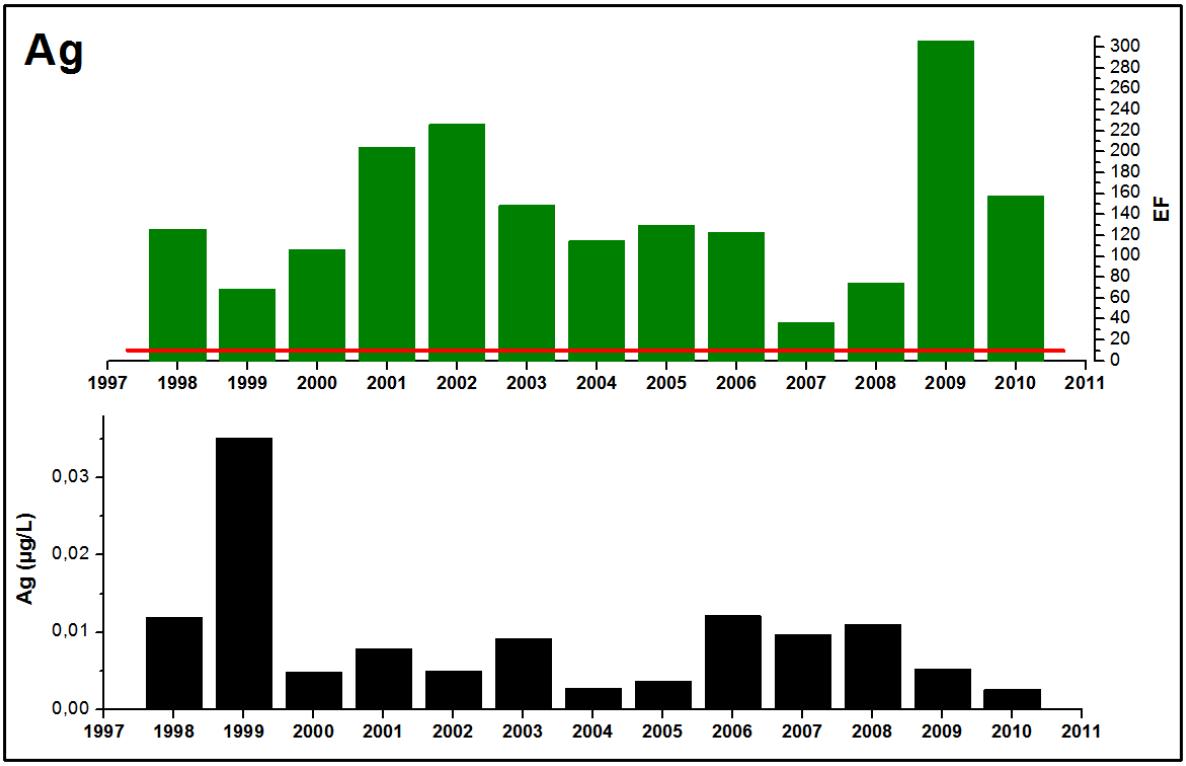

Figure 56: Ag annual concentrations and enrichment factors from 1998 to 2010

The silver EF it is well beyond the limit of ten, and not just occasionally.

This could be explained by the characteristics of the area: the Monte Rosa massif and the surrounding areas are historically famous for gold and silver mining activities, since preroman times (*Strabo* I century b.C. - I century A.D.) and until recent times (*Pipino* 2003).

It is conceivable that the average UCC concentration of silver of the Wedepohl's (*Wedepohl* 1995) study cannot be applied in this area without the consequence of a certain overestimation of the EF.

3.6.3 COBALT, NICKEL and VANADIUM

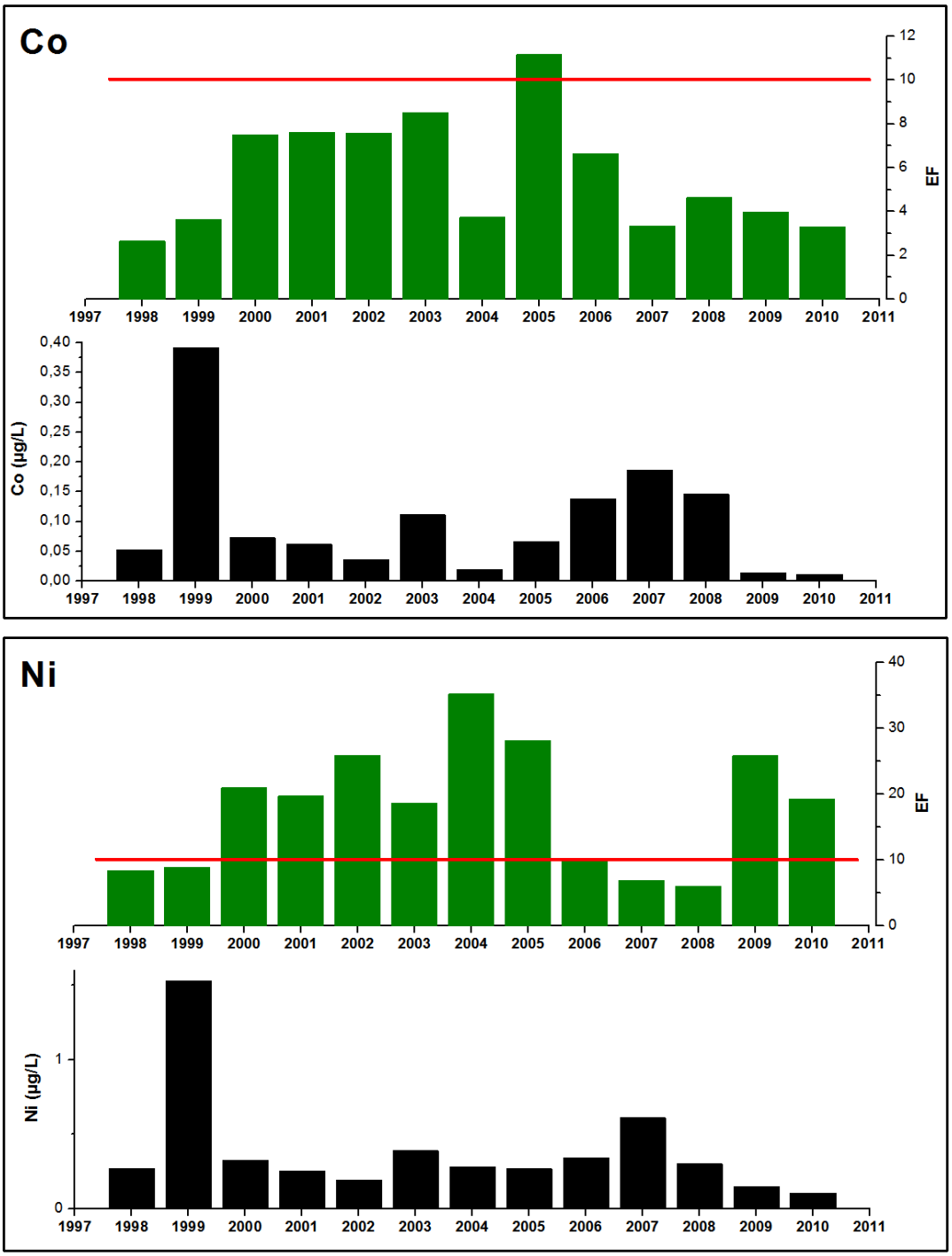

Figures 57 and 58: Co and Ni annual concentrations and enrichment factors from 1998 to 2010

Co, Ni and V present the same concentration patterns and a similar EF patterns. They are three metals strongly related to coal and oil combustion activity such as power plants, industrial, commercial and residential boilers (*Barbante*, *Schwikowski* et al. 2004) (*Barbante*, *Boutron* et al. 2002). Even if the time span of the CG11 core is quite short and thus subject to a high influence of each year

variability, it is possible to see how the concentration values of Ni and Co detected in it are consistent with the values given for the same elements in the Barbante's study of 2004 (*Barbante*, *Schwikowski* et al. 2004).

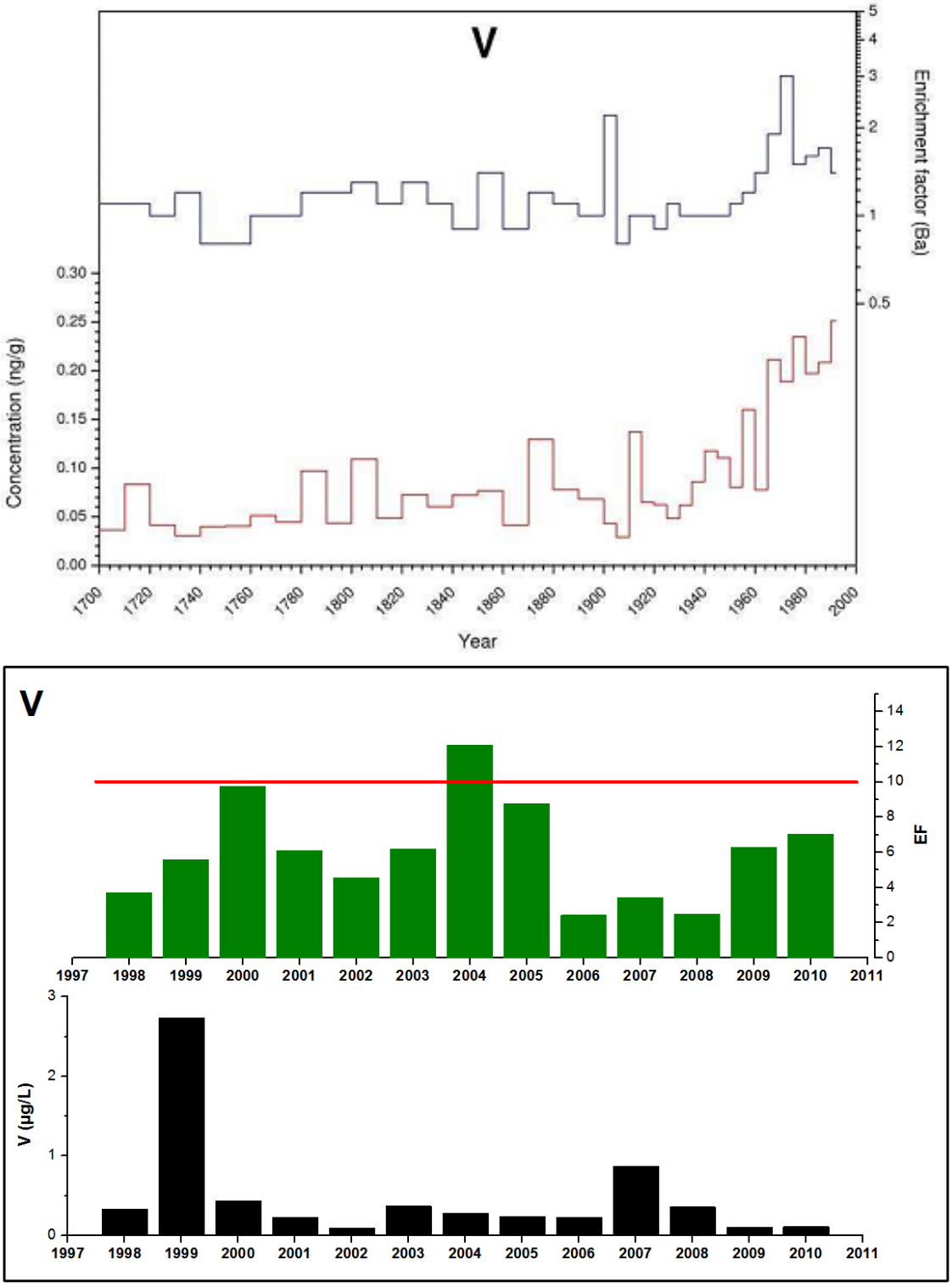

Figure 59: V concentrations and enrichment factors from 1700 to 2000 (CG03) (*Gabrieli* 2008)

Figure 60: V annual concentrations and enrichment factors from 1998 to 2010 (CG11)

Here the after 1970s (until 2000) mean values of Ni and Co are respectively ca. 0,14 μg/L and ca. 0,22 μg/L while the mean values over the 1998-2010 period detected in the CG11 core are respectively ca. 0,38 μg/L and 0,10 μg/L (it must be noted that these means would even be lower if the 1999 unusual high concentration were not taken into account).

V values are not present in the Barbante's work of 2004 and are a bit more difficult to correlate but seem to reasonably fall in an interval of seasonal values for the year 1990-1991 (V seems to undergo a strong seasonal variation) reported in Col du Dôme ice (*Barbante*, *Boutron* et al. 2002); CG11 core V mean value for the 2000-2010 period is 0,30 μg/L while the mean for 1990-1991 on Col du Dôme and on Colle Gnifetti (*Gabrieli* 2008) is ca. 0,20 μg/L.

The EF trends anyway show how the anthropogenic source of Ni should be considered quite higher than the one of V, which values instead tend to remain mainly within the limit of background concentrations.

Definitely both Ni and V (especially V) concentrations and depositional behaviours on the Alps are still relatively unknown if compared to other elements such as Pb, Cd, U et cetera.

3.6.4 CADMIUM, COPPER and TIN

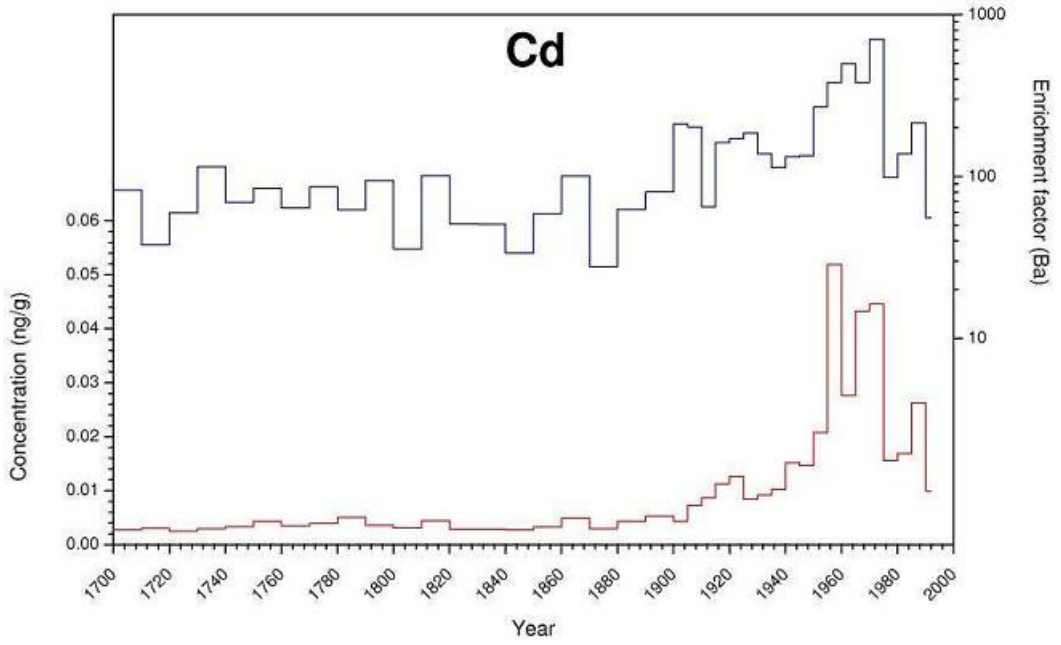

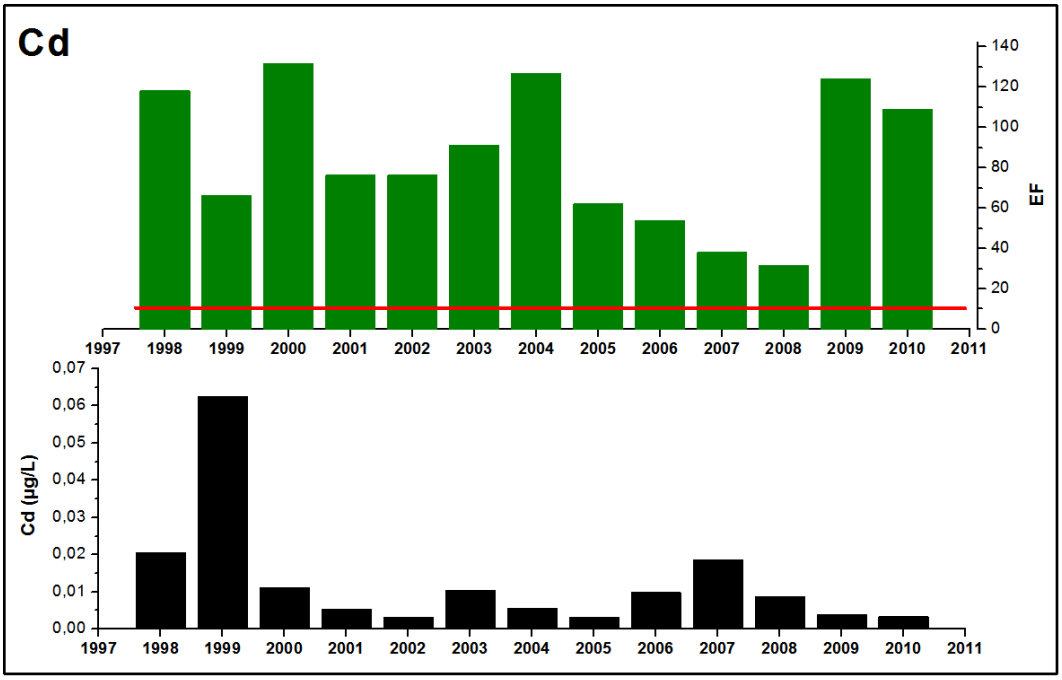

Figure 61: Cd concentrations and enrichment factors from 1700 to 2000 (CG03) (*Gabrieli* 2008)

Figure 62: Cd annual concentrations and enrichment factors from 1998 to 2010 (CG11)

Cadmium and copper EFs are remarkably high, marking a strong anthropogenic input; Cd and Cu traditional main source is non-ferrous metal production (*Pacyna* 1984) (*Pacyna* and *Pacyna* 2001). Since the beginning of the XXI century Cd main source shifted (from 10 to 60%) to fuel combustion for the production of energy and heat (*Pacyna*, *Pacyna* et al. 2007).

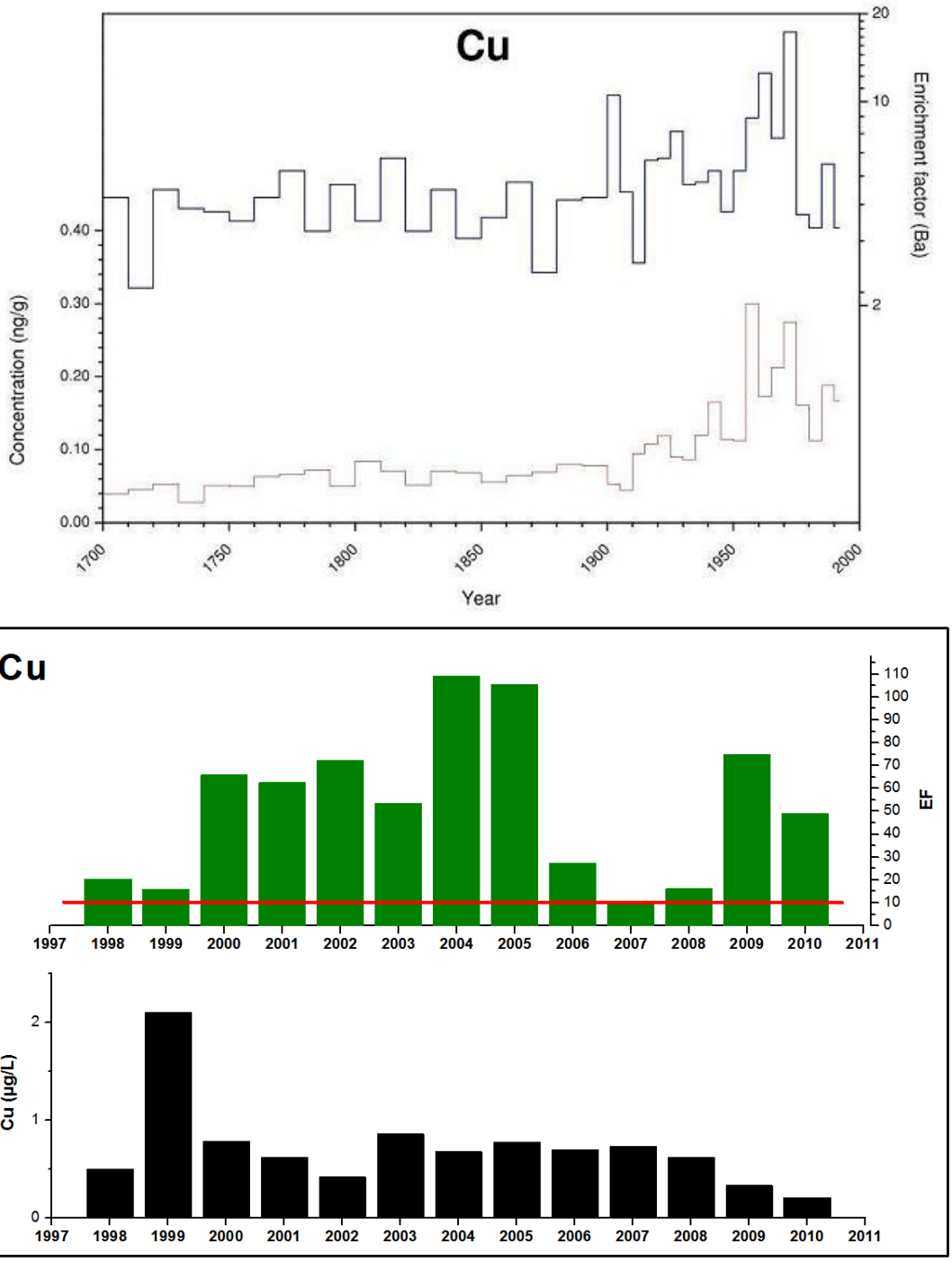

Figure 63: Cu concentrations and enrichment factors from 1700 to 2000 (CG03) (*Gabrieli* 2008)

Figure 64: Cu annual concentrations and enrichment factors from 1998 to 2010 (CG11)

Cd concentrations seem to well correlate with previous studies while Cu concentrations from CG11 could either be a little bit overestimated, maybe due to a not perfect calibration for this element (that cannot be further adjusted because of the scarcity of points in the regression line), or simply agreeing with the increasing copper production and smelting (according to the ICSG-International Copper Study Group).

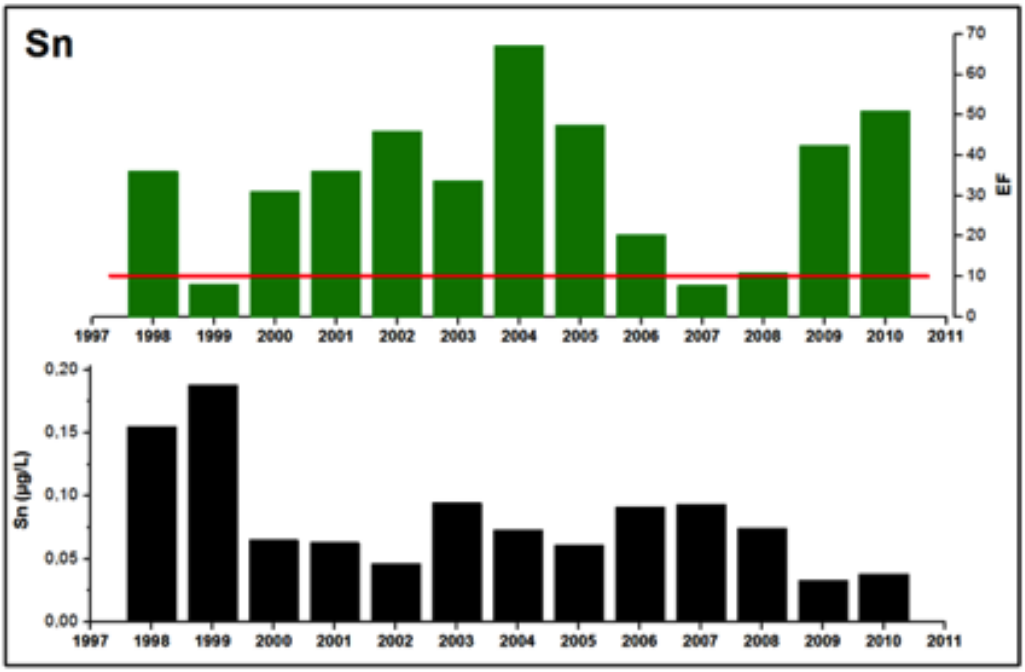

Figure 65: Sn annual concentrations and enrichment factors from 1998 to 2010

Gabrieli's work report a Cd and Cu concentration of respectively 0,0099 µg/L and 0,167 µg/L for the period 1990-1992; these values must be placed in a stable or decreasing trend due to the always more widespread use of new filter systems for smelting and power industries since the 1970s. The values for Cd and Cu obtained from the CG11 for the period 2000-2010 are respectively 0,0075 µg/L and 0,613 µg/L while the Barbante's study (*Barbante*, *Schwikowski* et al. 2004) brings a value of 0,412 µg/L for after 1970s Cu concentration but also shows an abrupt increase in the period 1990-2000 that would seem to well correlate with the CG11 estimation.

Tin is an element that is not so common, at least averagely, in the area of study: no particular association with any of the peculiar metals of the area (such as gold, silver or iron) has been reported and it is also clear that there is, in practice, a total absence of any Sn ore such as Cassiterite, Stannite et cetera.

Studies on European contamination by trace metals emission of Nriagu and Pacyna (*Nriagu and Pacyna* 1988) (*Pacyna* and *Pacyna* 2001) identify oil and coal combustion (for industrial or domestic purposes) and nonferrous metal production (specifically Ni-Cu production) as the main sources of Sn contamination in Europe.

This could explain the resemblance that the concentration trends of Sn and Cu present as well as the high EF. Furthermore an association between the trends of

Cu and Sn can be hinted from the factorial analysis at paragraph 3.5.2: both EFA and PCA plots on raw data place the two metals aside (see figures 46 and 47).

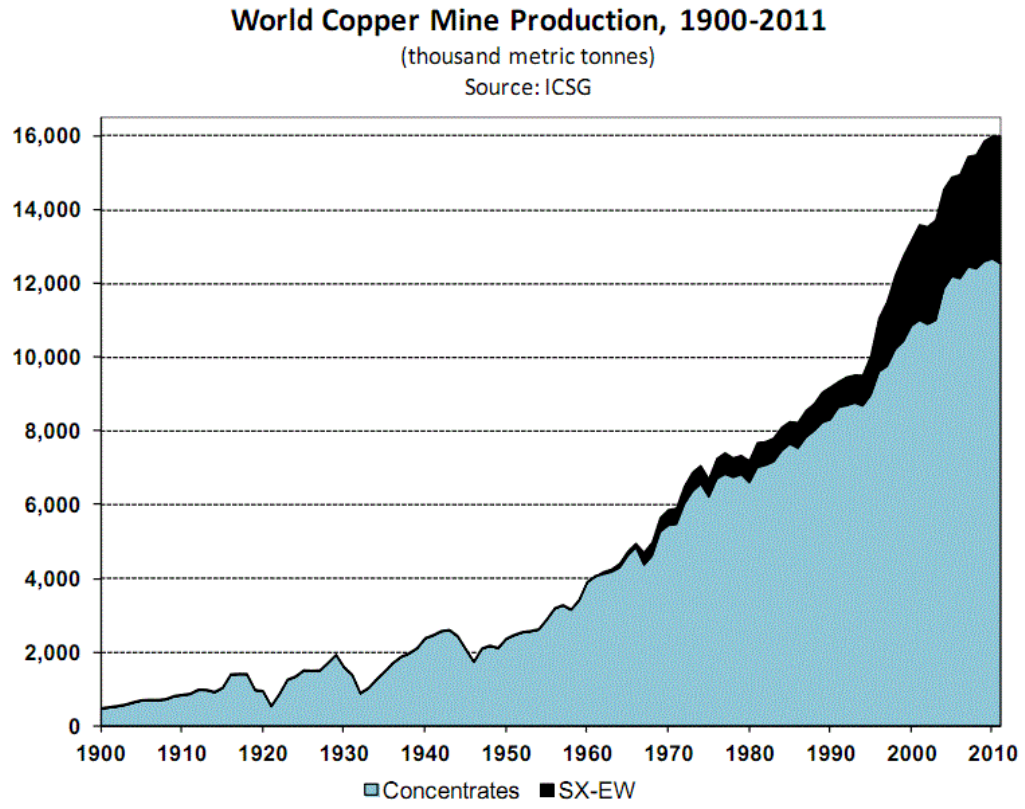

Figure 66: world copper mine production 1900-2011 (source: ICGS)

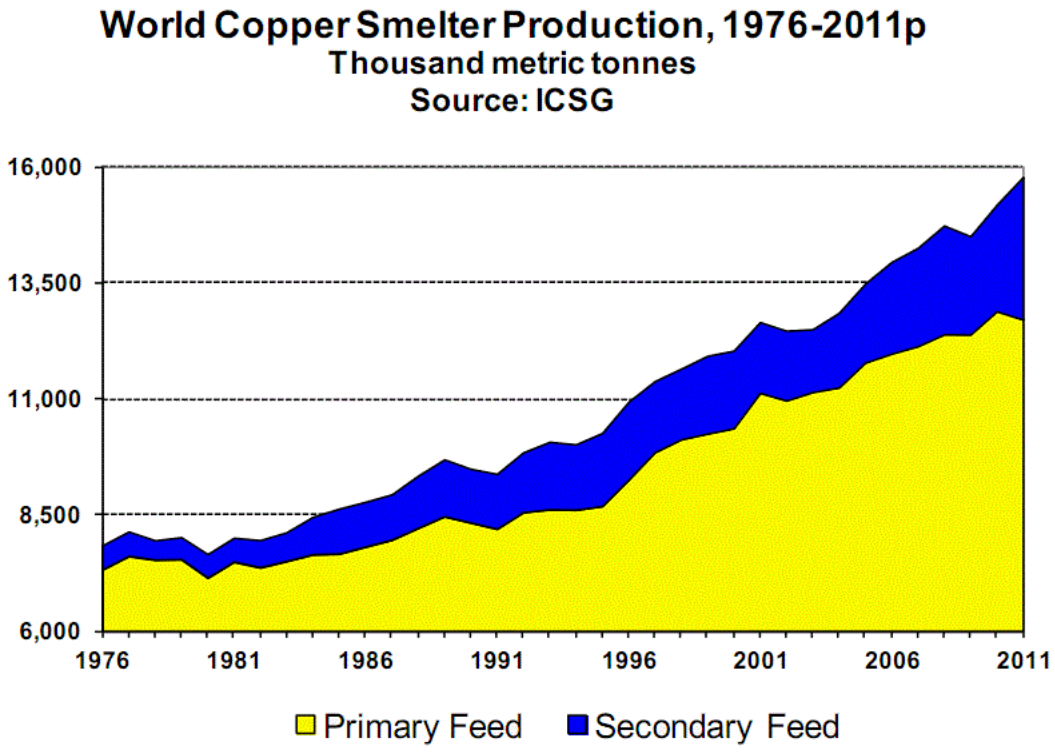

Figure 67: world copper smelter production 1976-2011 (source: ICSG)

3.6.5 URANIUM

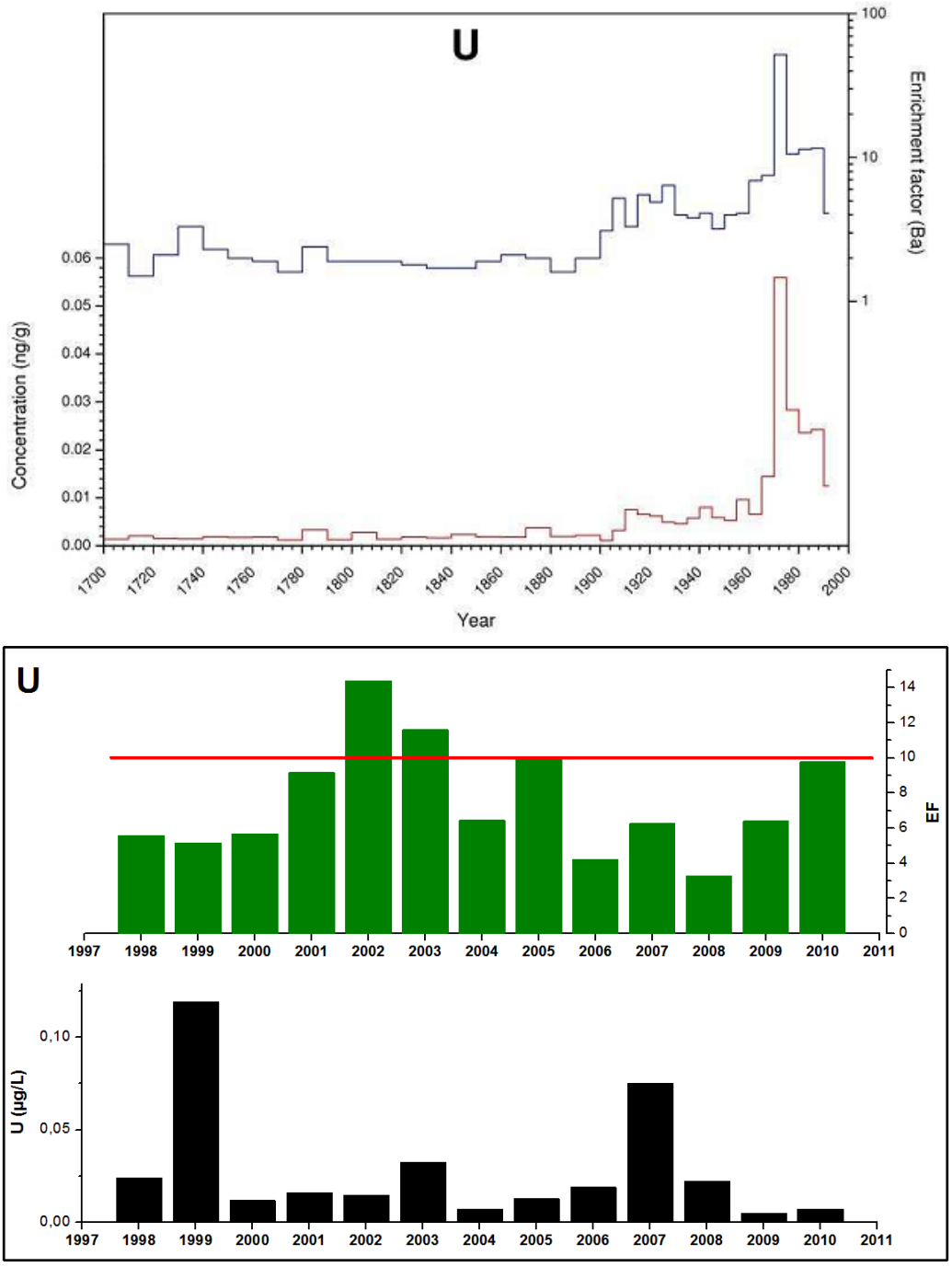

Figure 68: U concentrations and enrichment factors from 1700 to 2000 (CG03) (*Gabrieli* 2008)

Figure 69: U annual concentrations and enrichment factors from 1998 to 2010 (CG11)

Uranium concentration in the particulate aerosol and therefore in the ice records began to rise in the 1920s, probably as a side effect of the increase of other metal mining activity. It continued to rise after the second world war, when both in France and in the GDR there were two important mining projects (in the Limousin and Saxony-Thuringia, the two main uraniferous areas in Europe) to

supply uranium for weapons and energy production; after an abrupt increase during the 1970s it reached a peak during the 1980s and started to decrease (*Gabrieli* 2008), probably due to the start of a shift in energy production models and to a general disarmament (reduction in number of nuclear weapons).
The CG11 U mean value for the decade 2000-2010 (the two previous year are omitted to avoid the 1999 unusual high concentrations) is ca. 0,02 μg/L, which is in good accord with Gabrieli's work value (ca. 0,24 μg/L) for the decade 1980-1990. The CG11 and CG03 U values are less correlated to the Barbante's work (*Barbante*, *Schwikowski* et al. 2004) that shows a value around 0,4 μg/L for the same period; the decreasing trend seems anyway to coincide.
In the histogram above it is clear how this decrement of European Uranium mining activity that started in the 1980s seems to have brought the U concentration in the particulate aerosol back to pre WWII values, almost to background levels.

3.6.6 THALLIUM

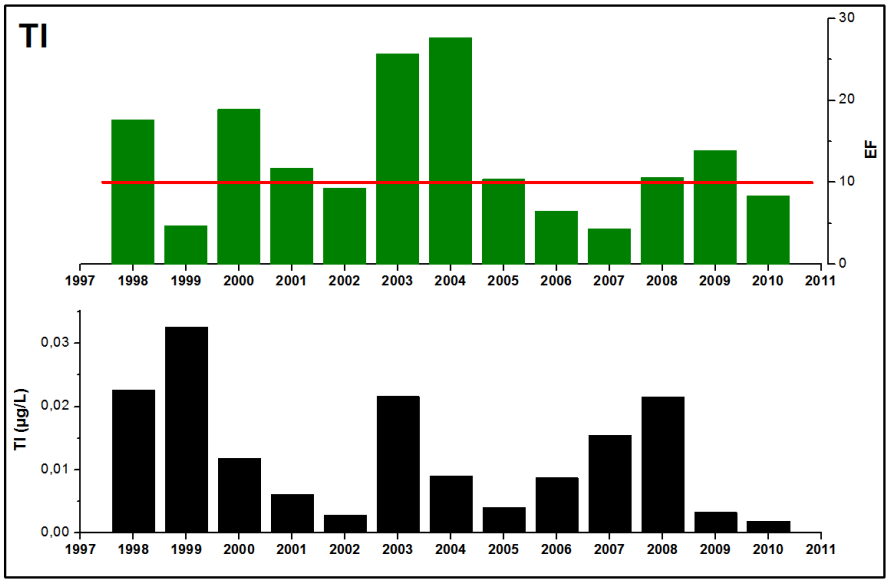

Figure 70: Tl concentration and enrichment factor trends from 1998 to 2010

Thallium is modestly abundant in the Earth crust (ca. 0,7 µg/L) (sources: USGS) (*Wedepohl* 1995) but there is no reason to think that it should be found at higher concentrations than average on the Monte Rosa massif.

According to Nriagu and Pacyna (*Nriagu and Pacyna* 1988) (*Pacyna* and *Pacyna* 2001) the two main sources for Tl pollution in Europe are coal combustion (electric, industrial and domestic utilities) and cement production. The fact that its concentration and EF trends look so different from the ones of other elements treated above can be due to the different distribution of pollution sources in respect of these other elements (coal but not oil combustion, nothing else than cement production).

It appears that in no previous studies on western-alps ice core Tl was ever analysed so there are no other values with which is possible to make a reasonable comparison.

Nonetheless, if we assume that concentrations and EF here measured and calculated are reasonably correct, it is possible to see a decrease in Thallium pollution at least for the last five years.

Of course further and more detailed analysis on a longer time span would be necessary to confirm this hypothesis. Pacyna in (*Pacyna* and *Pacyna* 2001) makes a comparison between estimated 1983 and 1995 Tl emissions, registering an increment of about 60% but it must be noted that the comparison is made on a world basis and it cannot tell in detail if the European region followed this trend or not.

3.6.7 BISMUTH

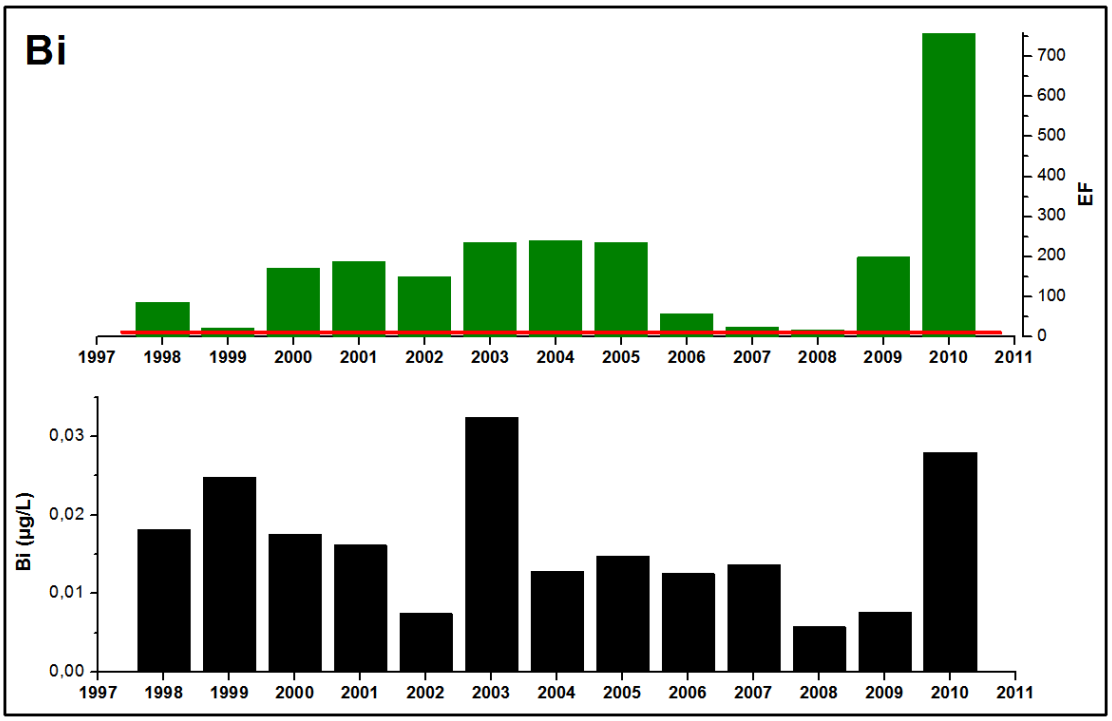

Figure 71: Bi concentration and enrichment factor trends from 1998 to 2010

Bismuth ores are not common and have not been reported in or around the area of study. This means that the Wedepohl's UCC mean value (*Wedepohl* 1995) can be assumed as reliable in this study case and therefore the high EF values of Bi calculated must be explained mainly with anthropogenic sources.

Bi and Pb pollution have similar sources but the two trends seems to lack any correspondence. Furthermore the Bi concentration values obtain by Barbante and Gabrieli on the ice of Colle Gnifetti (*Barbante*, *Schwikowski* et al. 2004) (*Gabrieli* 2008) of ca. 0,002-0,004 µg/L for the decade 1980-1990 appear to not correlate with the CG11 data of ca. 0,015 µg/L for the decade 2000-2010.

The most likable explanation, given that the CG11 Bi calibration was thorough, could be find in a marked variability of Bi concentration on the short term, considering the short time span covered by the CG11 core.

3.6.8 CHROMIUM

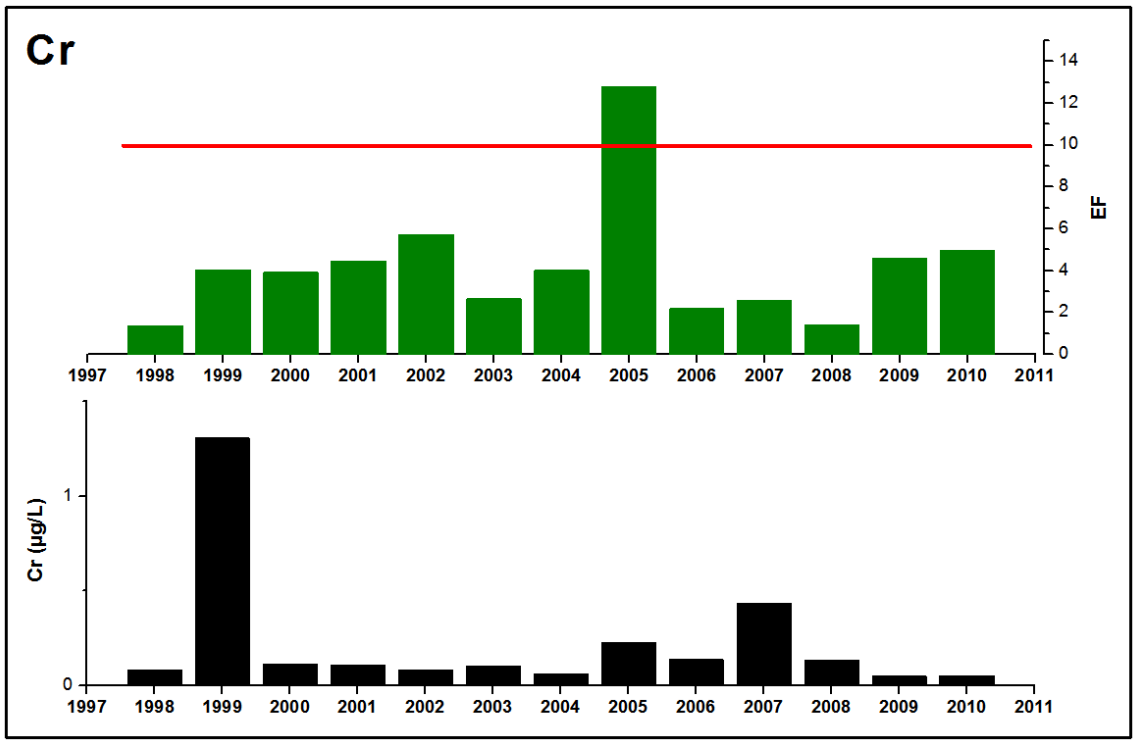

Figure 72: Cr concentration and enrichment factor trends from 1998 to 2010

Chromium most common pollution sources can be traced to coal and oil combustion and iron-steel manufactory. The CG11 value of ca. 0,22 µg/L is quite in accord with the ca. 0,35 µg/L value of the work of Barbante (*Barbante*, *Schwikowski* et al. 2004); the lower concentration mean and quite low EF values of the period 1998-2010 could mean a slight decrement of the Cr pollution.

3.6.9 MANGANESE

Manganese has many common pollution sources such as coal and oil combustion (mainly coal), nonferrous metal mining and Cu-Ni production, steel iron manufactory and refuse incineration (Nriagu and Pacyna 1988). CG11 Mn concentration values for the period 1998-2010 are ca. 2,8 µg/L and its EF is always under the limit of 10.

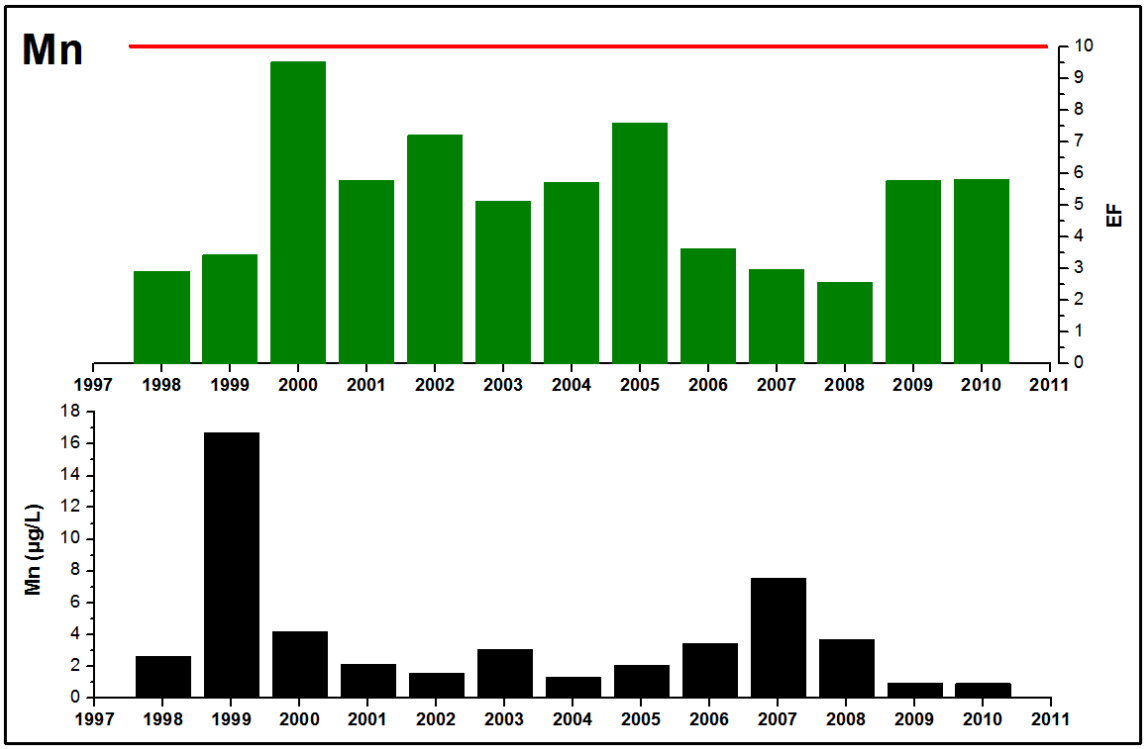

Figure 73: Mn concentration and enrichment factor trends from 1998 to 2010

3.6.10 RUBIDIUM, STRONTIUM, CESIUM and GALLIUM

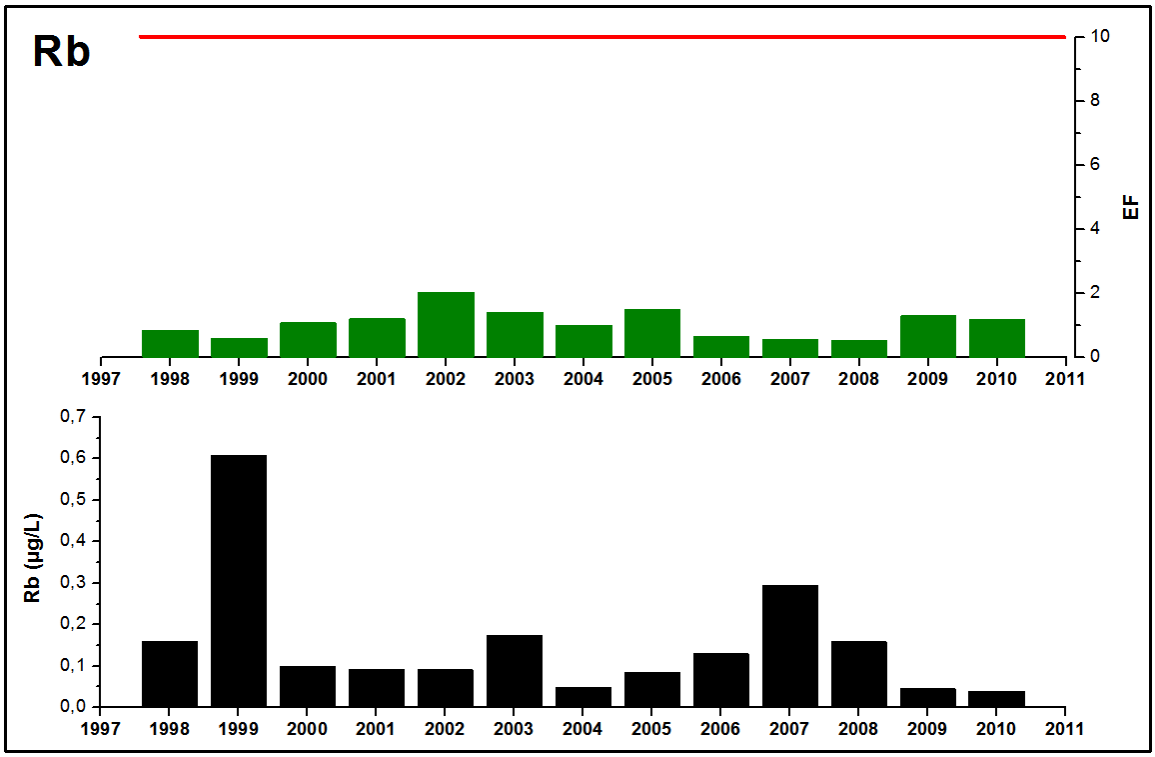

Figure 74: Rb concentration and enrichment factor trends from 1998 to 2010

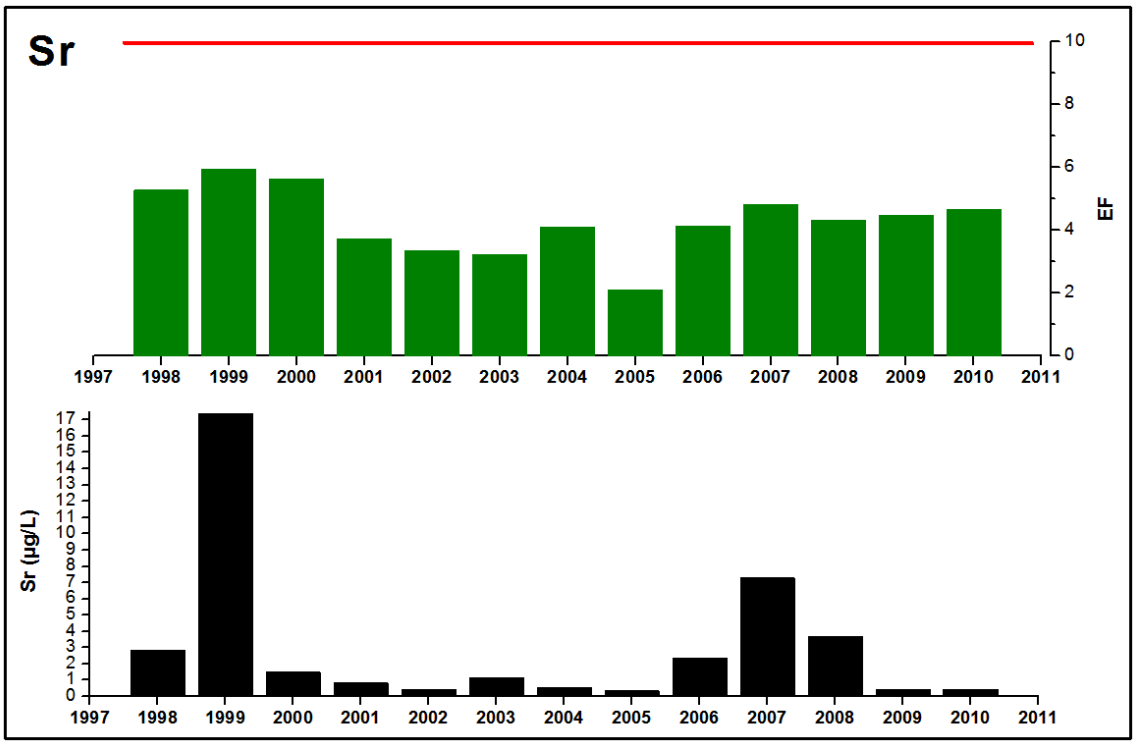

Figure 75: Sr concentration and enrichment factor trends from 1998 to 2010

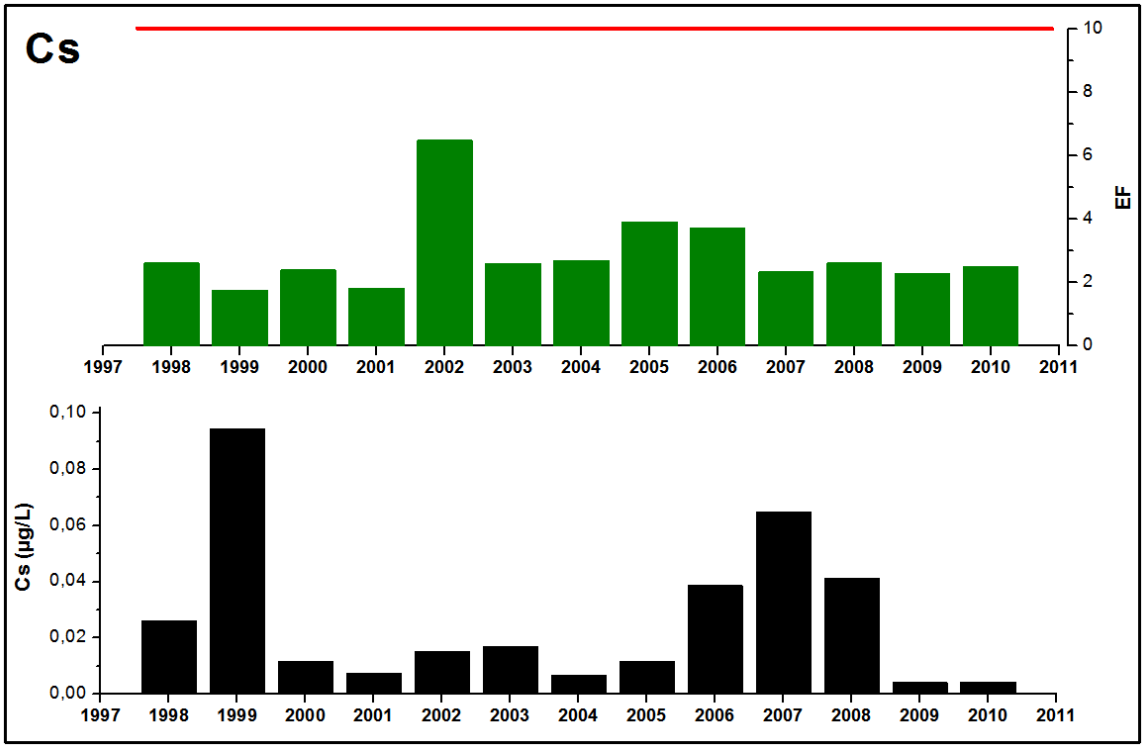

Figure 76: Cs concentration and enrichment factor trends from 1998 to 2010

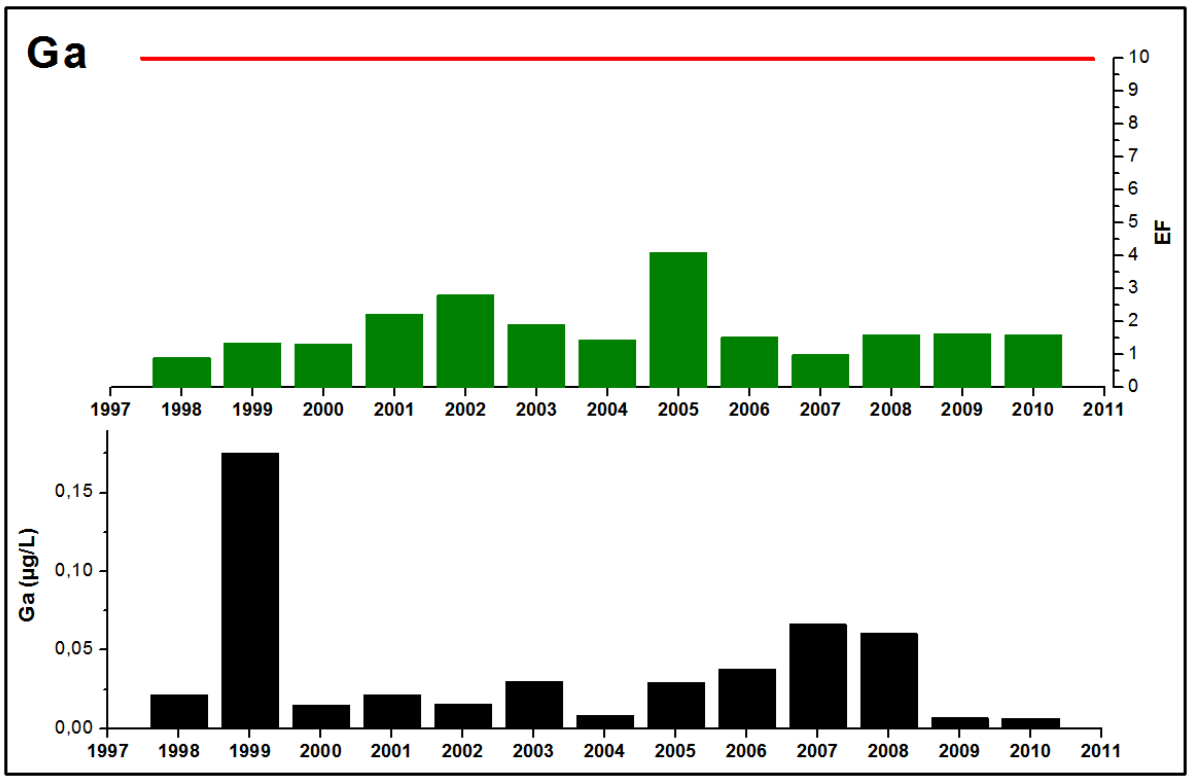

Figure 77: Ga concentration and enrichment factor trends from 1998 to 2010

Few or none records are available for these four less abundant crustal elements in alpine ice cores. For example Gabrieli's work describe the concentration of Rb but only at a several metres depth, which is not correlatable to a 1998-2010 value in any case.

CG11 mean concentration values for Rb, Sr, Cs and Ga are respectively 0,11 µg/L, 1,7 µg/L, 0,02 µg/L and 0,03 µg/L. All their EF values are well under the limit of 10, which is well in accord with their main crustal nature.

4. CONCLUSIONS

In the summer of 2003 an 11 m firn-ice core was drilled and recovered from the western Alps saddle of Colle Gnifetti, part of the massif of the Monte Rosa.

This core, called CG11, covers the time interval 1998-2010 and it is meant to continue the previous work on the Colle Gnifetti ice core: CG03, which was 81 m long and covered the last 10,000 years. On the other hand, where the CG03 study analysed trace elements, PAHs, Pu and lead isotopes, the CG11 core was analysed only for trace elements concentrations.

The dating process was performed by comparing the CG11 high resolution crustal profiles (analysed specifically for the dating process) and other dated crustal elements profiles of previous studies of colle Gnifetti ice cores such as the CG03 of Gabrieli (*Gabrieli* 2008) and the CG08, an unpublished Swiss work.

The results of the analysis of CG11 were then correlated with the trace elements values of other studies on ice cores from colle Gnifetti or other glaciers of the western Alps and analysed for possible trends and connections.

A newer and quicker approach for the process of ice decontamination with commercial ceramic knives was successfully tested and implemented. This new system has proven to be quicker than the previous approach, which comprises a steel blade that must be submerged in acid for weeks prior to each use, and does not seem to introduce any significant contamination, at least in the case of Alpine ice cores.

An attempt to refine the calculation of the Enrichment Factor with a focus on the geology of the study area proved to be practically impossible, due to the few crustal elements analysed and to the strong background noise brought both from the contamination of the high definition crustal samples and from the lack of other kinds of analyses such as microscopical analysis or pH analysis.

The CG11 trace elements concentration values were analysed statistically with various tools as EFA, PCA and clustering. This contributed to outlining possible associations that were more evident once the enrichment factors were calculated and plotted.

Lead appeared to be well in accord with previous studies; stable, if not decreasing thanks to governmental regulations and, maybe, the last economic

crisis. Silver was obviously related to the mineralogical nature of the site, rich in gold and silver ores.

Nickel, Copper, Cadmium and Tin were found to be in slight growth, linked together by their common source, but still well related to previous studies. Similarly, Cobalt and Vanadium even if the former showed a slight decreasing trend and the latter a more undefined pattern.

Uranium is well correlated with previous study and confirms the decreasing trend highlighted by these studies. It is now under the 10 EF limit, arbitrarily assumed to be the minimum EF level indicating an anthropogenic input.

Chromium is well correlated with values mentioned in the study of Barbante (*Barbante*, *Schwikowski* et al. 2004) on the Mont Blanc and shows a decreasing trend while Bismuth has values that are not correlatable with previous studies; they seem to be out by a factor 2-3. -The reason for their failure to match could be found in an imperfect calibration or in the high yearly variability.

Manganese is well under the 10 EF limit and quite stable while the values for Thallium are not comparable to any other previous study and appear to vary strongly.

Overall, it must be noted how the short time span covered by the CG11 core (only 12 years) limits any kind of trend extrapolation on the trace elements concentration values, starting from a statistical analysis. This fact limits most of the conclusions reached on TE trends to the rank of a “educated guess”, which will need to be confirmed by subsequent/future studies. One of the first will surely be the CG08 Swiss study that will hopefully provide additional sustainable evidence to the conclusions reached here. In any event, it seems that within only a decade or two, a new study based on a longer core, covering a longer time span, that would include also the period 1997-2011, would be able to clear the field from any doubt on the TE trends so roughly outlined in this thesis.

5. REFERENCES

Alean, J., *W. Haeberli*, et al. (1983). "Snow accumulation, firn temperature and solar radiation in the area of the Colle Gnifetti core drilling site (Monte Rosa, Swiss Alps): distribution patterns and interrelationships." Zeitschrift fur Gletscherkunde und Glazialgeologie **19**(2): 131-147.

Araguás-Araguás, L., *K. Froehlich*, et al. (2000). "Deuterium and oxygen-18 isotope composition of precipitation and atmospheric moisture." Hydrological Processes **14**(8): 1341-1355.

Barbante, C., et al. (1997). "Direct determination of heavy metals at picogram per gram levels in Greenland and Antarctic snow by double focusing inductively coupled plasma mass spectrometry." (9): 233.

Barbante, C., *C. Boutron*, et al. (2002). "Seasonal variations in nickel and vanadium in Mont Blanc snow and ice dated from the 1960s and 1990s." Journal of Environmental Monitoring **4**(6): 960-966.

Barbante, C., *M. Schwikowski*, et al. (2004). "Historical Record of European Emissions of Heavy Metals to the Atmosphere Since the 1650s from Alpine Snow/Ice Cores Drilled near Monte Rosa." Environmental Science & Technology **38**(15): 4085-4090.

Beltrando, M., *R. Compagnoni*, et al. (2010). "(Ultra-) High-pressure metamorphism and orogenesis: An Alpine perspective." Gondwana Research **18**(1): 147-166.

Berg, T., *W. Aas*, et al. (2008). "Atmospheric trace metal concentrations at Norwegian background sites during 25 years and its relation to European emissions." Atmospheric Environment **42**(32): 7494-7501.

Bolius, D. (2006). "Paleo climate reconstruction based on ice cores from the Andes and the Alps." PhD thesis, University Bern.

Brown, J. D. (2009). "Principal components analysis and exploratory factor analysis – Definitions, differences and choices." Shiken: JALT Testing & Evaluation SIG Newsletter.

Candelone, J.-P., *S. Hong*, et al. (1994). "An improved method for decontaminating polar snow or ice cores for heavy metal analysis." Analytica Chimica Acta **299**(1): 9-16.

Christner, B. C., *J. A. Mikucki*, et al. (2005). "Glacial ice cores: A model system for developing extraterrestrial decontamination protocols." Icarus **174**(2): 572-584.

Döscher, A., *H. W. Gäggeler*, et al. (1996). "A historical record of ammonium concentrations from a glacier in the Alps." Geophysical Research Letters **23**(20): 2741-2744.

Eichler, A., *M. Schwikowski*, et al. (2000). "Glaciochemical dating of an ice core from upper Grenzgletscher (4200 m a.s.l.)." Journal of Glaciology **46**(154): 507-515.

Eisen, O., *U. W. E. Nixdorf*, et al. (2003). "Alpine ice cores and ground penetrating radar: combined investigations for glaciological and climatic interpretations of a cold Alpine ice body." Tellus B **55**(5): 1007-1017.

Ferrari, C. P., *T. Clotteau*, et al. (2001). "Heavy metals in ancient tropical ice: initial results." Atmospheric Environment **35**(33): 5809-5815.

Fischer, L. K., A.; Huggel, C.; Noetzli J. (2006). "Geology, glacier retreat and permafrost degradation as controlling factors of slope instabilities in a high-mountain rock wall: the Monte Rosa east face."

Gabrieli, J. (2008). "Trace elements and Polycyclic Aromatic Hydrocarbons (PAHs) in snow and ice sampled at Colle Gnifetti, Monte Rosa (4450 m), during the last 10,000 years: environmental and climatic implications." phD thesis, University Ca' Foscari of Venice.

Gabrieli, J., *P. Vallelonga*, et al. (2010). "Post 17th-Century Changes of European PAH Emissions Recorded in High-Altitude Alpine Snow and Ice." Environmental Science & Technology **44**(9): 3260-3266.

Gabrielli, P., *C. Barbante*, et al. (2004). "Meteoric smoke fallout over the Holocene epoch revealed by iridium and platinum in Greenland ice." Nature **432**(7020): 1011-1014.

Gabrielli, P., *G. Cozzi*, et al. (2008). "Trace elements in winter snow of the Dolomites (Italy): A statistical study of natural and anthropogenic contributions." Chemosphere **72**(10): 1504-1509.

Gaggeler, H., *H. R. Von Gunten*, et al. (1983). "210Pb- dating of cold alpine firn/ ice cores from Colle Gnifetti, Switzerland." Journal of Glaciology **29**(101): 165-177.

Gambaro, A., *R. Zangrando*, et al. (2008). "Direct Determination of Levoglucosan at the Picogram per Milliliter Level in Antarctic Ice by High-Performance Liquid Chromatography/Electrospray Ionization Triple Quadrupole Mass Spectrometry." Analytical Chemistry **80**(5): 1649-1655.

Giacosa, P. (1896). "Indagini sulle acque e sulle nevi delle alte regioni." Bollettino del Club Alpino Italiano **1**: 45-64.

Gudmundsson, G. H., *A. Bauder*, et al. (1999). "Estimating rates of basal motion and internal ice deformation from continuous tilt measurements." Annals of Glaciology **28**: 247-252.

Häberli, W., *W. Schmid*, et al. (1988). "On the geometry, flow and age of firn and ice at the Colle Gnifetti core drilling site." Zeitschrift fur Gletscherkunde und Glazialgeologie **24**: 1-19.

Hong, S., *C. Barbante*, et al. (2004). "Atmospheric heavy metals in tropical South America during the past 22,000 years recorded in a high altitude ice core from Sajama, Bolivia." Journal of environmental monitoring : JEM **6**(4): 322-326.

Hovmand, M. F., *K. Kemp*, et al. (2008). "Atmospheric heavy metal deposition accumulated in rural forest soils of southern Scandinavia." Environmental Pollution **155**(3): 537-541.

Jenk, T. M., *S. Szidat*, et al. (2009). "A novel radiocarbon dating technique applied to an ice core from the Alps indicating late Pleistocene ages." Journal of Geophysical Research D: Atmospheres **114**(14).

Jenk, T. M., *S. Szidat*, et al. (2007). "Microgram level radiocarbon (14C) determination on carbonaceous particles in ice." Nuclear Instruments and Methods in Physics Research Section B: Beam Interactions with Materials and Atoms **259**(1): 518-525.

Kappenberger, G., Kerkmann, J., (1997). "Il tempo in montagna. Manuale di meteorologia alpina."

Kaufmann, J. B., *K. M. Till*, et al. (1992). The Science of Global Change, American Chemical Society.

Keck, L. (2000). "Climate significance of Alpine ice core stable isotope records." PhD thesis, University Heidelberg.

Kirchgeorg, T., *I. Weinberg*, et al. (2010). "Perfluorinated compounds in marine surface waters: data from the Baltic Sea and methodological challenges for future studies." Environmental Chemistry **7**(5): 429-434.

Lantzy, R. J. and *F. T. Mackenzie* (1979). "Atmospheric trace metals: global cycles and assessment of man's impact." Geochimica et Cosmochimica Acta **43**(4): 511-525.

Lavanchy, V. M. H., *H. W. Gäggeler*, et al. (1999). "Historical record of carbonaceous particle concentrations from a European high-alpine glacier (Colle Gnifetti, Switzerland)." J. Geophys. Res. **104**(D17): 21227-21236.

Legrand, M., *M. De Angelis*, et al. (1992). "Large perturbations of ammonium and organic acids content in the summit‐Greenland Ice Core. Fingerprint from forest fires?" Geophys. Res. Lett. **19**(5): 473-475.

Legrand, M., *S. Preunkert*, et al. (2002). Seasonally resolved Alpine and Greenland ice core records of anthropogenic HCl Emissions over the 20th century.

Li, J., *J. R. Anderson*, et al. (2003). "TEM study of aerosol particles from clean and polluted marine boundary layers over the North Atlantic." J. Geophys. Res. **108**(D6): 4189.

Liu, K.-b., *C. A. Reese*, et al. (2005). "Ice-core pollen record of climatic changes in the central Andes during the last 400 yr." Quaternary Research **64**(2): 272-278.

Lüthi, M. and *M. Funk* (2000). "Dating ice cores from a high Alpine glacier with a flow model for cold firn." Annals of Glaciology **31**: 69-79.

Mann, M. E., *Z. Zhang*, et al. (2008). "Proxy-based reconstructions of hemispheric and global surface temperature variations over the past two millennia." Proceedings of the National Academy of Sciences **105**(36): 13252-13257.

Nriagu, J. O. (1979). "Global inventory of natural and anthropogenic emissions of trace metals into the atmosphere." Nature **279**: 409-411.

Nriagu, J. O. and J. M. Pacyna (1988). "Quantitative assessment of worldwide contamination of air, water and soils by trace metals." Nature **333**(6169): 134-139.

Oeschger, H. (1977). "First results from Alpine core drilling projects." Zeitschrift fur Gletscherkunde und Glazialgeologie **13**: 193-208.

Olivier, S., *S. Bajo*, et al. (2004). "Plutonium from Global Fallout Recorded in an Ice Core from the Belukha Glacier, Siberian Altai." Environmental Science & Technology **38**(24): 6507-6512.

Pacyna, E. G., *J. M. Pacyna*, et al. (2007). "Current and future emissions of selected heavy metals to the atmosphere from anthropogenic sources in Europe." Atmospheric Environment **41**(38): 8557-8566.

Pacyna, J. M. (1984). "Estimation of the atmospheric emissions of trace elements from anthropogenic sources in Europe." Atmospheric Environment (1967) **18**(1): 41-50.

Pacyna, J. M. (1986). "Atmospheric trace elements from natural and anthropogenic sources." Toxic Metals in the Atmosphere.

Pacyna, J. M. and *E. G. Pacyna* (2001). "An assessment of global and regional emissions of trace metals to the atmosphere from anthropogenic sources worldwide." Environmental Reviews **9**(4): 269.

Pacyna, J. M., *M. T. Scholtz*, et al. (1995). "Global budget of trace metal sources." Environmental Reviews **3**(2): 145-159.

Pacyna, J. M., *A. Semb*, et al. (1984). "Emission and long-range transport of trace elements in Europe." Tellus B **36B**(3): 163-178.

Palmer, A. S., *T. D. van Ommen*, et al. (2001). "High-precision dating of volcanic events (A.D. 1301–1995) using ice cores from Law Dome, Antarctica." J. Geophys. Res. **106**(D22): 28089-28095.

Pipino, G. (2003). "Oro, miniere, storia: miscellanea di giacimentologia e storia mineraria italiana."

Planchon, F. A. M., *C. F. Boutron*, et al. (2001). "Ultrasensitive determination of heavy metals at the sub-picogram per gram level in ultraclean Antarctic snow samples by inductively coupled plasma sector field mass spectrometry." Analytica Chimica Acta **450**(1–2): 193-205.

Rampino, M. R. and *S. Self* (1993). "Volcanic winter and accelerated glaciation following the Toba supereruption." Nature **359**: 50-52.

Raynaud, D., Blunier, T., Ono Y., Delmas, R.J., (2003). "The Late Quaternary history of atmospheric trace gases and aerosols: interactions between climate and biogeochemical cycles." Paleoclimate, global change and the future(Springer Verlag): 13-33.

Schotterer, U., *H. Oeschger*, et al. (1985). "Information on paleo-precipitation on a high-altitude glacier Monte Rosa, Switzerland." Zeitschrift fur Gletscherkunde und Glazialgeologie **21**: 379-388.

Schwikowski, B. M., *A. Döscher*, et al. (1999). "Anthropogenic versus natural sources of atmospheric sulphate from an Alpine ice core." Tellus B **51**(5): 938-951.

Schwikowski, M. (2004). Reconstruction of European Air Pollution from Alpine Ice Cores

Earth Paleoenvironments: Records Preserved in Mid- and Low-Latitude Glaciers. L. DeWayne Cecil, J. Green and L. Thompson, Springer Netherlands. **9:** 95-119.

Siegenthaler, U. and *H. Oeschger* (1980). "Correlation of 18O in precipitation with temperature and altitude." Nature **285**(5763): 314-317.

Sigl, M. (2009). "Ice core based reconstruction of past climate conditions from Colle Gnifetti, Swiss Alps " PhD thesis, University Bern.

Strabo (I century b.C. - I century A.D.). "Geography." **V book**.

Vallelonga, P., *K. Van de Velde*, et al. (2002). "Recent advances in measurement of Pb isotopes in polar ice and snow at sub-picogram per gram concentrations using thermal ionisation mass spectrometry." Analytica Chimica Acta **453**(1): 1-12.

Villa, S., *C. Negrelli*, et al. (2006). "Analysis of a firn core for assessing POP seasonal accumulation on an Alpine glacier." Ecotoxicology and Environmental Safety **63**(1): 17-24.

Villa, S., *M. Vighi*, et al. (2003). "Historical Trends of Organochlorine Pesticides in an Alpine Glacier." Journal of Atmospheric Chemistry **46**(3): 295-311.

Wagenbach, *D.*, et al. (1988). "The Anthropogenic Impact of Snow Chemistry on Colle Gnifetti, Swiss Alps." Annals of Glaciology **10**.

Warneke, T., *I. W. Croudace*, et al. (2002). "A new ground-level fallout record of uranium and plutonium isotopes for northern temperate latitudes." Earth and Planetary Science Letters **203**(3–4): 1047-1057.

Wedepohl, H. K. (1995). "The composition of the continental crust." Geochimica et Cosmochimica Acta **59**(7): 1217-1232.

Weisel, C. P. (1981). "The atmospheric flux of elements from the ocean." **PhD Thesis, University of Rhode Island, R. I. Kingston**.

6. ATTACHMENTS

6.1 CG11 CORE PROFILE

The following CG11 ice core profile has been created using the observational data recorded first on the field during the drilling campaign, and later in the Ca' Foscari Environmental Science department cold room during the core cutting process.

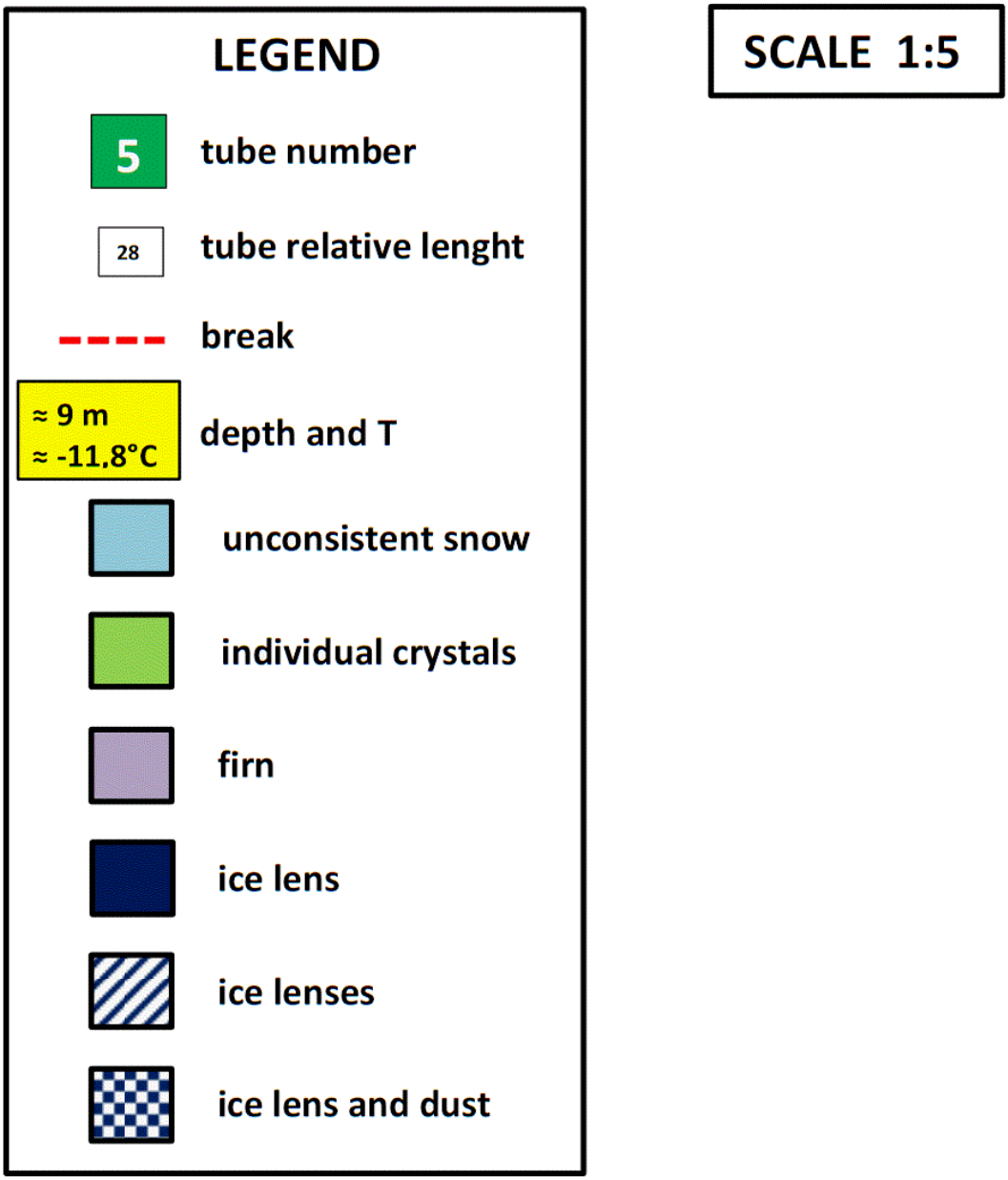

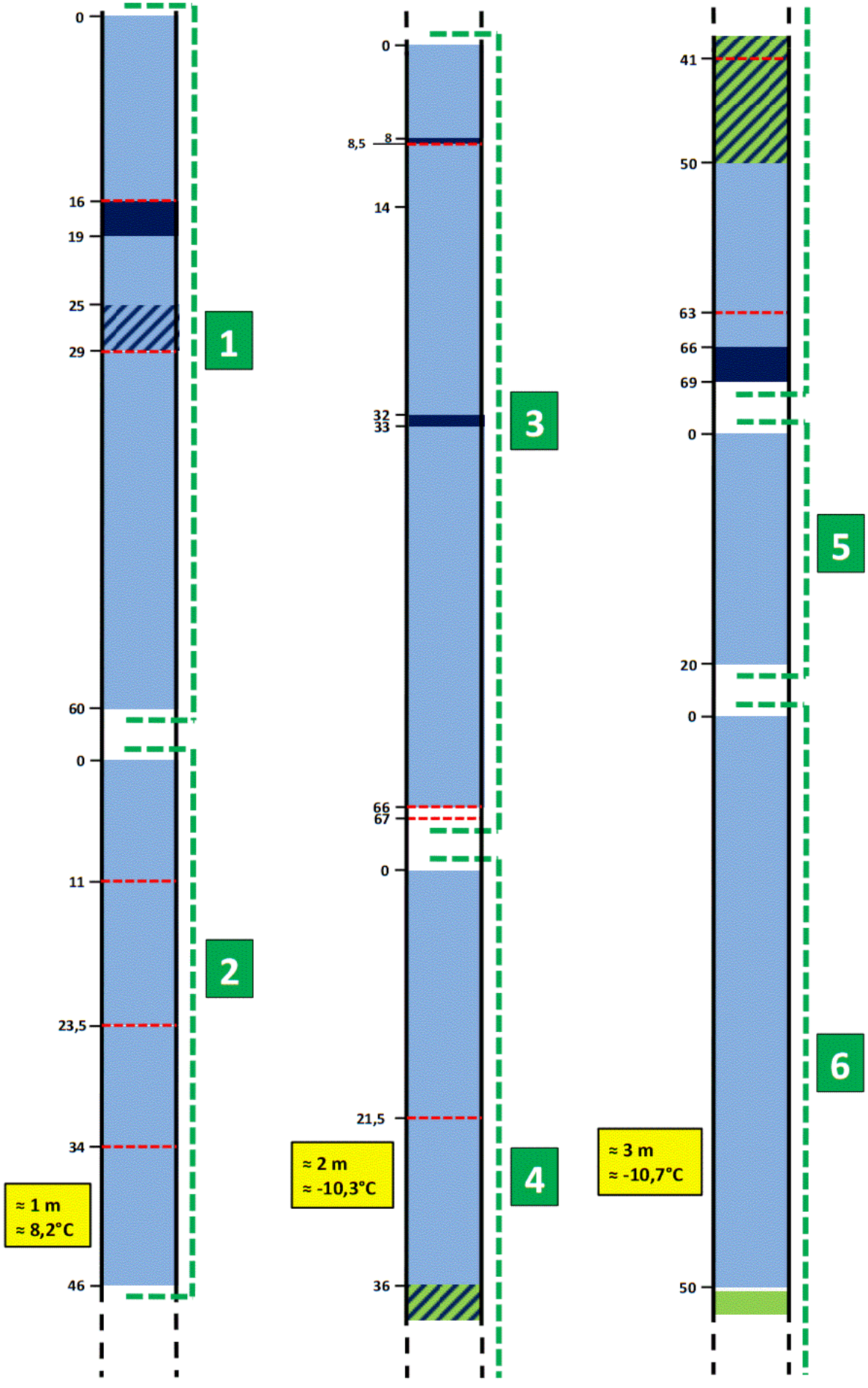
0
16
19
25
29
1
60
0
11
2
23,5
34
≈ 1 m
≈ 8,2°C
46
0
8,5
8
14
32
33
3
66
67
0
21,5
≈ 2 m
≈ -10,3°C
4
36
41
50
63
66
69
0
5
20
0
6
≈ 3 m
≈ -10,7°C
50

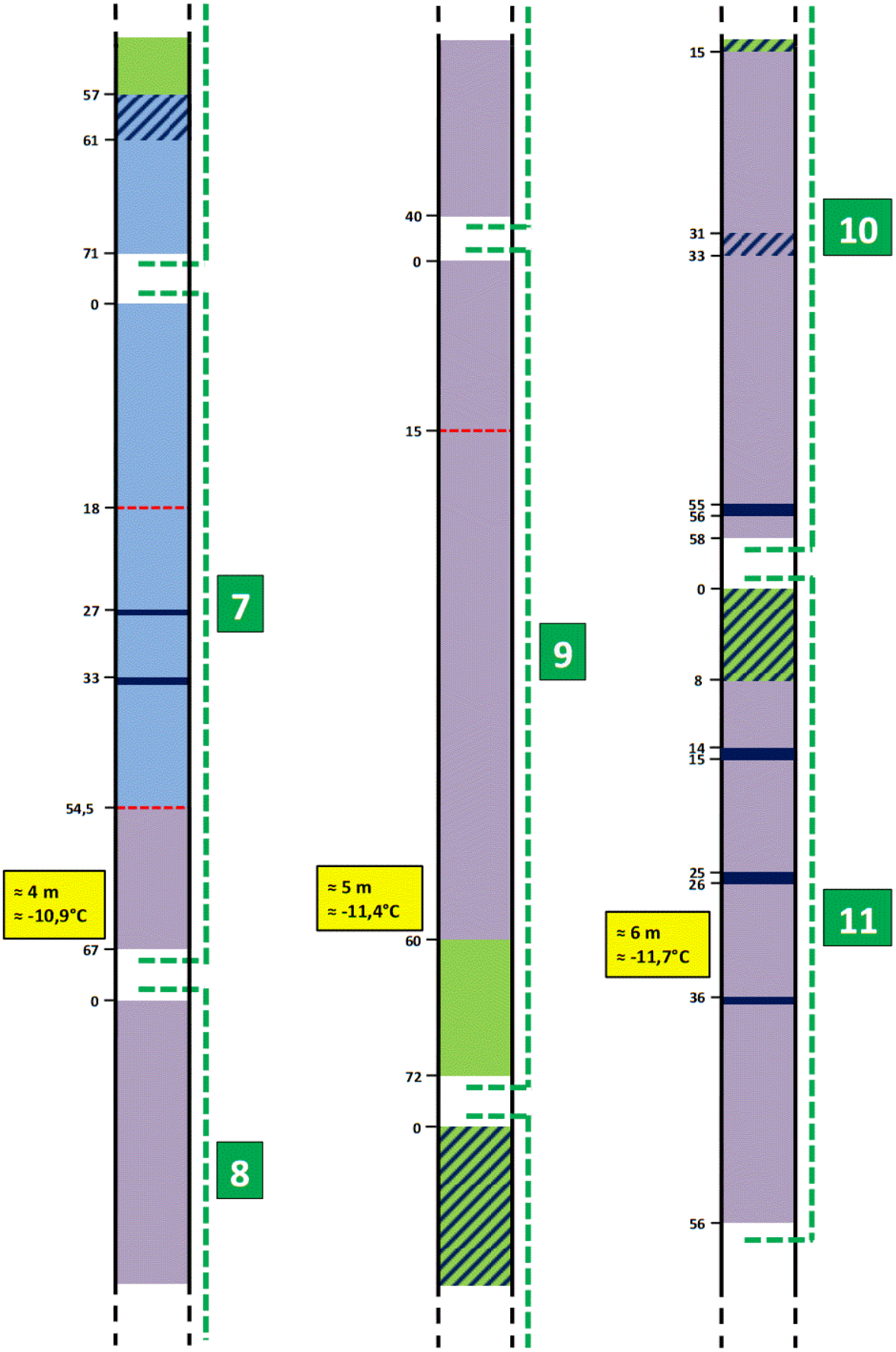
57
61
71
0
18
27
33
54,5
67
0
7
8
≈ 4 m
≈ -10,9°C
40
0
15
60
72
0
9
≈ 5 m
≈ -11,4°C
15
31
33
55
56
58
0
8
14
15
25
26
36
56
10
11
≈ 6 m
≈ -11,7°C

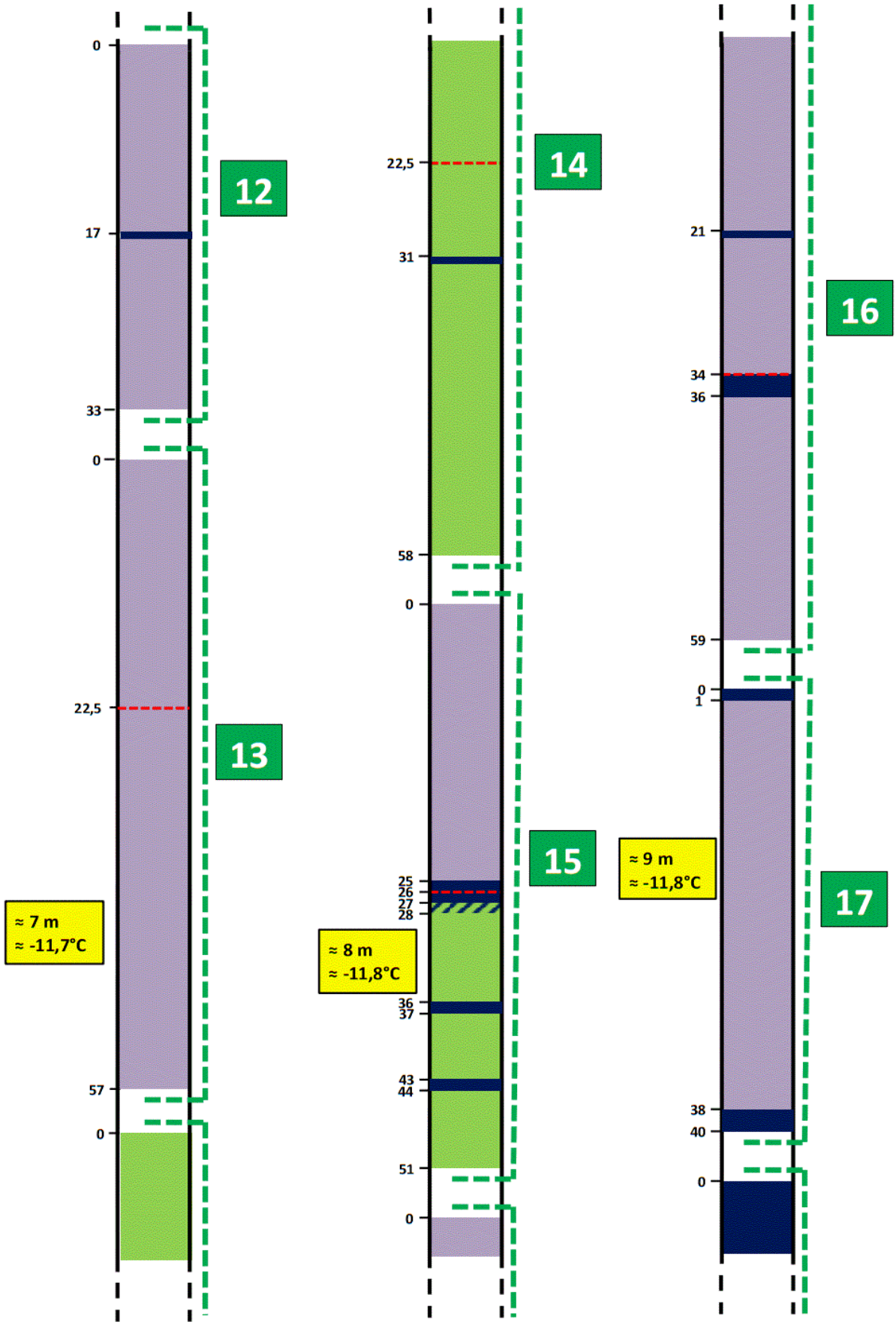
0
17
33
0
22,5
57
0
12
13
≈ 7 m
≈ -11,7°C
22,5
31
58
0
25
26
27
28
36
37
43
44
51
0
14
15
≈ 8 m
≈ -11,8°C
21
34
36
59
0
1
38
40
0
16
17
≈ 9 m
≈ -11,8°C

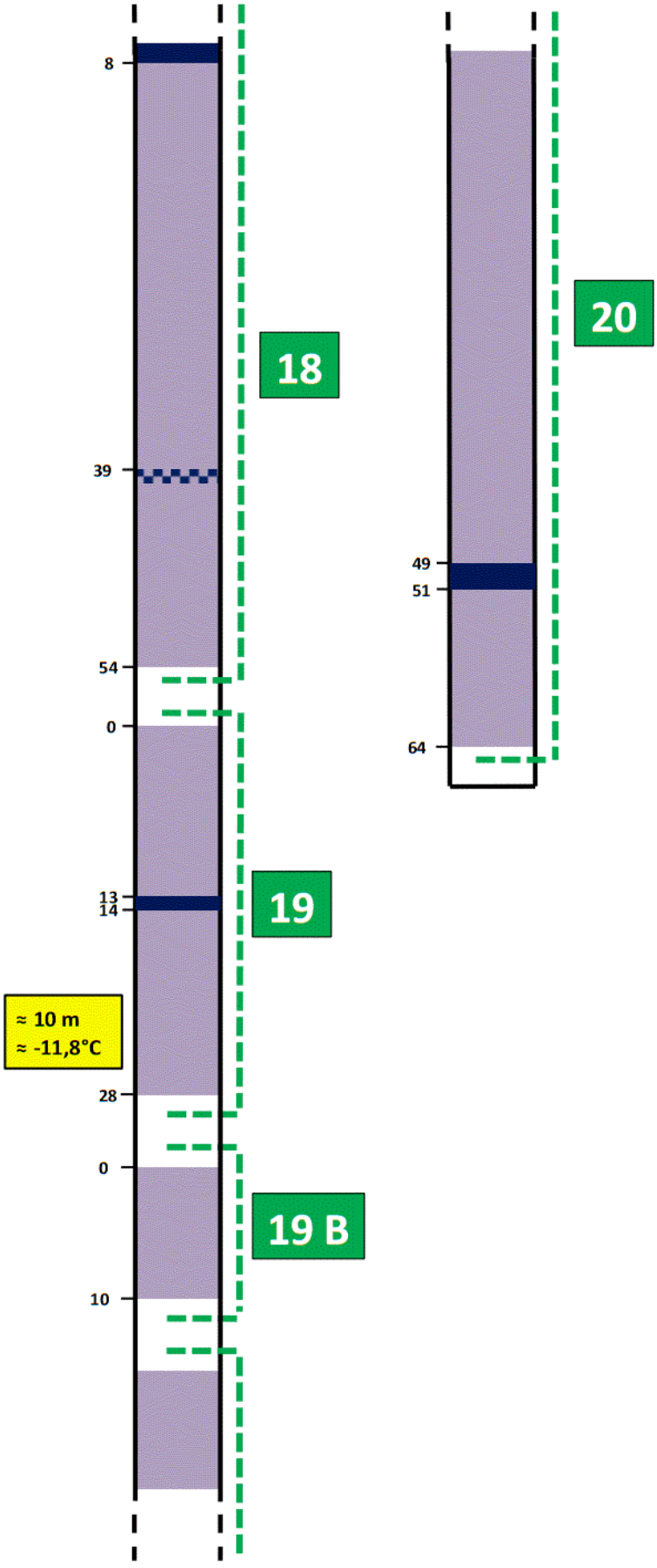
8
39
54
0
13
14
28
0
10
18
19
19 B
≈ 10 m
≈ -11,8°C
49
51
64
20

6.2 TABLES AND MATRICES PRODUCED BY EFA AND PCA CALCULATIONS

Variables	Na	Mg	Al	K	Ca	Ti	Fe	Ba
Na	**1**	0,840	0,347	0,827	0,610	0,448	0,337	0,475
Mg	0,840	**1**	0,538	0,803	0,836	0,664	0,572	0,710
Al	0,347	0,538	**1**	0,448	0,522	0,605	0,585	0,508
K	0,827	0,803	0,448	**1**	0,674	0,546	0,553	0,605
Ca	0,610	0,836	0,522	0,674	**1**	0,678	0,595	0,732
Ti	0,448	0,664	0,605	0,546	0,678	**1**	0,736	0,604
Fe	0,337	0,572	0,585	0,553	0,595	0,736	**1**	0,602
Ba	0,475	0,710	0,508	0,605	0,732	0,604	0,602	**1**

Table 19: box-cox transformed Q2 data EFA-PCA correlation matrix (Pearson)

	F1	F2	F3	F4	Initial communality	Final communality
Na	**0,771**	0,587	0,152	-0,195	1,000	**1,000**
Mg	**0,927**	0,234	0,002	0,099	1,000	0,923
Al	**0,698**	-0,462	0,538	0,006	1,000	0,990
K	**0,822**	0,273	-0,002	-0,137	1,000	0,769
Ca	**0,866**	0,028	-0,130	0,303	1,000	0,859
Ti	**0,770**	-0,246	-0,086	-0,007	1,000	0,661
Fe	**0,766**	-0,454	-0,290	-0,301	1,000	0,968
Ba	**0,765**	-0,079	-0,122	0,184	1,000	0,640

Table 20: box-cox transformed Q2 data EFA factor pattern

Variables	Na	Mg	K	Ca	Ti	Fe	Ba
Na	**1**	0,843	-0,192	-0,238	-0,048	-0,090	-0,036
Mg	0,843	**1**	-0,226	-0,283	-0,066	-0,065	-0,060
K	-0,192	-0,226	**1**	0,686	0,513	0,524	0,110
Ca	-0,238	-0,283	0,686	**1**	0,636	0,574	0,137
Ti	-0,048	-0,066	0,513	0,636	**1**	0,704	0,044
Fe	-0,090	-0,065	0,524	0,574	0,704	**1**	0,081
Ba	-0,036	-0,060	0,110	0,137	0,044	0,081	**1**

Table 21: ranked Q2 data correlation matrix (Pearson)

	F1	F2	F3	Initial communality	Final communality
Na	-0,450	**0,745**	-0,045	1,000	0,760
Mg	-0,501	**0,820**	-0,029	1,000	0,925
K	**0,707**	0,151	0,021	1,000	0,524
Ca	**0,821**	0,157	0,018	1,000	0,699
Ti	**0,721**	0,379	0,105	1,000	0,674
Fe	**0,696**	0,339	0,065	1,000	0,604
Ba	0,192	0,011	**-0,969**	1,000	0,975

Table 22: ranked Q2 data EFA factor pattern

Variables	Na	Mg	K	Ca	Ti	Fe	Ba
Na	**1**	0,843	-0,181	-0,230	-0,041	-0,091	-0,040
Mg	0,843	**1**	-0,217	-0,275	-0,056	-0,066	-0,063
K	-0,181	-0,217	**1**	0,683	0,510	0,527	0,113
Ca	-0,230	-0,275	0,683	**1**	0,632	0,577	0,140
Ti	-0,041	-0,056	0,510	0,632	**1**	0,709	0,046
Fe	-0,091	-0,066	0,527	0,577	0,709	**1**	0,081
Ba	-0,040	-0,063	0,113	0,140	0,046	0,081	**1**

Table 23: ranked Q2 data PCA correlation matrix (Pearson)

	F1	F2	F3	F4	F5	F6	F7	F8
Na	0,760	0,578	0,194	0,062	0,026	-0,077	-0,138	-0,145
Mg	0,926	0,250	-0,006	-0,057	0,107	0,034	-0,170	0,187
Al	0,688	-0,425	0,485	-0,330	-0,045	0,017	0,014	-0,010
K	0,846	0,352	0,108	0,151	-0,237	-0,001	0,258	0,056
Ca	0,878	0,032	-0,231	-0,145	0,232	0,292	0,103	-0,066
Ti	0,811	-0,344	-0,005	0,240	0,318	-0,243	0,078	-0,001
Fe	0,761	-0,447	-0,045	0,354	-0,226	0,158	-0,131	-0,027
Ba	0,810	-0,106	-0,402	-0,286	-0,219	-0,201	-0,024	-0,029

Table 24: box-cox transformed Q2 data PCA factor loadings

	F1	F2	F3	F4	F5	F6	F7
Na	-0,411	0,858	0,066	0,125	-0,061	-0,003	-0,268
Mg	-0,433	0,854	0,037	0,045	0,036	-0,043	0,275
K	0,797	0,118	0,012	0,507	0,247	0,177	0,011
Ca	0,866	0,097	0,016	0,221	-0,329	-0,287	0,024
Ti	0,781	0,370	-0,120	-0,302	-0,230	0,307	0,021
Fe	0,780	0,332	-0,077	-0,352	0,330	-0,201	-0,048
Ba	0,178	-0,022	0,980	-0,084	0,003	0,026	0,006

Table 25: ranked Q2 data PCA factor loadings

Table 26: raw E2 data EFA-PCA correlation matrix (Pearson)

/ariable	Ca	Mg	Na	K	Fe	Al	Ti	Ba	Li	Be	Rb	Sr	Ag	Sn	Cs	Tl	Pb	U	Bi	Cd	V	Cr	Mn	Co	Ni	Cu	Ga
Ca	**1**	0,972	0,876	0,923	0,956	0,967	0,823	0,963	0,300	0,973	0,864	0,984	0,543	0,443	0,812	0,607	0,731	0,910	0,212	0,859	0,844	0,950	0,959	0,841	0,838	0,536	0,971
Mg	0,972	**1**	0,936	0,972	0,988	0,994	0,902	0,996	0,474	0,985	0,935	0,996	0,620	0,574	0,894	0,685	0,802	0,967	0,255	0,911	0,917	0,977	0,994	0,911	0,904	0,612	0,978
Na	0,876	0,936	**1**	0,905	0,915	0,924	0,866	0,929	0,524	0,920	0,897	0,922	0,609	0,574	0,845	0,674	0,769	0,925	0,251	0,873	0,892	0,913	0,925	0,860	0,863	0,585	0,895
K	0,923	0,972	0,905	**1**	0,981	0,974	0,916	0,973	0,528	0,940	0,968	0,954	0,656	0,713	0,927	0,796	0,885	0,960	0,378	0,918	0,930	0,950	0,984	0,961	0,943	0,734	0,963
Fe	0,956	0,988	0,915	0,981	**1**	0,996	0,934	0,986	0,485	0,966	0,949	0,976	0,640	0,623	0,918	0,725	0,839	0,962	0,311	0,907	0,916	0,978	0,988	0,943	0,920	0,679	0,991
Al	0,967	0,994	0,924	0,974	0,996	**1**	0,914	0,992	0,476	0,973	0,935	0,987	0,643	0,580	0,909	0,698	0,811	0,962	0,269	0,910	0,905	0,974	0,987	0,930	0,900	0,628	0,989
Ti	0,823	0,902	0,866	0,916	0,934	0,914	**1**	0,895	0,521	0,865	0,932	0,870	0,698	0,696	0,887	0,722	0,855	0,901	0,316	0,884	0,937	0,948	0,920	0,906	0,922	0,747	0,904
Ba	0,963	0,996	0,929	0,973	0,986	0,992	0,895	**1**	0,512	0,977	0,936	0,992	0,607	0,595	0,907	0,702	0,812	0,966	0,258	0,900	0,909	0,963	0,988	0,924	0,904	0,621	0,977
Li	0,300	0,474	0,524	0,528	0,485	0,476	0,521	0,512	**1**	0,458	0,564	0,432	0,260	0,621	0,580	0,524	0,480	0,602	0,268	0,412	0,482	0,405	0,480	0,565	0,523	0,454	0,409
Be	0,973	0,985	0,920	0,940	0,966	0,973	0,865	0,977	0,458	**1**	0,914	0,986	0,546	0,510	0,832	0,660	0,754	0,972	0,278	0,867	0,884	0,963	0,974	0,860	0,881	0,582	0,960
Rb	0,864	0,935	0,897	0,968	0,949	0,935	0,932	0,936	0,564	0,914	**1**	0,906	0,666	0,780	0,916	0,860	0,933	0,963	0,466	0,913	0,960	0,934	0,955	0,954	0,983	0,814	0,925
Sr	0,984	0,996	0,922	0,954	0,976	0,987	0,870	0,992	0,432	0,986	0,906	**1**	0,585	0,515	0,870	0,641	0,767	0,951	0,208	0,890	0,892	0,966	0,983	0,881	0,875	0,560	0,974
Ag	0,543	0,620	0,609	0,656	0,640	0,643	0,698	0,607	0,260	0,546	0,666	0,585	**1**	0,506	0,698	0,576	0,639	0,606	0,217	0,792	0,695	0,652	0,629	0,696	0,631	0,476	0,616
Sn	0,443	0,574	0,574	0,713	0,623	0,580	0,696	0,595	0,621	0,510	0,780	0,515	0,506	**1**	0,718	0,866	0,894	0,643	0,631	0,663	0,748	0,582	0,630	0,787	0,808	0,908	0,581
Cs	0,812	0,894	0,845	0,927	0,918	0,909	0,887	0,907	0,580	0,832	0,916	0,870	0,698	0,718	**1**	0,740	0,858	0,881	0,280	0,875	0,875	0,869	0,907	0,945	0,883	0,677	0,892
Tl	0,607	0,685	0,674	0,796	0,725	0,698	0,722	0,702	0,524	0,660	0,860	0,641	0,576	0,866	0,740	**1**	0,907	0,764	0,673	0,742	0,775	0,669	0,724	0,842	0,850	0,880	0,702
Pb	0,731	0,802	0,769	0,885	0,839	0,811	0,855	0,812	0,480	0,754	0,933	0,767	0,639	0,894	0,858	0,907	**1**	0,820	0,517	0,855	0,921	0,821	0,844	0,910	0,952	0,915	0,822
U	0,910	0,967	0,925	0,960	0,962	0,962	0,901	0,966	0,602	0,972	0,963	0,951	0,606	0,643	0,881	0,764	0,820	**1**	0,394	0,886	0,908	0,942	0,966	0,912	0,921	0,675	0,938
Bi	0,212	0,255	0,251	0,378	0,311	0,269	0,316	0,258	0,268	0,278	0,466	0,208	0,217	0,631	0,280	0,673	0,517	0,394	**1**	0,313	0,342	0,271	0,295	0,444	0,462	0,671	0,304
Cd	0,859	0,911	0,873	0,918	0,907	0,910	0,884	0,900	0,412	0,867	0,913	0,890	0,792	0,663	0,875	0,742	0,855	0,886	0,313	**1**	0,929	0,914	0,919	0,894	0,889	0,661	0,886
V	0,844	0,917	0,892	0,930	0,916	0,905	0,937	0,909	0,482	0,884	0,960	0,892	0,695	0,748	0,875	0,775	0,921	0,908	0,342	0,929	**1**	0,944	0,941	0,895	0,967	0,773	0,889
Cr	0,950	0,977	0,913	0,950	0,978	0,974	0,948	0,963	0,405	0,963	0,934	0,966	0,652	0,582	0,869	0,669	0,821	0,942	0,271	0,914	0,944	**1**	0,980	0,896	0,922	0,664	0,971
Mn	0,959	0,994	0,925	0,984	0,988	0,987	0,920	0,988	0,480	0,974	0,955	0,983	0,629	0,630	0,907	0,724	0,844	0,966	0,295	0,919	0,941	0,980	**1**	0,925	0,934	0,672	0,974
Co	0,841	0,911	0,860	0,961	0,943	0,930	0,906	0,924	0,565	0,860	0,954	0,881	0,696	0,787	0,945	0,842	0,910	0,912	0,444	0,894	0,895	0,896	0,925	**1**	0,935	0,796	0,933
Ni	0,838	0,904	0,863	0,943	0,920	0,900	0,922	0,904	0,523	0,881	0,983	0,875	0,631	0,808	0,883	0,850	0,952	0,921	0,462	0,889	0,967	0,922	0,934	0,935	**1**	0,862	0,902
Cu	0,536	0,612	0,585	0,734	0,679	0,628	0,747	0,621	0,454	0,582	0,814	0,560	0,476	0,908	0,677	0,880	0,915	0,675	0,671	0,661	0,773	0,664	0,672	0,796	0,862	**1**	0,665
Ga	0,971	0,978	0,895	0,963	0,991	0,989	0,904	0,977	0,409	0,960	0,925	0,974	0,616	0,581	0,892	0,702	0,822	0,938	0,304	0,886	0,889	0,971	0,974	0,933	0,902	0,665	**1**

	F1	F2	Initial communality	Final communality	Specific variance
Ca	**0,913**	0,334	0,991	0,945	0,055
Mg	**0,973**	0,229	0,996	0,998	0,002
Na	**0,919**	0,162	0,903	0,871	0,129
K	**0,989**	0,028	0,991	0,979	0,021
Fe	**0,983**	0,147	0,993	0,988	0,012
Al	**0,975**	0,208	0,994	0,993	0,007
Ti	**0,941**	-0,004	0,982	0,885	0,115
Ba	**0,973**	0,202	0,990	0,986	0,014
Li	**0,523**	-0,209	0,906	0,318	0,682
Be	**0,943**	0,255	0,995	0,955	0,045
Rb	**0,988**	-0,113	0,993	0,990	0,010
Sr	**0,950**	0,297	0,993	0,991	0,009
Ag	**0,667**	-0,031	0,827	0,446	0,554
Sn	**0,734**	-0,637	0,968	0,945	0,055
Cs	**0,927**	-0,008	0,959	0,860	0,140
Tl	**0,812**	-0,480	0,954	0,889	0,111
Pb	**0,910**	-0,341	0,990	0,944	0,056
U	**0,969**	0,072	0,988	0,944	0,056
Bi	0,390	**-0,563**	0,808	0,469	0,531
Cd	**0,932**	0,044	0,950	0,871	0,129
V	**0,958**	-0,045	0,992	0,920	0,080
Cr	**0,965**	0,189	0,995	0,968	0,032
Mn	**0,984**	0,153	0,990	0,992	0,008
Co	**0,966**	-0,118	0,990	0,948	0,052
Ni	**0,968**	-0,162	0,988	0,964	0,036
Cu	**0,764**	-0,565	0,970	0,903	0,097
Ga	**0,964**	0,178	0,992	0,961	0,039

Table 27: raw E2 data EFA factor pattern

Variables	Ca	Mg	Na	K	Fe	Al	Ti	Ba	Be	Rb	Sr	Ag	Sn	Cs	Tl	Pb	U	Bi	Cd	V	Cr	Mn	Co	Ni	Cu	Ga
Ca	**1**	0,948	0,840	0,904	0,791	-0,282	-0,232	-0,244	-0,003	-0,269	-0,194	-0,255	-0,241	-0,323	-0,302	-0,334	-0,177	-0,002	-0,286	-0,240	-0,173	-0,316	-0,314	-0,347	-0,258	-0,214
Mg	0,948	**1**	0,856	0,928	0,862	-0,256	-0,209	-0,209	0,032	-0,248	-0,169	-0,236	-0,281	-0,290	-0,303	-0,335	-0,159	-0,028	-0,289	-0,252	-0,181	-0,291	-0,289	-0,311	-0,262	-0,190
Na	0,840	0,856	**1**	0,777	0,606	-0,162	-0,132	-0,144	0,092	-0,175	-0,070	-0,199	-0,104	-0,243	-0,216	-0,201	-0,090	0,141	-0,174	-0,123	-0,038	-0,178	-0,204	-0,259	-0,155	-0,108
K	0,904	0,928	0,777	**1**	0,873	-0,304	-0,274	-0,260	0,002	-0,298	-0,223	-0,267	-0,295	-0,312	-0,363	-0,371	-0,167	-0,064	-0,321	-0,306	-0,251	-0,336	-0,333	-0,365	-0,333	-0,237
Fe	0,791	0,862	0,606	0,873	**1**	-0,348	-0,283	-0,296	-0,061	-0,323	-0,316	-0,288	-0,360	-0,292	-0,410	-0,425	-0,207	-0,096	-0,405	-0,378	-0,298	-0,390	-0,364	-0,350	-0,355	-0,271
Al	-0,282	-0,256	-0,162	-0,304	-0,348	**1**	0,962	0,850	0,824	0,926	0,818	0,694	0,794	0,902	0,865	0,878	0,823	0,649	0,699	0,868	0,916	0,884	0,905	0,769	0,805	0,985
Ti	-0,232	-0,209	-0,132	-0,274	-0,283	0,962	**1**	0,833	0,821	0,946	0,763	0,726	0,800	0,929	0,868	0,882	0,856	0,696	0,695	0,855	0,925	0,874	0,915	0,803	0,817	0,969
Ba	-0,244	-0,209	-0,144	-0,260	-0,296	0,850	0,833	**1**	0,786	0,851	0,879	0,569	0,719	0,756	0,853	0,797	0,734	0,586	0,753	0,856	0,826	0,883	0,855	0,703	0,815	0,829
Be	-0,003	0,032	0,092	0,002	-0,061	0,824	0,821	0,786	**1**	0,810	0,776	0,599	0,670	0,785	0,769	0,756	0,785	0,681	0,694	0,788	0,830	0,806	0,792	0,686	0,702	0,842
Rb	-0,269	-0,248	-0,175	-0,298	-0,323	0,926	0,946	0,851	0,810	**1**	0,818	0,726	0,835	0,952	0,933	0,928	0,908	0,720	0,797	0,905	0,889	0,943	0,977	0,832	0,816	0,922
Sr	-0,194	-0,169	-0,070	-0,223	-0,316	0,818	0,763	0,879	0,776	0,818	**1**	0,598	0,704	0,701	0,855	0,772	0,694	0,589	0,801	0,874	0,791	0,897	0,831	0,682	0,733	0,790
Ag	-0,255	-0,236	-0,199	-0,267	-0,288	0,694	0,726	0,569	0,599	0,726	0,598	**1**	0,630	0,758	0,702	0,710	0,704	0,557	0,680	0,657	0,675	0,645	0,714	0,737	0,643	0,680
Sn	-0,241	-0,281	-0,104	-0,295	-0,360	0,794	0,800	0,719	0,670	0,835	0,704	0,630	**1**	0,793	0,847	0,899	0,767	0,797	0,786	0,867	0,786	0,814	0,826	0,727	0,761	0,802
Cs	-0,323	-0,290	-0,243	-0,312	-0,292	0,902	0,929	0,756	0,785	0,952	0,701	0,758	0,793	**1**	0,862	0,894	0,925	0,700	0,746	0,812	0,836	0,863	0,931	0,829	0,771	0,908
Tl	-0,302	-0,303	-0,216	-0,363	-0,410	0,865	0,868	0,853	0,769	0,933	0,855	0,702	0,847	0,862	**1**	0,942	0,807	0,705	0,884	0,941	0,845	0,915	0,925	0,805	0,803	0,856
Pb	-0,334	-0,335	-0,201	-0,371	-0,425	0,878	0,882	0,797	0,756	0,928	0,772	0,710	0,899	0,894	0,942	**1**	0,819	0,751	0,873	0,910	0,846	0,887	0,905	0,806	0,797	0,874
U	-0,177	-0,159	-0,090	-0,167	-0,207	0,823	0,856	0,734	0,785	0,908	0,694	0,704	0,767	0,925	0,807	0,819	**1**	0,724	0,753	0,785	0,815	0,851	0,906	0,783	0,767	0,831
Bi	-0,002	-0,028	0,141	-0,064	-0,096	0,649	0,696	0,586	0,681	0,720	0,589	0,557	0,797	0,700	0,705	0,751	0,724	**1**	0,653	0,731	0,780	0,665	0,675	0,688	0,729	0,686
Cd	-0,286	-0,289	-0,174	-0,321	-0,405	0,699	0,695	0,753	0,694	0,797	0,801	0,680	0,786	0,746	0,884	0,873	0,753	0,653	**1**	0,840	0,708	0,825	0,816	0,720	0,720	0,683
V	-0,240	-0,252	-0,123	-0,306	-0,378	0,868	0,855	0,856	0,788	0,905	0,874	0,657	0,867	0,812	0,941	0,910	0,785	0,731	0,840	**1**	0,881	0,923	0,899	0,786	0,810	0,855
Cr	-0,173	-0,181	-0,038	-0,251	-0,298	0,916	0,925	0,826	0,830	0,889	0,791	0,675	0,826	0,836	0,845	0,846	0,815	0,780	0,708	0,881	**1**	0,859	0,877	0,821	0,889	0,919
Mn	-0,316	-0,291	-0,178	-0,336	-0,390	0,884	0,874	0,883	0,806	0,943	0,897	0,645	0,814	0,863	0,915	0,887	0,851	0,665	0,825	0,923	0,859	**1**	0,966	0,803	0,807	0,857
Co	-0,314	-0,289	-0,204	-0,333	-0,364	0,905	0,915	0,855	0,792	0,977	0,831	0,714	0,826	0,931	0,925	0,905	0,906	0,675	0,816	0,899	0,877	0,966	**1**	0,853	0,829	0,890
Ni	-0,347	-0,311	-0,259	-0,365	-0,350	0,769	0,803	0,703	0,686	0,832	0,682	0,737	0,727	0,829	0,805	0,806	0,783	0,688	0,720	0,786	0,821	0,803	0,853	**1**	0,873	0,770
Cu	-0,258	-0,262	-0,155	-0,333	-0,355	0,805	0,817	0,815	0,702	0,816	0,733	0,643	0,761	0,771	0,803	0,797	0,767	0,729	0,720	0,810	0,889	0,807	0,829	0,873	**1**	0,804
Ga	-0,214	-0,190	-0,108	-0,237	-0,271	0,985	0,969	0,829	0,842	0,922	0,790	0,680	0,802	0,908	0,856	0,874	0,831	0,686	0,683	0,855	0,919	0,857	0,890	0,770	0,804	**1**

Table 28: ranked E2 data EFA correlation matrix (Pearson)

	F1	F2	F3	F4	Initial communality	Final communality	Specific variance
Ca	-0,345	**0,892**	-0,064	-0,055	1,000	0,922	0,078
Mg	-0,335	**0,934**	-0,016	0,050	1,000	0,987	0,013
Na	-0,217	**0,818**	-0,143	-0,111	1,000	0,748	0,252
K	-0,380	**0,875**	0,030	0,038	1,000	0,913	0,087
Fe	-0,414	**0,753**	0,177	0,064	1,000	0,773	0,227
Al	**0,941**	0,062	0,098	0,201	1,000	0,939	0,061
Ti	**0,943**	0,112	0,191	0,125	1,000	0,953	0,047
Ba	**0,877**	0,078	-0,195	0,235	1,000	0,869	0,131
Be	**0,822**	0,342	0,000	0,132	1,000	0,810	0,190
Rb	**0,972**	0,075	0,081	0,052	1,000	0,961	0,039
Sr	**0,857**	0,111	-0,351	0,200	1,000	0,909	0,091
Ag	**0,743**	-0,001	0,155	-0,084	1,000	0,583	0,417
Sn	**0,874**	0,046	-0,064	-0,265	1,000	0,840	0,160
Cs	**0,934**	0,028	0,302	0,013	1,000	0,965	0,035
Tl	**0,952**	0,000	-0,143	-0,033	1,000	0,929	0,071
Pb	**0,951**	-0,015	-0,036	-0,144	1,000	0,926	0,074
U	**0,883**	0,160	0,188	-0,048	1,000	0,843	0,157
Bi	**0,748**	0,286	0,025	-0,392	1,000	0,795	0,205
Cd	**0,847**	-0,015	-0,235	-0,157	1,000	0,797	0,203
V	**0,940**	0,067	-0,212	-0,038	1,000	0,935	0,065
Cr	**0,925**	0,153	0,035	-0,014	1,000	0,881	0,119
Mn	**0,952**	0,022	-0,136	0,105	1,000	0,935	0,065
Co	**0,968**	0,027	0,032	0,065	1,000	0,942	0,058
Ni	**0,866**	-0,039	0,135	-0,116	1,000	0,784	0,216
Cu	**0,872**	0,030	0,004	-0,083	1,000	0,769	0,231
Ga	**0,930**	0,135	0,142	0,159	1,000	0,929	0,071

Table 29: ranked E2 data EFA factor pattern

Variable	Ca	Mg	Na	K	Fe	Al	Ti	Ba	Be	Rb	Sr	Ag	Sn	Cs	Tl	Pb	U	Bi	Cd	V	Cr	Mn	Co	Ni	Cu	Ga
Ca	**1**	0,945	0,831	0,899	0,812	-0,301	-0,241	-0,271	0,000	-0,300	-0,232	-0,278	-0,258	-0,336	-0,345	-0,373	-0,181	-0,005	-0,319	-0,267	-0,170	-0,335	-0,330	-0,364	-0,261	-0,226
Mg	0,945	**1**	0,848	0,925	0,886	-0,273	-0,216	-0,235	0,037	-0,277	-0,206	-0,258	-0,300	-0,301	-0,345	-0,374	-0,161	-0,033	-0,322	-0,279	-0,179	-0,309	-0,303	-0,326	-0,265	-0,200
Na	0,831	0,848	**1**	0,764	0,623	-0,177	-0,138	-0,169	0,099	-0,203	-0,105	-0,221	-0,114	-0,253	-0,256	-0,236	-0,090	0,144	-0,204	-0,147	-0,029	-0,193	-0,216	-0,274	-0,154	-0,116
K	0,899	0,925	0,764	**1**	0,896	-0,328	-0,288	-0,292	-0,001	-0,334	-0,266	-0,295	-0,322	-0,331	-0,412	-0,416	-0,177	-0,077	-0,360	-0,339	-0,259	-0,360	-0,354	-0,387	-0,345	-0,254
Fe	0,812	0,886	0,623	0,896	**1**	-0,353	-0,286	-0,301	-0,063	-0,330	-0,322	-0,294	-0,374	-0,300	-0,419	-0,432	-0,214	-0,098	-0,413	-0,383	-0,306	-0,395	-0,370	-0,355	-0,362	-0,276
Al	-0,301	-0,273	-0,177	-0,328	-0,353	**1**	0,962	0,846	0,819	0,925	0,818	0,683	0,788	0,901	0,864	0,877	0,819	0,636	0,689	0,866	0,917	0,881	0,902	0,762	0,800	0,985
Ti	-0,241	-0,216	-0,138	-0,288	-0,286	0,962	**1**	0,830	0,817	0,947	0,765	0,719	0,796	0,929	0,870	0,885	0,854	0,687	0,688	0,854	0,925	0,871	0,913	0,798	0,812	0,969
Ba	-0,271	-0,235	-0,169	-0,292	-0,301	0,846	0,830	**1**	0,781	0,846	0,878	0,553	0,710	0,750	0,848	0,790	0,727	0,570	0,744	0,852	0,826	0,880	0,852	0,695	0,813	0,825
Be	0,000	0,037	0,099	-0,001	-0,063	0,819	0,817	0,781	**1**	0,806	0,781	0,582	0,648	0,772	0,767	0,755	0,772	0,663	0,685	0,788	0,821	0,801	0,785	0,674	0,688	0,838
Rb	-0,300	-0,277	-0,203	-0,334	-0,330	0,925	0,947	0,846	0,806	**1**	0,814	0,715	0,832	0,956	0,931	0,926	0,911	0,709	0,789	0,903	0,892	0,943	0,978	0,829	0,816	0,922
Sr	-0,232	-0,206	-0,105	-0,266	-0,322	0,818	0,765	0,878	0,781	0,814	**1**	0,588	0,706	0,703	0,851	0,765	0,698	0,582	0,796	0,872	0,801	0,899	0,834	0,679	0,739	0,791
Ag	-0,278	-0,258	-0,221	-0,295	-0,294	0,683	0,719	0,553	0,582	0,715	0,588	**1**	0,612	0,749	0,691	0,702	0,693	0,537	0,668	0,647	0,665	0,634	0,705	0,728	0,632	0,670
Sn	-0,258	-0,300	-0,114	-0,322	-0,374	0,788	0,796	0,710	0,648	0,832	0,706	0,612	**1**	0,781	0,849	0,907	0,920	0,696	0,880	0,908	0,854	0,887	0,907	0,805	0,801	0,875
Cs	-0,336	-0,301	-0,253	-0,331	-0,300	0,901	0,929	0,750	0,772	0,956	0,703	0,749	0,781	**1**	0,866	0,900	0,920	0,684	0,740	0,814	0,828	0,861	0,930	0,824	0,760	0,906
Tl	-0,345	-0,345	-0,256	-0,412	-0,419	0,864	0,870	0,848	0,767	0,931	0,851	0,691	0,849	0,866	**1**	0,941	0,810	0,696	0,880	0,940	0,852	0,917	0,928	0,803	0,807	0,856
Pb	-0,373	-0,374	-0,236	-0,416	-0,432	0,877	0,885	0,790	0,755	0,926	0,765	0,702	0,907	0,900	0,941	**1**	0,824	0,748	0,870	0,908	0,854	0,887	0,907	0,805	0,801	0,875
U	-0,181	-0,161	-0,090	-0,177	-0,214	0,819	0,854	0,727	0,772	0,911	0,698	0,693	0,752	0,920	0,810	0,824	**1**	0,708	0,749	0,787	0,805	0,849	0,905	0,776	0,755	0,826
Bi	-0,005	-0,033	0,144	-0,077	-0,098	0,636	0,687	0,570	0,663	0,709	0,582	0,537	0,785	0,684	0,696	0,748	0,708	**1**	0,641	0,726	0,770	0,654	0,676	0,676	0,718	0,674
Cd	-0,319	-0,322	-0,204	-0,360	-0,413	0,689	0,688	0,744	0,685	0,789	0,796	0,668	0,781	0,740	0,880	0,870	0,749	0,641	**1**	0,836	0,705	0,821	0,812	0,713	0,716	0,675
V	-0,267	-0,279	-0,147	-0,339	-0,383	0,866	0,854	0,852	0,788	0,903	0,872	0,647	0,873	0,814	0,940	0,908	0,787	0,726	0,836	**1**	0,888	0,923	0,899	0,782	0,812	0,854
Cr	-0,170	-0,179	-0,029	-0,259	-0,306	0,917	0,925	0,826	0,821	0,892	0,801	0,665	0,817	0,828	0,852	0,854	0,805	0,770	0,705	0,888	**1**	0,858	0,875	0,816	0,884	0,919
Mn	-0,335	-0,309	-0,193	-0,360	-0,395	0,881	0,871	0,880	0,801	0,943	0,899	0,634	0,811	0,861	0,917	0,887	0,849	0,654	0,821	0,923	0,858	**1**	0,965	0,798	0,803	0,803
Co	-0,330	-0,303	-0,216	-0,354	-0,370	0,902	0,913	0,852	0,785	0,978	0,834	0,705	0,822	0,930	0,928	0,907	0,905	0,663	0,812	0,899	0,875	0,965	**1**	0,848	0,824	0,886
Ni	-0,364	-0,326	-0,274	-0,387	-0,355	0,762	0,798	0,695	0,674	0,829	0,679	0,728	0,717	0,824	0,803	0,805	0,776	0,676	0,713	0,782	0,816	0,798	0,848	**1**	0,870	0,762
Cu	-0,261	-0,265	-0,154	-0,345	-0,362	0,800	0,812	0,813	0,688	0,816	0,739	0,632	0,751	0,760	0,807	0,801	0,755	0,718	0,716	0,812	0,884	0,803	0,824	0,870	**1**	0,799
Ga	-0,226	-0,200	-0,116	-0,254	-0,276	0,985	0,969	0,825	0,838	0,922	0,791	0,670	0,797	0,906	0,856	0,875	0,826	0,674	0,675	0,854	0,919	0,852	0,886	0,762	0,799	**1**

Table 30: ranked E2 data PCA correlation matrix (Pearson)

	F1	F2	F3	F4
Ca	0,913	-0,334	-0,088	-0,188
Mg	0,971	-0,225	0,029	-0,061
Na	0,923	-0,170	0,099	0,010
K	0,988	-0,033	0,016	-0,026
Fe	0,982	-0,148	0,007	-0,050
Al	0,973	-0,205	0,015	-0,041
Ti	0,944	-0,007	-0,009	0,124
Ba	0,971	-0,200	0,072	-0,055
Li	0,539	0,279	0,758	0,181
Be	0,943	-0,251	0,052	-0,173
Rb	0,987	0,103	0,008	-0,012
Sr	0,949	-0,291	0,024	-0,093
Ag	0,683	0,021	-0,341	0,565
Sn	0,735	0,621	0,073	0,109
Cs	0,932	-0,002	0,084	0,193
Tl	0,815	0,483	-0,056	-0,042
Pb	0,911	0,323	-0,113	0,048
U	0,970	-0,069	0,128	-0,089
Bi	0,399	0,706	-0,155	-0,404
Cd	0,936	-0,057	-0,158	0,172
V	0,960	0,031	-0,068	0,092
Cr	0,965	-0,193	-0,076	-0,036
Mn	0,982	-0,154	0,008	-0,052
Co	0,967	0,110	0,009	0,056
Ni	0,968	0,149	-0,033	-0,025
Cu	0,767	0,560	-0,111	-0,082
Ga	0,964	-0,180	-0,055	-0,104

Table 31: raw E2 data PCA factor loadings

	F1	F2	F3	F4
Ca	-0,371	0,884	-0,045	0,058
Mg	-0,360	0,913	0,007	-0,051
Na	-0,241	0,847	-0,196	0,185
K	-0,413	0,865	0,056	-0,064
Fe	-0,431	0,791	0,200	-0,120
Al	0,939	0,070	0,048	-0,204
Ti	0,940	0,129	0,144	-0,134
Ba	0,877	0,076	-0,247	-0,249
Be	0,818	0,377	-0,050	-0,182
Rb	0,972	0,073	0,082	-0,075
Sr	0,861	0,099	-0,338	-0,177
Ag	0,749	-0,009	0,396	0,098
Sn	0,874	0,048	-0,094	0,304
Cs	0,931	0,039	0,284	-0,065
Tl	0,956	-0,016	-0,103	0,024
Pb	0,955	-0,026	-0,006	0,133
U	0,883	0,182	0,212	0,005
Bi	0,741	0,311	0,014	0,484
Cd	0,851	-0,029	-0,192	0,186
V	0,942	0,067	-0,198	0,050
Cr	0,926	0,181	-0,026	0,023
Mn	0,951	0,029	-0,145	-0,105
Co	0,967	0,036	0,033	-0,084
Ni	0,870	-0,035	0,213	0,119
Cu	0,877	0,048	-0,022	0,112
Ga	0,928	0,150	0,084	-0,170

Table 32: ranked E2 data PCA factor loadings

6.1 DATED PROFILES OF BOTH SERIES OF ELEMENTS ANALYSED (HIGH AND LOW RESOLUTION)

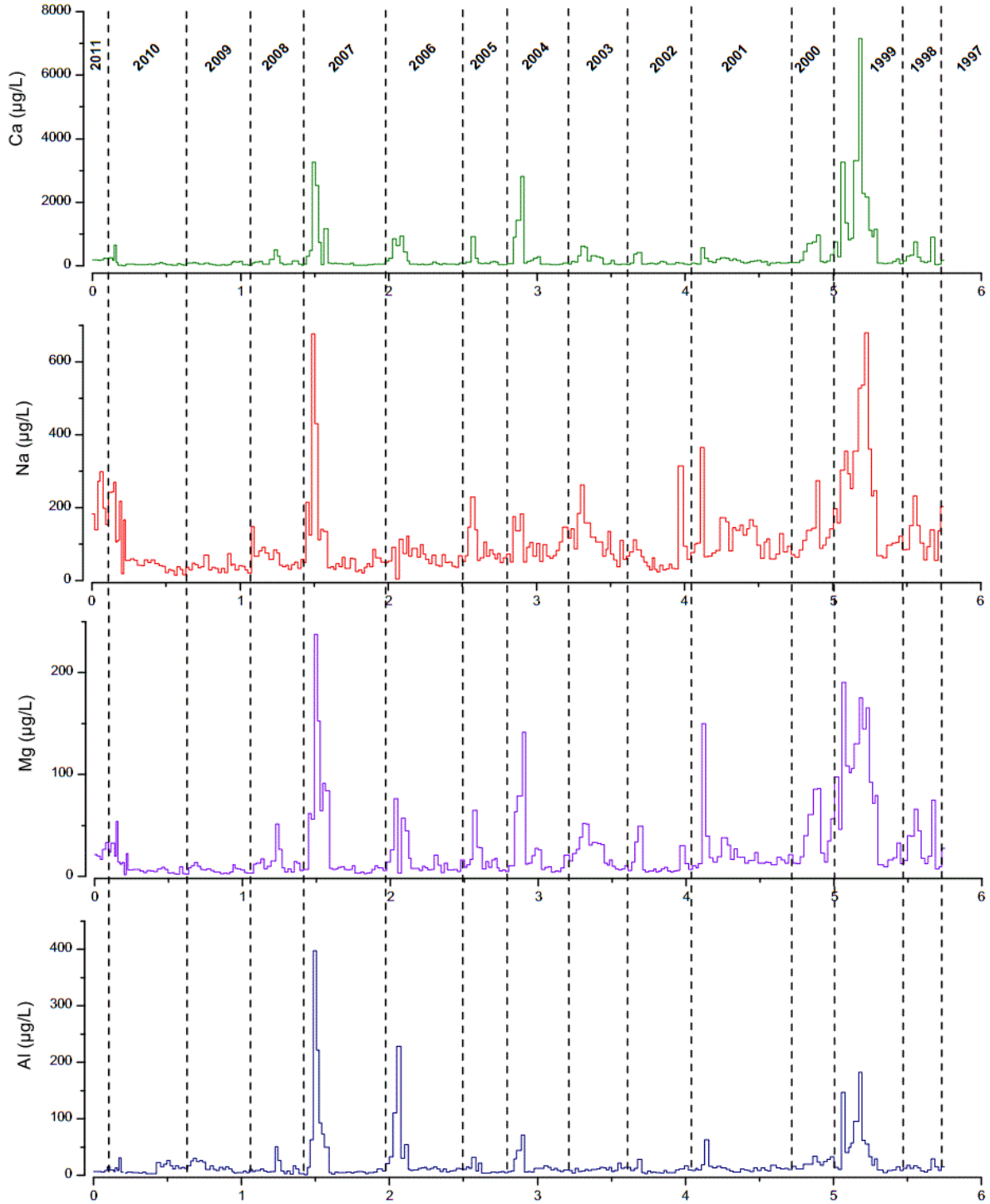

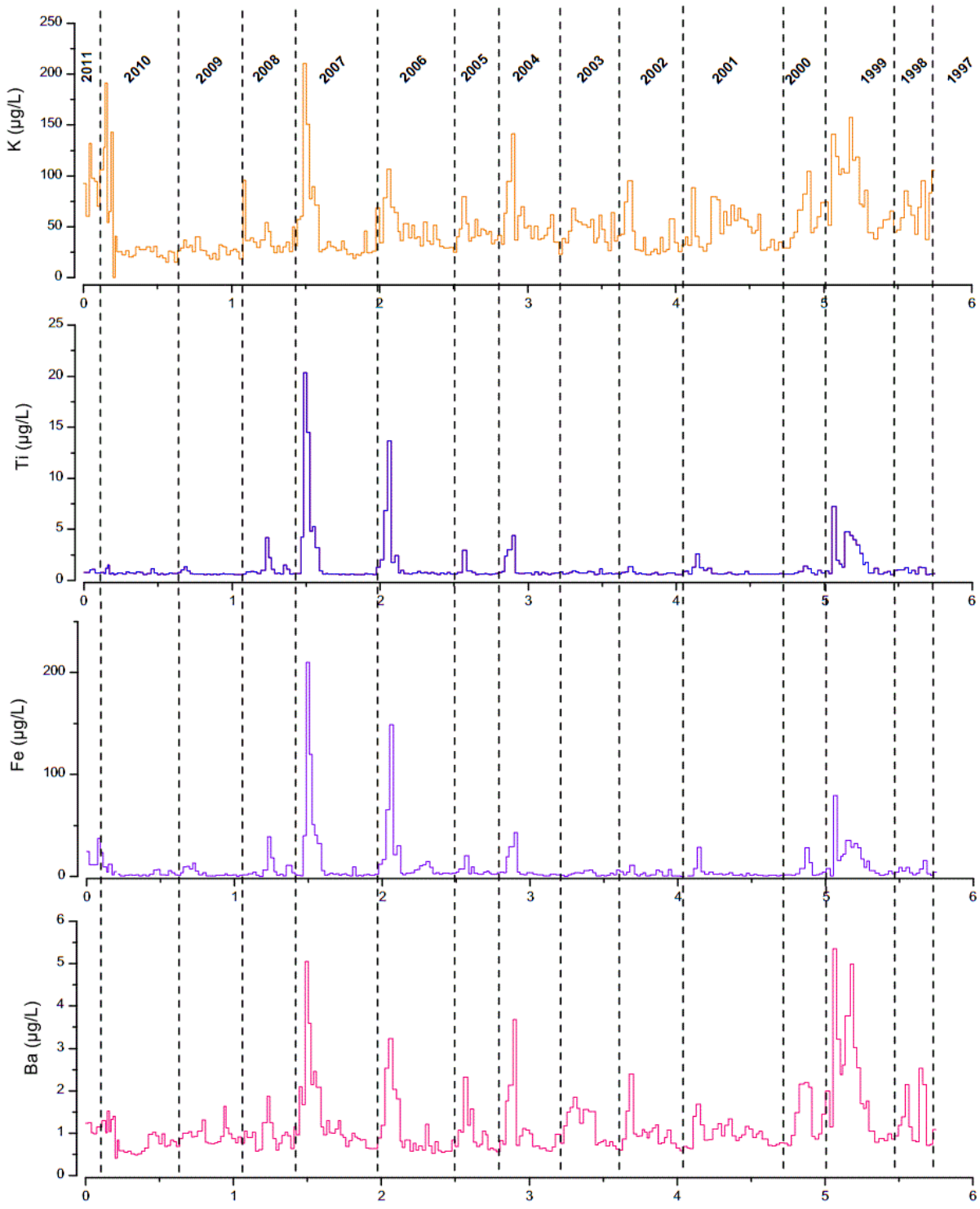
2011
2010
2009
2008
2007
2006
2005
2004
2003
2002
2001
2000
1999
1998
1997
K (µg/L)
Ti (µg/L)
Fe (µg/L)
Ba (µg/L)

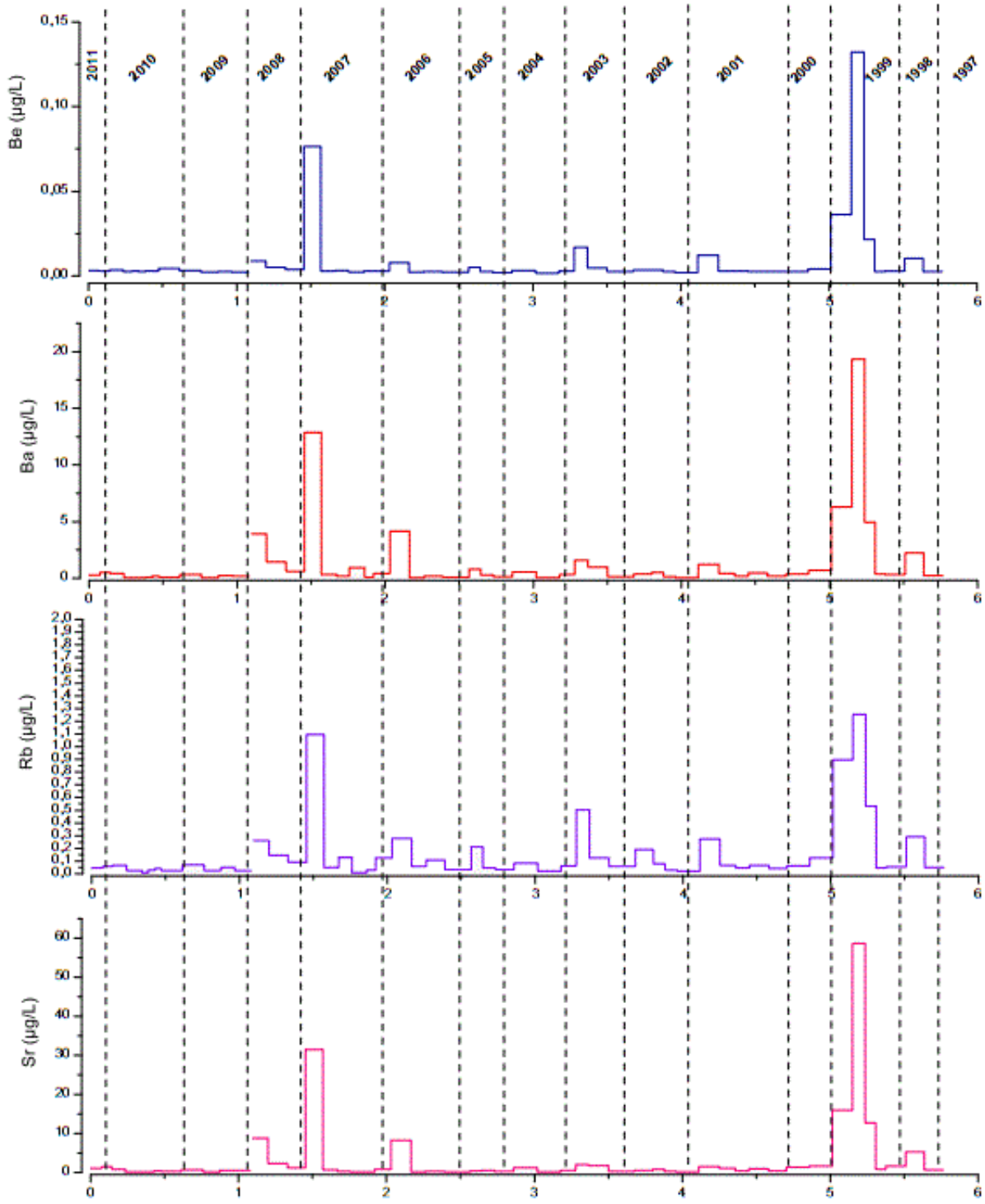
Be (µg/L)
Ba (µg/L)
Rb (µg/L)
Sr (µg/L)
2011
2010
2009
2008
2007
2006
2005
2004
2003
2002
2001
2000
1999
1998
1997

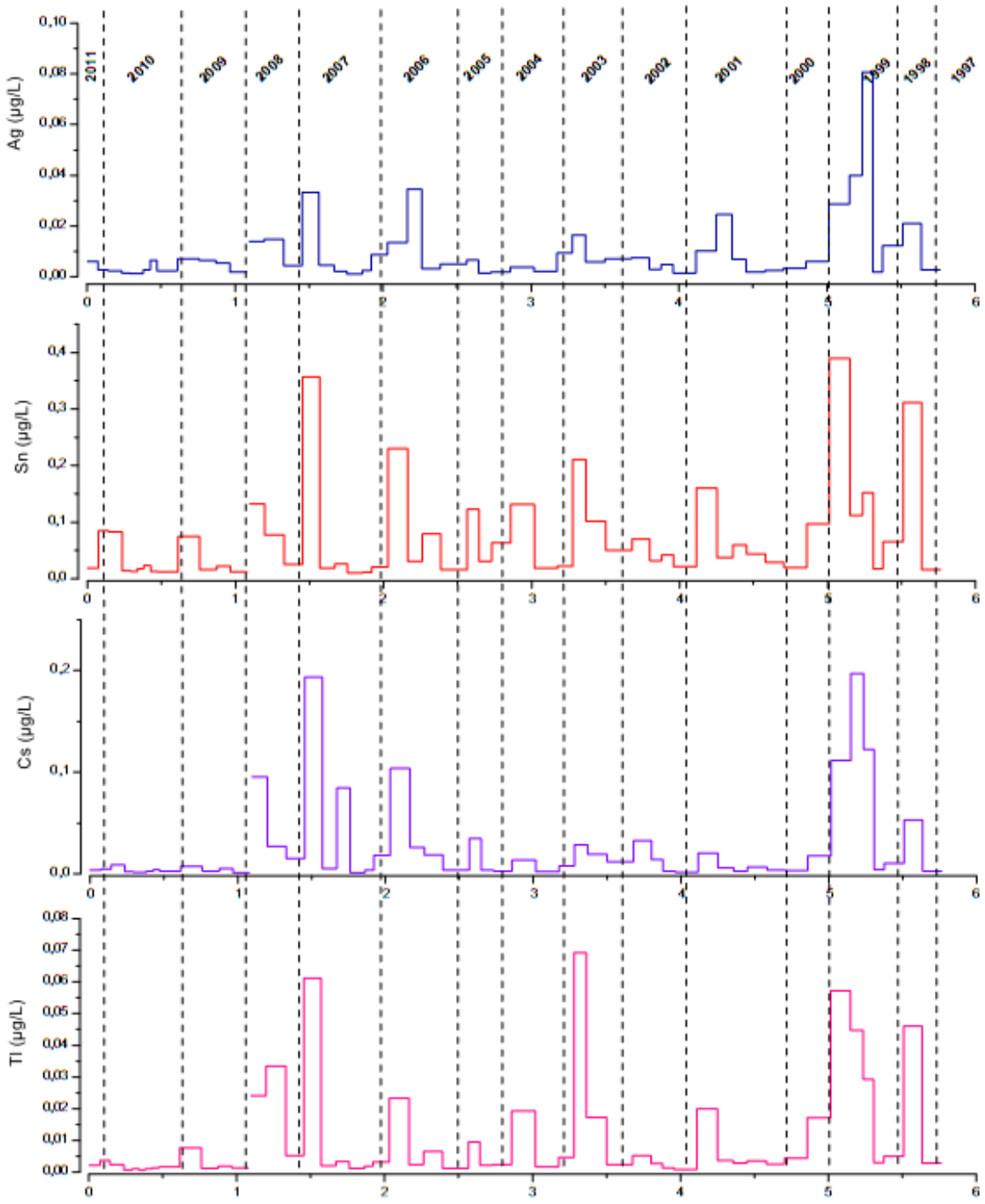
2011
2010
2009
2008
2007
2006
2005
2004
2003
2002
2001
2000
1999
1998
1997
Ag (µg/L)
Sn (µg/L)
Cs (µg/L)
Tl (µg/L)

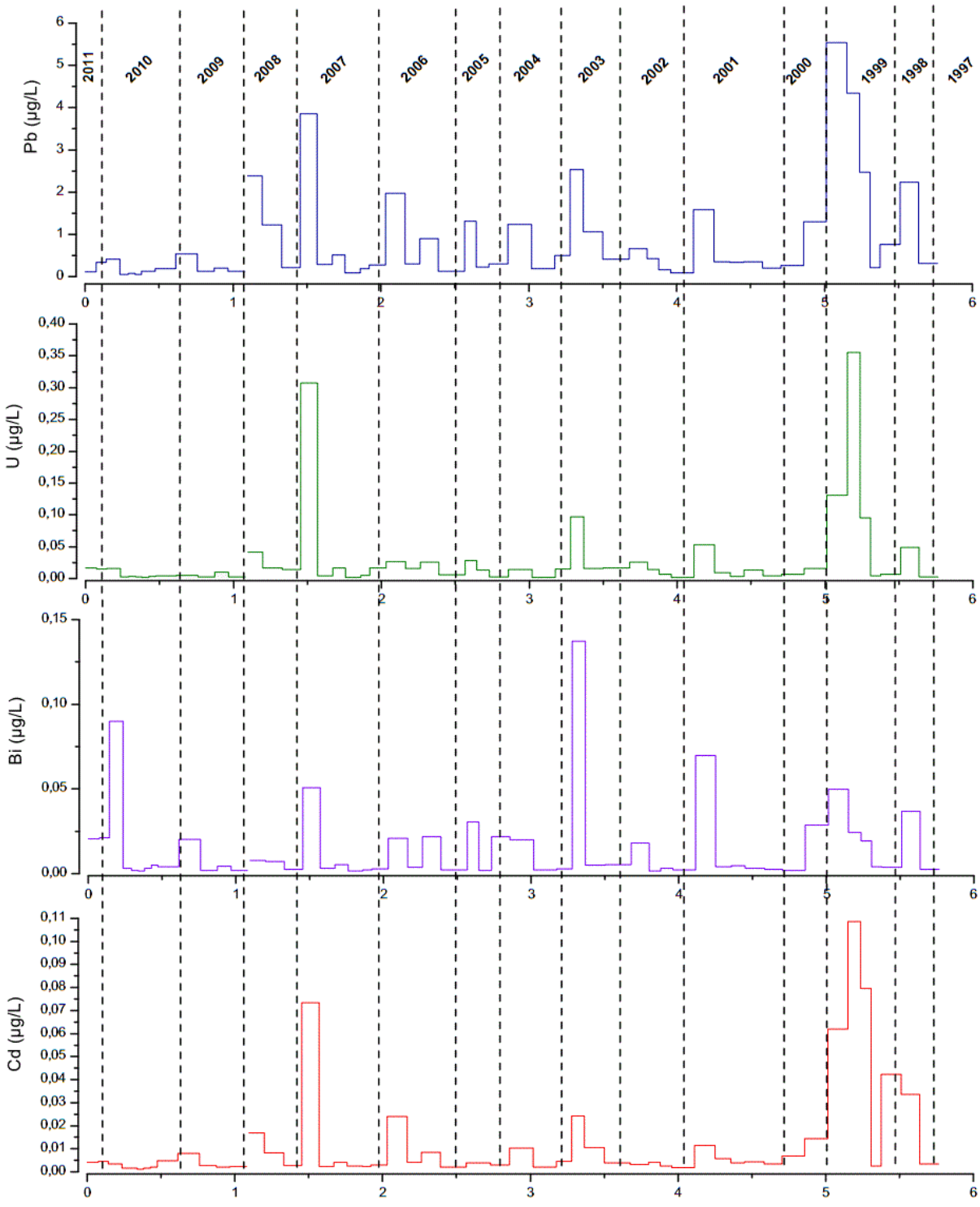
2011
2010
2009
2008
2007
2006
2005
2004
2003
2002
2001
2000
1999
1998
1997
Pb (µg/L)
U (µg/L)
Bi (µg/L)
Cd (µg/L)

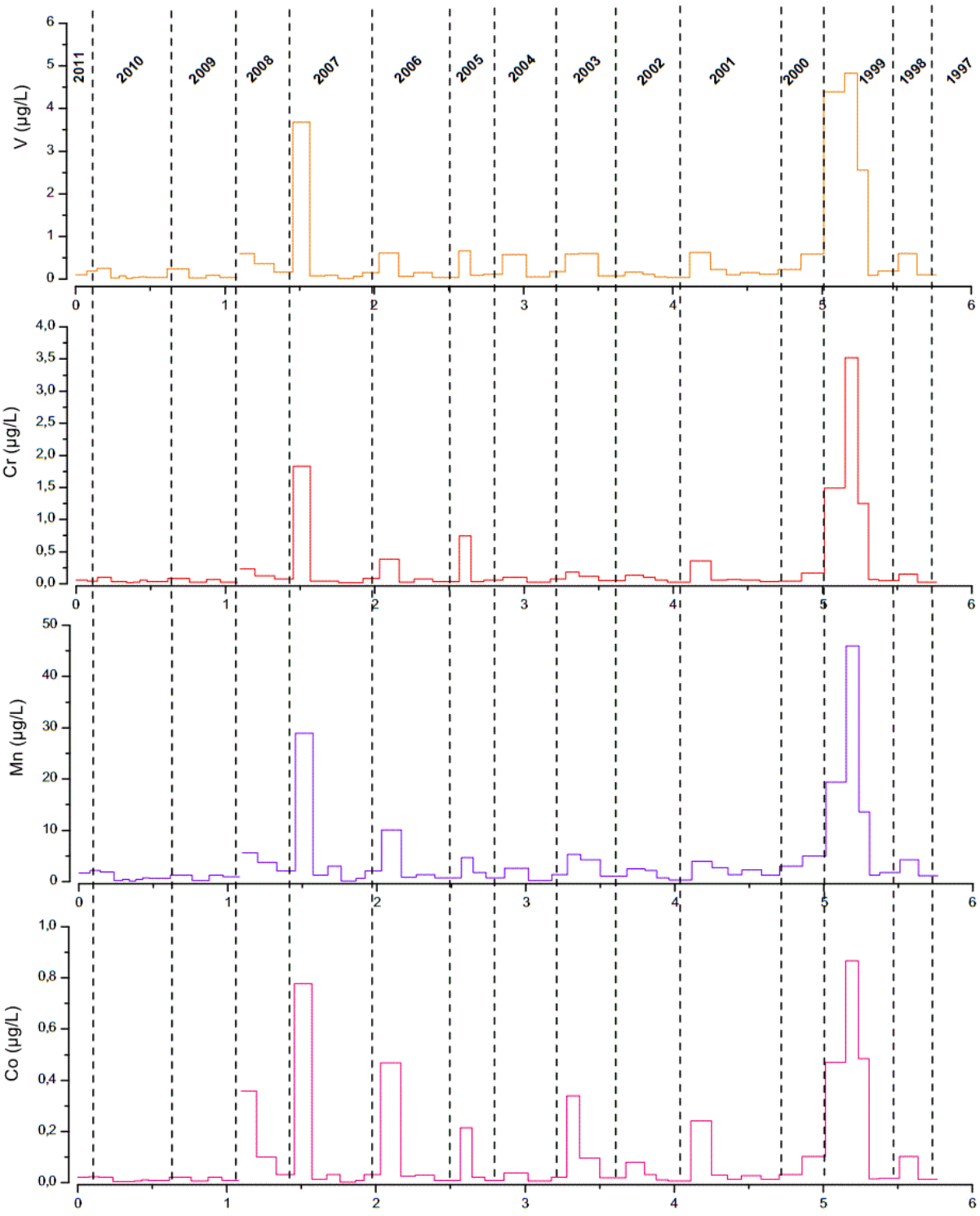
2011
2010
2009
2008
2007
2006
2005
2004
2003
2002
2001
2000
1999
1998
1997
V (µg/L)
Cr (µg/L)
Mn (µg/L)
Co (µg/L)

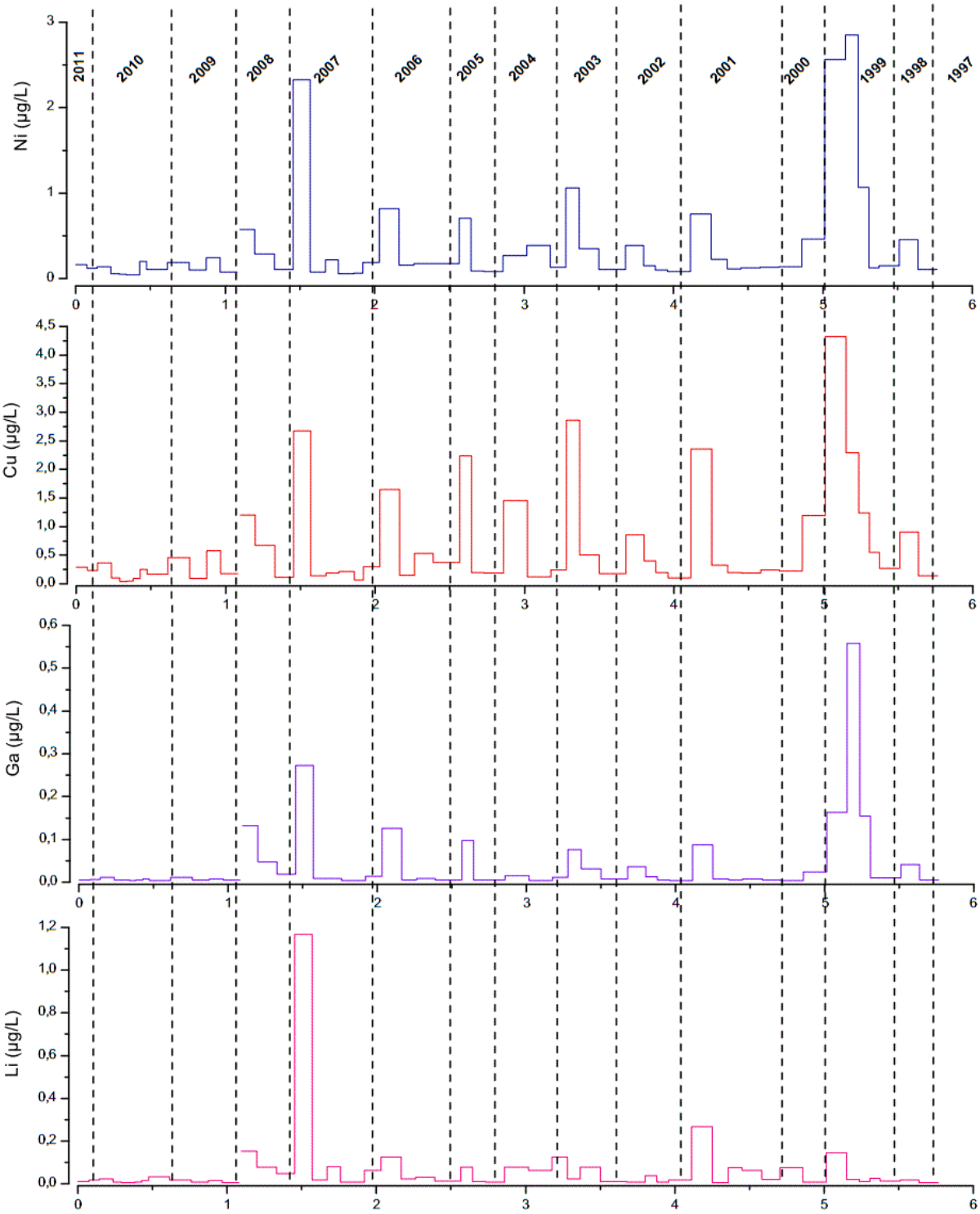
2011
2010
2009
2008
2007
2006
2005
2004
2003
2002
2001
2000
1999
1998
1997
Ni (µg/L)
Cu (µg/L)
Ga (µg/L)
Li (µg/L)